Engineering Journal

First Quarter 2021 | Volume 58, No. 1

Smarter. Stronger. Steel.

Engineering Journal

American Institute of Steel Construction

Dedicated to the development and improvement of steel construction, through the interchange of ideas, experiences, and data.

Engineering Journal (ISSN 0013-8029) is published quarterly. Subscriptions: Members: one subscription, $40 per year, included in dues; Additional Member Subscriptions: $40 per year. Non-Members U.S.: $160 per year. Foreign (Canada and Mexico): Members $80 per year. Non-Members $160 per year. Published by the American Institute of Steel Construction at 130 E Randolph Street, Suite 2000, Chicago, IL 60601.

Subscriptions: subscriptions@aisc.org, 312.670.2400

Archives: Search at **aisc.org/ej**. Article downloads are free for current members and are avaialable for a nominal fee for non-members.

DISCUSSION

Investigation on the Performance of a Mathematical Model to Analyze Concentrically Braced Frame Beams with V-Type Bracing Configurations

Paper by ALIREZA ASGARI HADAD and PATRICK J. FORTNEY
(2020, 2nd Quarter)

Discussion by CHARLES W. ROEDER, DAWN E. LEHMAN, QIYANG TAN, JEFFREY W. BERMAN, and ANDREW D. SEN

The paper "Investigation on the Performance of a Mathematical Model to Analyze Concentrically Braced Frame Beams with V-Type Bracing Configurations" (Hadad and Fortney, 2020) addresses a difficult problem that is not well understood by engineers. While that paper does not specifically limit its application to seismic design, the work was based upon the AISC *Seismic Provisions* and chevron-braced frame seismic behavior experiments. The authors of this discussion, hereafter referred to as the responders for clarity, have also studied chevron-configured concentrically braced frames. That research forms the basis of this discussion. In particular, this discussion aims to clarify the AISC *Seismic Provisions* and prior research results, which the responders believe is misinterpreted in the paper in question. Further, in the series of continuum finite element analyses on a beam with a plate discussed in the paper, it is of note that the model's boundary conditions, loading regime, and results are simplifications of those for beams in chevron-configured or multistory X-braced frames under seismic loading. This discussion addresses applicability of the paper to seismic design and does not apply to any other application.

There are several aspects of the original paper that need to be clarified. First, the findings of some of the cited research is misstated. For example, the paper states that the yielding-beam mechanism is inferior to the "nominally elastic" chevron-beam concept, but this is not correct. Research by the responders (Sen et al., 2016) shows that chevron-braced frames with yielding beams provide better distribution of inelastic deformation over the building height than those with "nominally elastic" beams, and they develop larger inelastic deformations prior to brace fracture. The expected brace forces for seismic design (i.e., Equations 1, 2, and 3 in the paper in question) are used as the basis of the analyses as specified in the AISC *Seismic Provisions*, but it is important to recognize that these are not the forces necessary to resist the design seismic lateral force for the system; instead, they are an idealized set of demands used in the capacity-based design process.

In seismic design of braced frames, the braces are initially designed to resist reduced forces [forces corresponding to the design basis earthquake reduced by the seismic reduction factor, R, as determined by ASCE/SEI 7, *Minimum Design Loads and Other Associated Criteria for Buildings and Other Structures* (ASCE, 2016)]. These reduced seismic design forces are expected to correspond to demands resulting from small, frequent earthquakes, and the structure is expected to remain elastic for that seismic hazard level. For special concentrically braced frames (SCBFs), collapse resistance of the structure is achieved by capacity-based design and detailing for ductility to ensure the system can sustain the cyclic inelastic deformation demands during large earthquakes. In such events, the braces are expected to buckle in compression, yield in tension, and sustain deterioration of their post-buckling compressive resistance at large inelastic deformations. Adjacent members, including the beams, columns, and gusset plates, are designed using capacity-based methods to ensure the braces develop their resistance and inelastic deformation capacity. The capacity-based design concept is not intended to guarantee that members or connections remain elastic during an earthquake; they are simply intended to ensure that the ductile element (the brace in this case) can develop its full deformation capacity by designing the adjacent members to sustain their maximum demands. A primary issue with the

Charles W. Roeder, Professor, Department of Civil and Environmental Engineering, University of Washington, Seattle, Wash. Email: croeder@uw.edu (corresponding)

Dawn E. Lehman, Professor, Department of Civil and Environmental Engineering, University of Washington, Seattle, Wash. Email: delehman@uw.edu

Qiyang Tan, Visiting Graduate Student, Department of Civil and Environmental Engineering, University of Washington, and PhD Candidate, Harbin Institute of Technology, Harbin, China. Email: qiyang_tan@163.com

Jeffrey W. Berman, Professor, Department of Civil and Environmental Engineering, University of Washington, Seattle, Wash. Email: jwberman@uw.edu

Andrew D. Sen, Assistant Professor, Department of Civil, Construction and Environmental Engineering, Marquette University, Milwaukee, Wis. Email: adsen@uw.edu

Paper No. 2018-07RD

stress evaluations proposed in the paper is that they will not necessarily achieve this goal.

The main objective of capacity-based design in SCBFs is to develop the inelastic deformation of the brace rather than to design for a set of fictitious forces. The gusset plates are designed for the expected brace capacities because they are directly connected to the brace. However, when braces are oriented for out-of-plane buckling, the gusset plates deform inelastically due to brace buckling and, as a consequence, sustain significant inelastic deformation demands, as shown in Figure 1. The actual local stresses developed in gusset plates after brace buckling are distributed unevenly and are much larger than those used in gusset-plate design calculations; as the authors recognize, this has been well established even in the absence of brace buckling (Richard, 1986). However, gusset plates that are very conservatively designed will still develop significant yielding because of this out-of-plane brace deformation demand (Lehman et al., 2008). Gusset plates sustain these demands because of the inherent ductility of steel, but welds joining gusset plates to beams and columns are vulnerable to tearing and fracture prior to brace fracture. Therefore, such welds should be designed to develop the plastic capacity of the gusset plate, not the expected brace forces, because inelastic action in the gusset plate is required to accommodate the deformation demands on the system. The User Note in AISC *Seismic Provisions* Section F2.6c.4 (AISC, 2016) is intended to address this goal. While the gusset plates should be designed to develop the expected brace forces, it is unwise to overdesign the gusset plate because that will require larger and more expensive welds on the gusset plate-to-beam or plate-to-column interface. The paper suggests that the welds joining a midspan gusset to the chevron beam should be designed for the in-plane shear, bending moment, and axial force from the gusset plate, but research funded by AISC has shown that this can lead to premature weld fracture, as illustrated in Figure 2 (Swatosh, 2015). Weld fracture should be prevented in seismic design because it prevents the braces and the SCBF from developing their full inelastic capacity. Moreover, weld fracture in some gusset plate connection configurations can also compromise the vertical load-resisting system, as shown in Figure 2.

A second issue with the research presented in the paper is the numerical simulation of the chevron beam. A finite element analysis of the beam and midspan plate was performed with the goals of improving the understanding of the behavior of beams in chevron-braced frames and supporting their proposed stress distribution at the gusset plate-to-chevron beam weld. There are several issues with the approach. First, the boundary conditions of the beam and other aspects of the modeling approach are not described, and these will influence the demands at that weld. It appears that the beam was simply supported, which is an idealized boundary condition and not representative of an actual SCBF. Second, a set of idealized point loads were applied to the gusset plate. However, the demand resulting from cyclic action on an SCBF does not result in a single set of forces, and as such, this approach is not sufficient to understand this complex stress state. Third, as a result of these two issues, the local demands are not properly simulated, but this is not recognized in the paper. Nevertheless, a detailed discussion of the local shear forces and bending moments of the beam in the midspan gusset-plate connection are provided, and it is asserted that these local effects

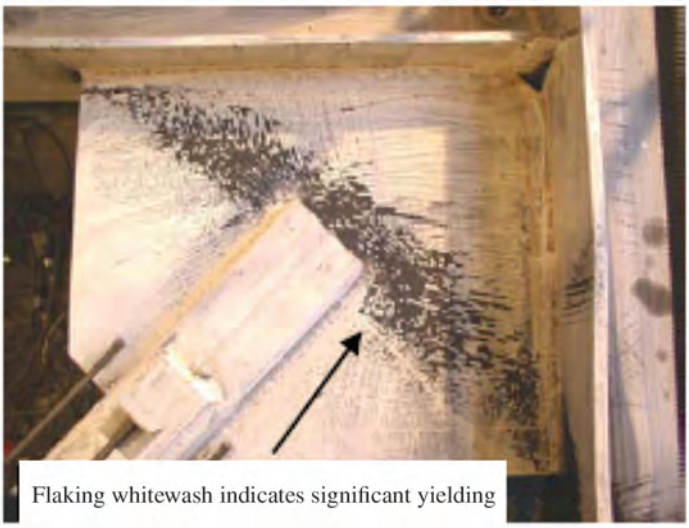

Fig. 1. Inelastic deformation of a gusset plate under seismic deformation.

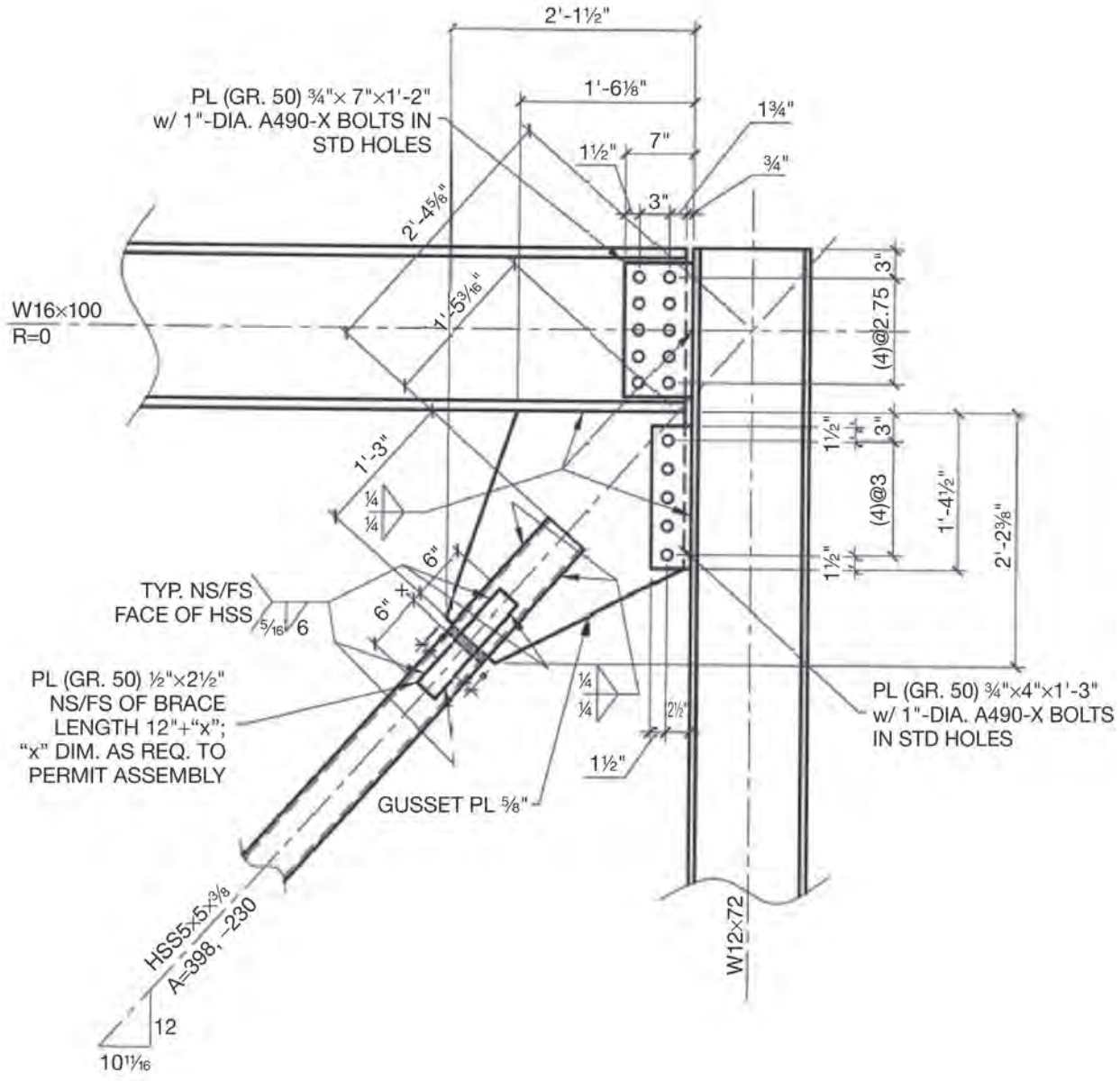

(a) Gusset-plate connection based on expected brace forces

Fig. 2(a). Fracture of gusset-plate welds designed by stress.

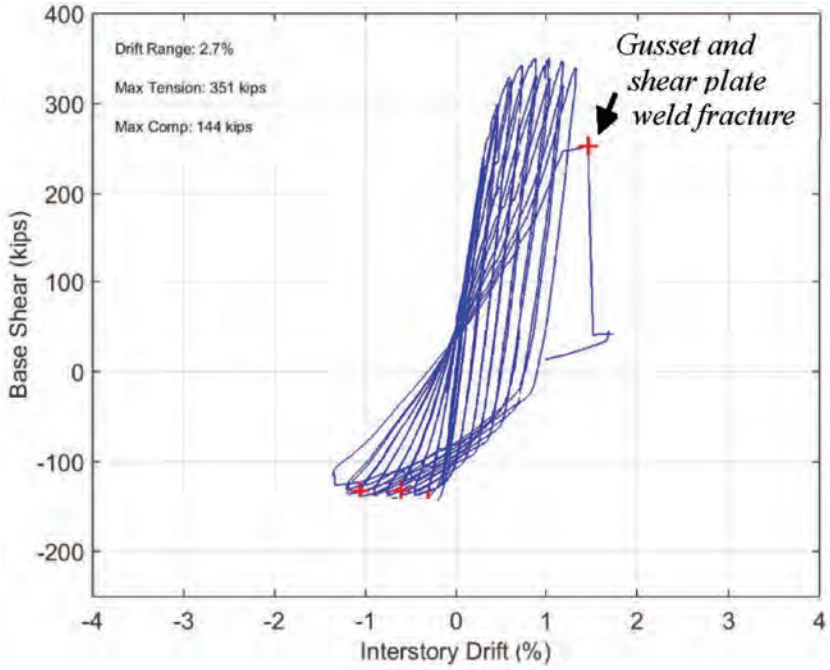

(b) Inelastic deformation of braced frames

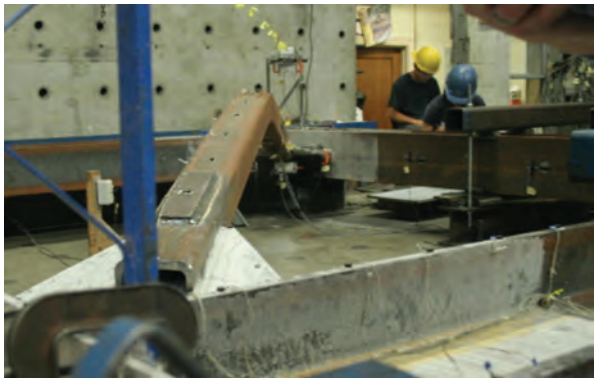

(c) Buckled brace just prior to connection weld fracture

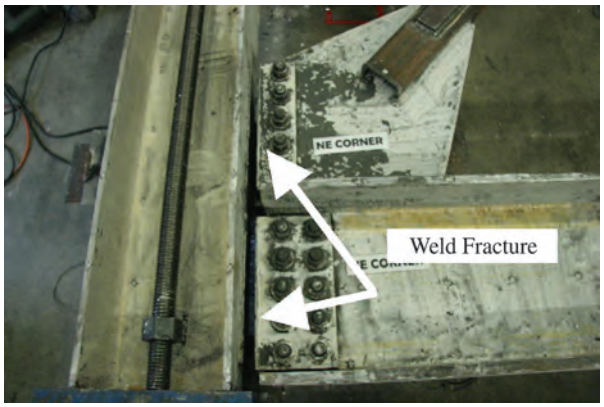

(d) Fractured weld

Fig. 2(b-d). Fracture of gusset-plate welds designed by stress.

control the design of the beam. This conclusion is incorrect because the simulation neglects the axial load, shear force, and bending moment demands in the beam outside the gusset area. These forces and moments are larger than the forces and moments in the gusset area as demonstrated in Figure 3, and they form the primary design considerations for the chevron beam.

Considering these three issues, there are several concerns with the paper's approach:

1. Using St. Venant's principle indicates that the local stresses in the beam in the vicinity of the gusset plate are not reliable when using this calculation method. The principle clearly states that an analysis will produce reasonable results at considerable distance from the load if the load is in equilibrium with the true condition but distributed differently; however, calculated stresses near or adjacent to the applied loads will be quite different under these conditions. Rather than use these reliable stresses away from the gusset plate, the analysis proposed in the paper focuses on local stresses in a disturbed region, and first principles indicates that this is not correct. In comparison, consider the analysis shown in Figure 4, which are the results from a nonlinear analysis of a full chevron-braced frame. The figure shows that the stresses and deformations in the beam when the full system is analyzed are very different from those described in the paper. The beams were designed for the forces of Equations 1, 2, and 3, but there is still significant yielding of the beam. Further, stresses are significantly higher in regions that are *not* adjacent to the midspan gusset plate; these higher stresses must be considered in design. They are neglected in the paper, however, and this is a primary concern to the responders.
2. The paper focuses on the stress-distribution transfer between the midspan gusset plate and the chevron beam; to achieve this, an idealized distribution of stresses is proposed, and these stresses are transferred to the beam as an external load. This approach does not represent the stress transfer because the gusset plate is attached to the beam by continuous welds (or bolts). Therefore, compatibility of the strain between the beam and gusset plate must be maintained at this interface, and these are truly internal stresses. The stresses and strains in the beam and gusset plate must be the same at this location, and the gusset plate and the beam join to resist the forces. The proposed idealization suggests that only the beam resists these forces; this is incorrect. The local effects predicted in the paper's proposed method do not represent the significant overall moment, shear, and axial load demands, and they do not consider that the chevron beam is strengthened significantly by the gusset plate in this region.
3. The axial load in the beam is neglected. A braced frame is often idealized as a truss. This idealization neglects the bending moment demands on the beams and column, but research by the responders indicates that it does

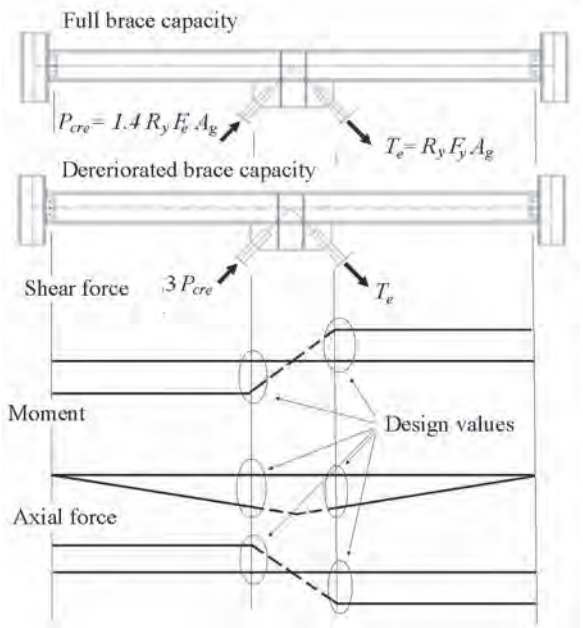

Fig. 3. Axial-load, shear-force, and bending-moment diagrams for idealized boundary condition for capacity-based design of chevron beams.

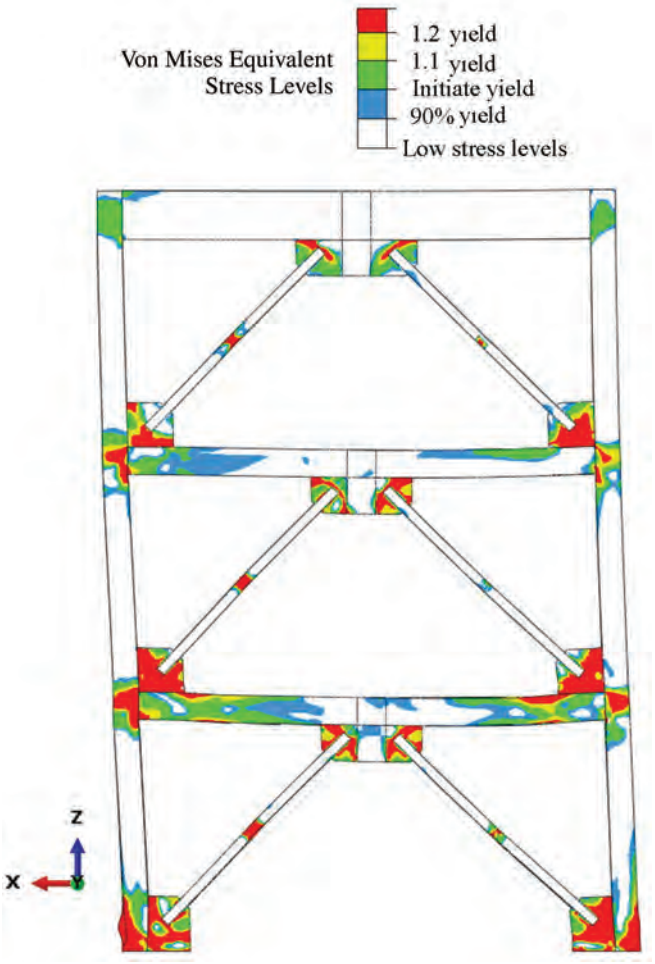

(a) Frame with chevron beam designed to current AISC Seismic Provisions *with* t_w/t_p *of 0.8 and with stiffeners*

Fig. 4(a). Nonlinear analyses of chevron-braced frames.

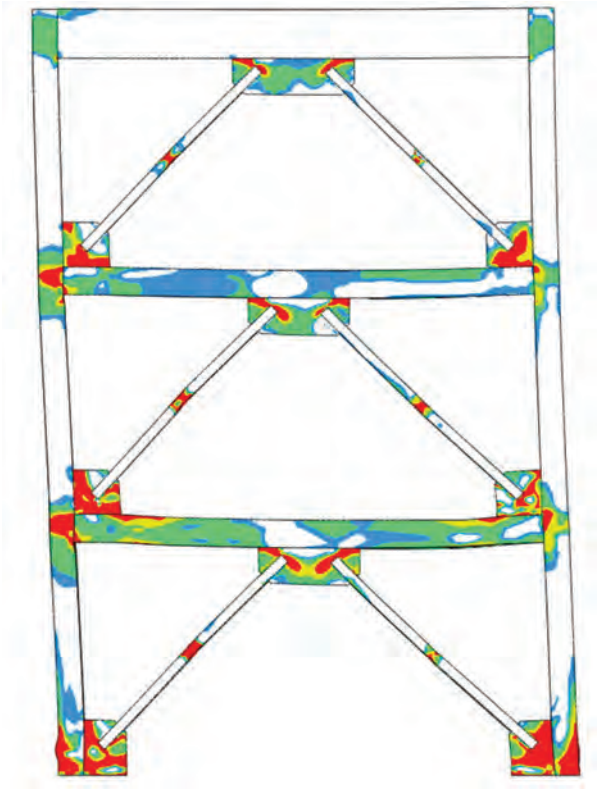

(b) Frame with chevron beam designed to current AISC Seismic Provisions *with* t_w/t_p *of 0.8 and with no stiffeners*

Fig. 4(b). Nonlinear analyses of chevron-braced frames.

provide a reliable estimate of the axial demands. As such, all primary members in SCBFs must be designed considering the axial forces. Neglecting these forces is not an acceptable approach for chevron-beam design. The chevron beam must be designed to develop the combined axial load and bending moment, not local stresses at the gusset plate.

4. In chevron-braced frames, the brace forces distributed over the region of the gusset plate and the extreme local stresses shown in the paper cannot occur. The stresses at the interface also include stresses induced by out-of-plane brace buckling deformations, which are not included in the proposed model. Further, the ends of the chevron beam may not be simply supported. There are often corner gusset plates for the bracing of the story above, and research has shown that these corner gusset plates will provide significant end restraint to the beam and develop significant end moments. This is clearly seen in the nonlinear analysis of Figure 4, but it is not considered in the paper. If there is no corner gusset plate, and the beam-to-column connection is a shear plate or similar connection, the end restraint and resulting moments are very small, as depicted in Figure 3. Figure 3 and the analytical results shown in Figure 4 indicate significant stress due to shear, bending, and axial force outside the gusset regions. Within the midspan gusset regions, the beams are more lightly stressed because the gusset plates stiffen and strengthen the beams in this location.

A BETTER WAY

Local beam forces result from post-buckling brace forces and the boundary conditions of the beam, and these local effects simply change the direction of shear, axial force, and bending moment vectors over the length of the midspan gusset plate. Figure 3 shows that the maximum moment, shear, and axial load are just outside the gusset plate, shown as dashed lines in Figure 3. Analysis of the frame shows the von Mises stresses resulting from combined moment, shear, and axial load are smaller in the region of the midspan gusset and largest just outside of the corner and midspan gusset plates (see Figure 4). Although these forces are affected by the local stresses argued in the paper, the only effect of these local stresses is to change direction and magnitude of these forces over the short length of the gusset plate, which is not the critical section of the beam. The actual shear and axial force must be largest in the beam section outside the

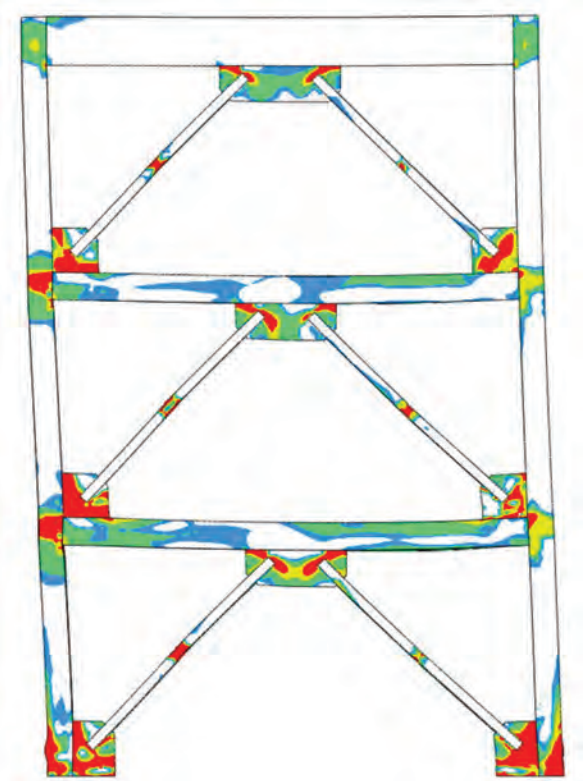

(c) Frame with chevron beam designed to current AISC Seismic Provisions *with* t_w/t_p *of 1.0 and with no stiffeners*

Fig. 4(c). Nonlinear analyses of chevron-braced frames.

gusset plates, shown by the solid lines. Note that Figure 3 assumes a pinned condition at the beam-to-column connection; if the stiffness of the corner gusset is included, then the demands and resulting stresses are also high just outside of the corner gusset plate, as shown in Figure 4. The moment will be slightly larger over the length of the midspan gusset, but the gusset plate adds considerable cross-sectional area and depth to the beam; thus, this larger moment is resisted by the combined capacity of the wide-flange section and gusset plate. The critical section is outside of the gusset plate—and, therefore, the bending moment at the edge of the gusset plate—needs to be checked in the beam design. It is important to note that the beam must be designed for the maximum combined axial, bending, and shear demands, which occur at the circled areas of the figure. This design requirement is not addressed in the paper.

While the responders disagree with results of the paper's stress-driven approach, they also recognize that additional checks are needed to evaluate the midspan gusset plate-to-beam connection in chevron-braced frames. The paper contends that seismic design requires a detailed stress calculation based on forces used as aids in capacity-based design. However, these calculated stresses are not accurate, and they will not capture the local stress demands that actually occur. As previously noted, the gusset-plate connection develops larger stresses than computed if the gusset plate is solely designed to develop the expected brace forces because out-of-plane brace buckling induces inelastic deformation demands on the gusset plate.

To accommodate these demands, gusset-plate welds should be sized to the plastic capacity of the gusset plate as stated in the User Note in AISC *Seismic Provisions* Section F2.6c.4. If the welds are designed to meet this user note, capacity-based design would logically require that the beam must also be capable of developing this resistance. For corner gusset plates where the beam is attached to the column as part of the beam-to-column connection, the beam flange could aid in developing this resistance. However, the beam flange is not restrained for midspan gusset plates, and hence the web of the chevron-beam must resist these demands. If the yield stress of the gusset plate and the beam are the same, this simply means that the thickness of the beam web, t_w, should be equal to or greater than the thickness of the gusset plate, t_{gp} (in multistory X-bracing, the thicker gusset plate controls). This is a very simple check, but it will ensure that stress and force demands required to develop the buckling capacity of the brace are resisted by the beam. Further, this again illustrates why it is so important that the gusset plate be large and strong enough to develop the brace capacity, but no larger or stronger than needed. If a larger plate is used, a thicker web is required.

This simple check may be difficult to satisfy in practice, however, because it is likely that the gusset plate will be thicker than the lightest beam needed to support chevron-beam forces. Figure 4 illustrates the impact of stiffeners and the gusset plate-to-beam web thickness ratio. The validity of this approach is illustrated in Figure 4 for frames subjected to large inelastic deformations. Figure 4(b) shows a chevron-beam web that is thinner than the gusset plate, and a significant amount of local yielding can be seen in the beam web above the midspan gusset plate. Figure 4(a) has the same beam and gusset plate, but stiffeners are applied to the beam web and midspan gusset plate. At the same inelastic deformation as in Figure 4(b), the beam web adjacent to the midspan gusset plate is quite clear of all yielding. Figure 4(c) has a beam with web thickness equal to the gusset-plate thickness and no beam-web or gusset-plate stiffeners. While the thinner beam web with stiffeners performed better, this frame with the thicker web and no stiffeners performed acceptably.

The results indicate the stiffeners can help achieve the desired response and a web thickness less than the gusset plate can be used; further research is being conducted by the responders to provide more guidance on this aspect of design and detailing. While adding stiffeners might be viewed as an undesirable expense, they serve multiple purposes here, which justify their cost. The bending moment in a chevron beam is largest at the midspan gusset plate, which means that bracing against lateral-torsional buckling is also required at this location. In addition, stiffeners can be used to attach transverse beams or elements used for lateral support and aid in transferring brace forces to the chevron beam.

An X-braced frame with top and bottom gusset plates is even more likely to require stiffeners with thin webs because stiffeners will facilitate force transfer between stories. The size of the stiffeners could be based on the size of the balance of the gusset-plate and beam-web thicknesses. A similar approach can be used for corner gusset plates, but this could be relaxed when the beam flange is attached to the column because this attachment stiffens the flange so that it also facilitates transfer of forces from the gusset plate to the beam or column.

CONCLUSIONS

The responders recognize that this is a difficult topic and more research is needed to define the optimal design procedure. However, the responders contend that the research presented herein justifies a simpler and more reliable method for evaluating beams and midspan gusset plates in seismic design of chevron or multi-story, X-braced frames versus that proposed in the paper. This research clearly suggests the following design method:

1. The brace is designed to develop the seismic design forces required by ASCE/SEI 7.
2. The expected tensile and compressive capacity of these selected braces are used to perform a capacity-based design of the gusset plates. The gusset plates should be strong enough to develop the expected resistance of the brace, but additional strength beyond this requirement is discouraged because overly strong gusset plates will require larger welds and adversely affect braced-frame performance.
3. The welds or bolts joining the gusset plate to the beams and the columns should be strong enough to develop the resistance of the gusset plate, ensuring they are able to accommodate the deformation demands of the gusset plate due to out-of-plane brace buckling.
4. The beams of chevron (V- and inverted V-configuration) and multi-story, X-braced frames should be capacity designed to develop the expected shear force, bending moment, and axial force in the beam from maximum elastic and plastic brace forces, including deterioration of the compressive capacity.
5. Because the midspan gusset plate stiffens and strengthens the beam where they are attached, the demands should be evaluated in the beam *adjacent* to the midspan gusset plate. No stress calculations for the beam in the midspan gusset plate region are recommended.
6. The midspan connection should fulfill one of two requirements. If the thickness of the beam web is equal to or greater than the thickness of the gusset plate, no further design checks are required. Otherwise, when the thickness of the gusset plate exceeds the thickness of the beam web, vertical stiffeners to the beam web and the gusset plate should be employed.

REFERENCES

AISC (2016), *Seismic Provisions for Structural Steel Buildings*, ANSI/AISC 341-16, American Institute of Steel Construction, Chicago, Ill.

ASCE (2016), *Minimum Design Loads and Associated Criteria for Buildings and Other Structures*, ASCE/SEI 7-16, American Society of Civil Engineers, Reston, Va.

Hadad, A.A. and Fortney, P.J. (2020), "Investigation on the Performance of a Mathematical Model to Analyze Concentrically Braced Frame Beams with V-Type Bracing Configurations," AISC, *Engineering Journal*, Vol. 57, No. 2, pp. 91–108.

Lehman, D.E., Roeder, C.W., Herman, D., Johnson, S., and Kotulka, B. (2008), "Improved Seismic Performance of Gusset Plate Connections," *Journal of Structural Engineering*, ASCE, Vol. 134, No. 6.

Richard, R.M. (1986), "Analysis of Large Bracing Connection Designs for Heavy Construction," *Proceedings of the National Steel Construction Conference*, AISC, June 12–14, Nashville, Tenn.

Sen, A.D., Roeder, C.W., Berman, J.W., Lehman, D.E., Li, C.-H., Wu, A.-C., and Tsai, K.-C., (2016), "Experimental Investigation of Chevron Concentrically Braced Frames with Yielding Beams," *Journal of Structural Engineering*, ASCE, Vol. 142, No. 12.

Swatosh, M. (2015), "AISC SCBF3," Report to AISC, University of Washington, Seattle, Wash.

AISC Provisions for Web Stability Under Local Compression Applied to HSS

FEI WEI and JEFFREY A. PACKER

ABSTRACT

The relevant limit states for local compression loading on the webs of a rectangular HSS member are reviewed, and the 2016 AISC *Specification* Chapter J provisions are adapted from their normal application to the single web of a W-shape or I-section to this case. Two recent laboratory tests on matched-width, rectangular HSS-to-HSS cross-connections are described to illustrate the behavior of such connections under branch axial compression. The data from these tests are supplemented by experimental results from a further 76 cross-connection tests, with the branches being either welded plates or welded HSS. From this 78-test database, the existing provisions for local yielding of the chord sidewalls, local crippling of the chord sidewalls, and buckling of the chord sidewalls are evaluated. Recommendations are made for handling transverse compression loading on HSS webs in the AISC *Specification*, and a design example is given to illustrate the approach.

KEYWORDS: hollow structural sections, cross-connections, web yielding, web crippling, web buckling, design procedures.

INTRODUCTION

Concentrated compression forces on rectangular HSS are relatively common, especially at bearing or reaction points of trusses and girders and at beam-to-column moment connections. This loading situation is covered in AISC *Specification* Section K2.3 (AISC, 2016), where one is directed to determine the connection available strength from the applicable limit states in Chapter J.

For loading across the full width of the HSS (or when the branch-to-chord width ratio $\beta = 1.0$), the two webs are loaded in compression, and yielding or instability of the chord/column webs will control the connection capacity. AISC *Specification* Section J10 (AISC, 2016) on "Flanges and Webs with Concentrated Forces," which is based on the behavior of I-shaped sections with a single web, specifies the applicable limit states. For laterally supported HSS connections these are (1) web local yielding (Section J10.2), (2) web local crippling (Section J10.3), and (3) web compression buckling (Section J10.5). In the following, these limit states are further described, applied to the case of HSS webs, and evaluated against test results for matched-width, HSS-to-HSS cross-connections and plate-to-HSS connections under transverse compression. For all three limit states, the AISC *Specification* considers separate cases of the concentrated compression load being applied: (1) away from the member end (termed "interior" herein) and being free of any end effects and (2) close to the member end (termed "end" herein). The latter would correspond to a compression load close to an open end of an HSS member, without a cap plate. This paper evaluates transversely loaded HSS connections remote from the member end.

Fei Wei, Structural Engineer, Cast Connex Corporation, Toronto, Ontario, Canada. E-mail: fei.wei@mail.utoronto.ca

Jeffrey A. Packer, Bahen/Tanenbaum Professor of Civil Engineering, Department of Civil & Mineral Engineering, University of Toronto, Toronto, Ontario, Canada. E-mail: jeffrey.packer@utoronto.ca (corresponding)

Paper No. 2019-11R

Web Local Yielding

Local yielding of the HSS webs is a possible limit state for both compression and tension concentrated loads, and it applies to T-, Y- and cross- (or X-) connections with $\beta \approx 1.0$. The applied load, acting over a bearing length of l_b, disperses at a slope of 2.5:1 to the "k line" and thus produces yielding over a length of $(5k + l_b)$ for an interior connection. This load-dispersion angle of 21.8° is a classical assumption throughout steel codes. The distance k, from the outer face of the flange to the web toe of the fillet for a wide flange or I-section, can be taken for a rectangular HSS as the outside corner radius, with a conservative value of $1.5t$, where t is the HSS member design thickness (AISC *Specification* Section J10 Commentary). The applicable connection nominal strength equations, in both wide-flange (or I-section) format and HSS format, are shown in Table 1 for interior- and end-loading situations. In laboratory experiments, this failure mode has been found to occur for short bearing lengths (such as with plate-to-HSS connections, as shown in Figure 1) and also for stocky chord walls with longer bearing lengths.

Web Local Crippling

This limit state is defined as the crumpling of the web into buckled waves directly beneath a compression load,

occurring in more slender webs, whereas web local yielding of that same area occurs for stockier webs (AISC *Specification* Section J10.3 Commentary). Research by Roberts (1981) on the compression of a single, slender, I-section web provided the basis for the nominal strength expressions in the AISC *Specification*. As shown in Table 1, modified versions are provided for interior- and end-loading situations. Because the overall member depth, d, is used in the I-section web crippling AISC *Specification* Equation J10-4, for consistency this is replaced by the HSS overall depth, H, in the conversion shown in Table 1. This is a small and conservative difference to the presentation in the 2010 AISC *Specification* Equation K2-10 (AISC, 2010). This limit state is applicable to "compressive single-concentrated forces" (*Specification* Section J10.3), hence to T- and Y-connections with $\beta \approx 1.0$. However, this failure mode has not been observed in rectangular HSS connections, which is presumed to be because the typical H/t values of HSS webs are below the wall slenderness requirement for this failure mode to govern. [Note that the tests reported by Roberts (1981) had overall height-to-web thickness ratios ranging from 75 to 505, with very few below 100.] Nevertheless, although the scope of the study presented herein is for HSS cross-connections, the applicable connection nominal strength equations for web local crippling, in both wide flange (or I-section) format and HSS format, are shown in Table 1.

Web Compression Buckling

This limit state involves overall buckling of the entire web and only applies to "a pair of compressive single-concentrated forces" (AISC *Specification* Section J10.5), hence to HSS cross-connections with $\beta \approx 1.0$, where compression force is transferred through the chord/column member. AISC *Specification* Section J10.5 Commentary notes that the nominal strength expression (for W- or I-shapes) is only valid for bearing lengths "…for which l_b/d is approximately less than 1." A validity range of l_b/d is hence included in Table 1. AISC *Specification* Equation J10-8 originates from Newlin and Chen (1971), who showed that their semi-empirical expression was a lower bound for web buckling failure loads achieved in a small number of transverse compression tests on point-loaded, wide-flange sections. AISC *Specification* Section J10 Commentary points out that *Specification* Equation J10-8 assumes pinned restraints at the ends of the web.

The dimension h is defined as the clear distance between flanges less the fillet or inside corner radius. Thus, in the conversion of web compression buckling formulas to HSS format, h is taken equal to $(H - 3t)$, which represents a maximum height of the flat part of the chord sidewall. For long bearing lengths, greater than the HSS overall depth, H, the web needs to be designed as a column member in accordance with AISC *Specification* Chapter E. Treating each HSS web as a column with a rectangular cross section is actually the method for handling web compression failure in Eurocode 3 (CEN, 2005), CIDECT Design Guide No. 3 (Packer et al., 2009), and ISO 14346 (ISO, 2013). This failure mode has been observed experimentally for full-width HSS-to-HSS cross-connections with H/t greater than about 15 (Figure 2). An earlier investigation on the influential parameters affecting the web strength of HSS chords under transverse compression, by Davies and Packer (1987), indicated that the bearing length parameter, l_b/H, affects the chord sidewall slenderness, H/t, at which failure changes from web bearing (local yielding) to web buckling.

For web compression buckling with $l_b > d$, or $H_b/\sin\theta > H$ (i.e., beyond the applicable limit of Table 1), each web is to be treated as a column of slenderness KL/r, where the effective length factor, K, can be taken as 1.0 (as suggested by AISC *Specification* Appendix Section 7.2.3, considering the main HSS through member as a non-sway frame). The column length, L, is taken as the sidewall flat dimension, equal to $(H - 3t)$. The radius of gyration, r, of a rectangular cross-section HSS wall is $t/\sqrt{12}$. Thus, the nominal

Fig. 1. Web local yielding failure in a full-width plate-to-HSS connection, with plates in compression.

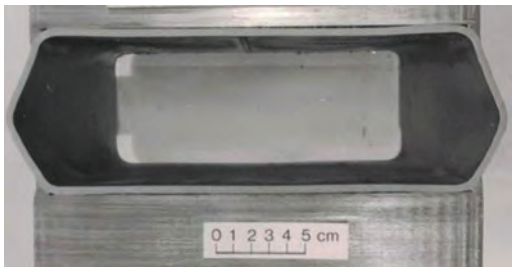

Fig. 2. Web buckling failure in a full-width ($\beta = 1.0$) HSS-to-HSS cross-connection, with branches in compression and $H/t = 23$.

Table 1. Nominal (and Available) Strengths of Web Compression Limit States for Wide Flange (I-Section) Shapes and Rectangular HSS Connections, per the AISC *Specification* (Equation Numbers and ϕ/Ω Values from the *Specification*)

Limit State	Wide Flange or I-Section, R_n (kips)	HSS-to-HSS Connection, P_n (kips)	ϕ (Ω)
Web local yielding, interior	for $l_{end} > d$ $F_{yw}t_w(5k + l_b)$ (J10-2)	for $l_{end} > H$ $\frac{2F_yt}{\sin\theta}\left(7.5t + \frac{H_b}{\sin\theta}\right)$ (1)	1.00 (1.50)
Web local yielding, end	for $l_{end} \le d$ $F_{yw}t_w(2.5k + l_b)$ (J10-3)	for $l_{end} \le H$ $\frac{2F_yt}{\sin\theta}\left(3.75t + \frac{H_b}{\sin\theta}\right)$ (2)	1.00 (1.50)
Web local crippling, interior	for $l_{end} \ge d/2$ $0.80t_w^2\left[1+3\left(\frac{l_b}{d}\right)\left(\frac{t_w}{t_f}\right)^{1.5}\right]\sqrt{\frac{EF_{yw}t_f}{t_w}}Q_f$ (J10-4)	for $l_{end} \ge H/2$ $\frac{1.6t^2}{\sin\theta}\left(1+\frac{3H_b}{\frac{\sin\theta}{H}}\right)\sqrt{EF_y}Q_f$ (3)	0.75 (2.00)
Web local crippling, end, and $l_b/d \le 0.2$	for $l_{end} < d/2$ $0.40t_w^2\left[1+3\left(\frac{l_b}{d}\right)\left(\frac{t_w}{t_f}\right)^{1.5}\right]\sqrt{\frac{EF_{yw}t_f}{t_w}}Q_f$ (J10-5a)	for $l_{end} < H/2$ and $H_b/H\sin\theta \le 0.2$ $\frac{0.8t^2}{\sin\theta}\left(1+\frac{4H_b}{\frac{\sin\theta}{H}}\right)\sqrt{EF_y}Q_f$ (4)	0.75 (2.00)
Web local crippling, end, and $l_b/d > 0.2$	for $l_{end} < d/2$ $0.40t_w^2\left[1+\left(4\frac{l_b}{d}-0.2\right)\left(\frac{t_w}{t_f}\right)^{1.5}\right]\sqrt{\frac{EF_{yw}t_f}{t_w}}Q_f$ (J10-5b)	for $l_{end} < H/2$ and $H_b/H\sin\theta > 0.2$ $\frac{0.8t^2}{\sin\theta}\left(0.8+\frac{4H_b}{\frac{\sin\theta}{H}}\right)\sqrt{EF_y}Q_f$ (5)	0.75 (2.00)
Web compression buckling, interior, and $l_b \le d$	for $l_{end} \ge d/2$ $\frac{24t_w^3\sqrt{EF_{yw}}}{h}Q_f$ (J10-8)	for $l_{end} \ge H/2$ and $H_b/H\sin\theta \le 1.0$ $\frac{1}{\sin\theta}\left(\frac{48t^3}{H-3t}\right)\sqrt{EF_y}Q_f$ (6)	0.90 (1.67)
Web compression buckling, end, and $l_b \le d$	for $l_{end} < d/2$ $\frac{12t_w^3\sqrt{EF_{yw}}}{h}Q_f$	for $l_{end} < H/2$ and $H_b/H\sin\theta \le 1.0$ $\frac{1}{\sin\theta}\left(\frac{24t^3}{H-3t}\right)\sqrt{EF_y}Q_f$ (7)	0.90 (1.67)

Note: l_{end} = distance from the near side of the connecting branch or plate to end of member

flexural buckling strength of the two HSS sidewalls can be calculated from AISC *Specification* Section E3, with an allowance for an inclined branch producing a longer web buckling length (Packer et al., 2009; IIW, 2012; ISO, 2013) by:

$$\frac{KL}{r} = \frac{L_c}{r} = 3.46\left(\frac{H}{t} - 3\right)\sqrt{\frac{1}{\sin\theta}} \quad (8)$$

and, for one sidewall, a "column" cross-sectional area given by $A_g = (7.5t + H_b/\sin\theta)t$, from Equation 1 in Table 1 for $l_{end} > H$, or $A_g = (3.75t + H_b/\sin\theta)t$ from Equation 2 in Table 1 if $l_{end} \le H$. For consistency with Equations 6 and 7 in Table 1, the factor Q_f (from AISC *Specification* Table K3.2) should also be included if chord compression stress is present.

A recent numerical study of welded, full-width, rectangular HSS cross-connections by Kuhn et al. (2019) showed that 0.25 represented a critical value for the bearing length-to-chord height ratio at which the failure mode changed from web yielding to web buckling. Thus, for rectangular HSS-to-HSS cross-connections and plate-to-HSS cross-connections with $(H_b/\sin\theta)/H \le 0.25$, web local yielding was deemed to govern and could be predicted by a model such as Equation 1. H_b represents either the HSS branch depth,

in the plane of the connection or, alternatively, the thickness of a transverse, full-width plate. If $(H_b/\sin\theta)/H > 0.25$, web compression buckling was deemed to govern and could be predicted by treating the two chord sidewalls as columns, for which a modification of Equation 1 could be used:

$$P_n = \frac{2\chi F_y t}{\sin\theta}\left(7.5t + \frac{H_b}{\sin\theta}\right) \quad (9)$$

where χ is a reduction factor applied to yield stress for column buckling. For fully welded branches to either side of the chord member, the end fixity of the sidewall "column" is likely closer to fixed-fixed than pin-ended. For fixed-fixed end conditions, Kuhn et al. (2019) noticed that most steel codes have a cold-formed column buckling curve that is almost linear when plotted over a practical chord sidewall slenderness range; hence they advocated a simple conservative estimation for χ using:

$$\chi = 1.15 - 0.013\frac{H}{t}\sqrt{\frac{1}{\sin\theta}} \le 1 \quad (10)$$

Equation 10, for $F_y \le 50$ ksi and $H/t \le 50$, is shown plotted in comparison to the 2016 AISC *Specification* column buckling curve in Figure 3. The vertical axis in this figure, χ, is equivalent to the AISC *Specification* buckling stress, F_{cr}, divided by the yield stress, F_y. An effective length factor of $K = 0.65$ is used as a design approximation to the theoretical fixed-fixed factor of $K = 0.5$. This approach advocated by Kuhn et al. (2019) is also evaluated against test data later in this paper, in addition to the current 2016 AISC *Specification* method.

EXPERIMENTS ON FULL-WIDTH RECTANGULAR HSS CROSS-CONNECTIONS

Two recent laboratory tests (Wei, 2019) on matched-width, rectangular HSS-to-HSS 90° cross-connections are described to illustrate the behavior under branch axial compression. These were tested to failure under displacement control, in quasi-static branch compression, as shown in Figure 4, using a 1,000-kip-capacity universal testing machine. As can be seen from Figure 4, the branch compression load was reacted by a steel plate, which was secured to the laboratory strong floor, and no lateral restraint was provided to the chord member. Displacement was captured at many points by a Metris K-610 3D Dynamic Laser Measuring System together with a linear variable differential transformer (LVDT). All members were made of cold-formed HSS to either ASTM A500 Grade B/C (ASTM, 2018) or CSA G40.20/G40.21 (CSA, 2013), and two chord sizes were used: HSS 8×8×¼ and HSS 8×8×⅜. A common branch size of HSS 8×4×½ was used, oriented such that $\beta = B_b/B = 1.0$ and $\eta = (H_b/\sin\theta)/B = 0.5$. The branch thickness was selected to be greater than that of the chord to be certain that local branch yielding would not occur before the chord webs failed. Measured geometric properties are given in Tables 2 and 3. Mechanical properties of the two chord members were determined by tensile tests on coupons cut from the flat regions where there was no weld seam. Average measured values (using three coupons from each HSS) are shown in Table 4.

In both connection tests, sidewall buckling was the observed failure mode, and the maximum load, P_a, was achieved prior to the 3%B connection ultimate deformation

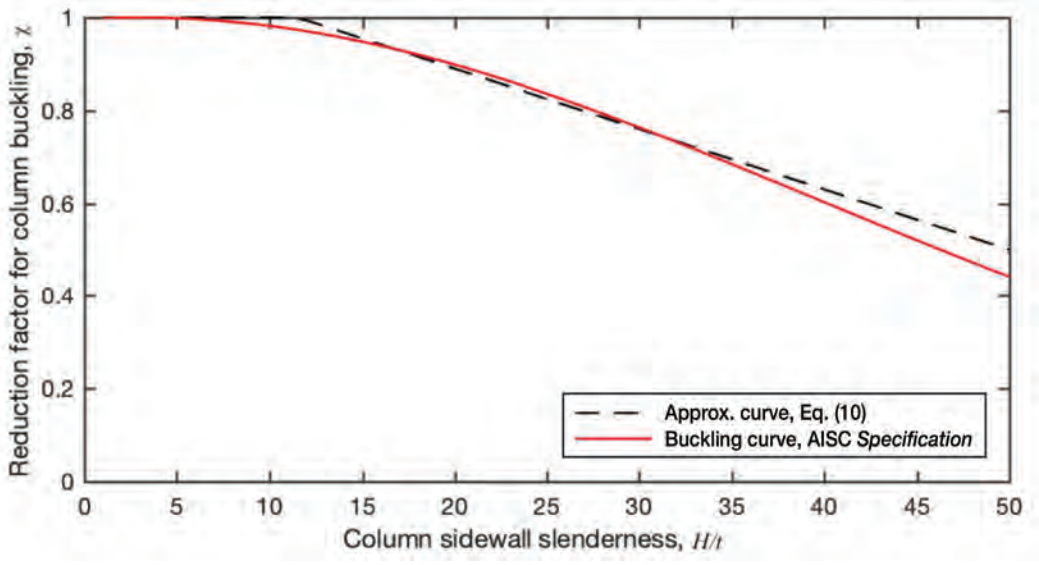

Fig. 3. AISC Specification *column buckling curve and the linear approximation of Equation 10, for* $F_y = 50$ *ksi.*

Table 2. Test Specimens and Measured Geometric Variables						
Specimen	Width Ratio β	Chord Slenderness Ratio $2\gamma = B/t$	Wall-Thickness Ratio $\tau = t_b/t$	Chord Length (in.)	Branch Length (in.)	Fillet Weld Size (leg) (in.)
X1	1.0	34.7	2.17	41.4	20.0	0.25
X2	1.0	23.6	1.47	38.1	20.0	0.22

Table 3. Average Measured Rectangular HSS Cross-Sectional Dimensions					
Designation	Width B (in.)	Height H (in.)	Wall Thickness t (in.)	Corner Radius	
				Outer (in.)	Inner (in.)
HSS 8×8×¼	7.98	7.98	0.23	0.59	0.36
HSS 8×8×⅜	8.03	8.03	0.34	0.94	0.60
HSS 8×4×½	8.02	4.02	0.50	1.01	0.51

Table 4. Average Measured Rectangular HSS Chord Material Properties						
Designation	E (ksi)	F_y (ksi)	ε_y	F_u (ksi)	ε_{rup}	F_y/F_u
HSS 8×8×¼	30,180	57.1	0.0039	70.3	0.308	0.81
HSS 8×8×⅜	28,630	56.9	0.0040	71.6	0.334	0.79

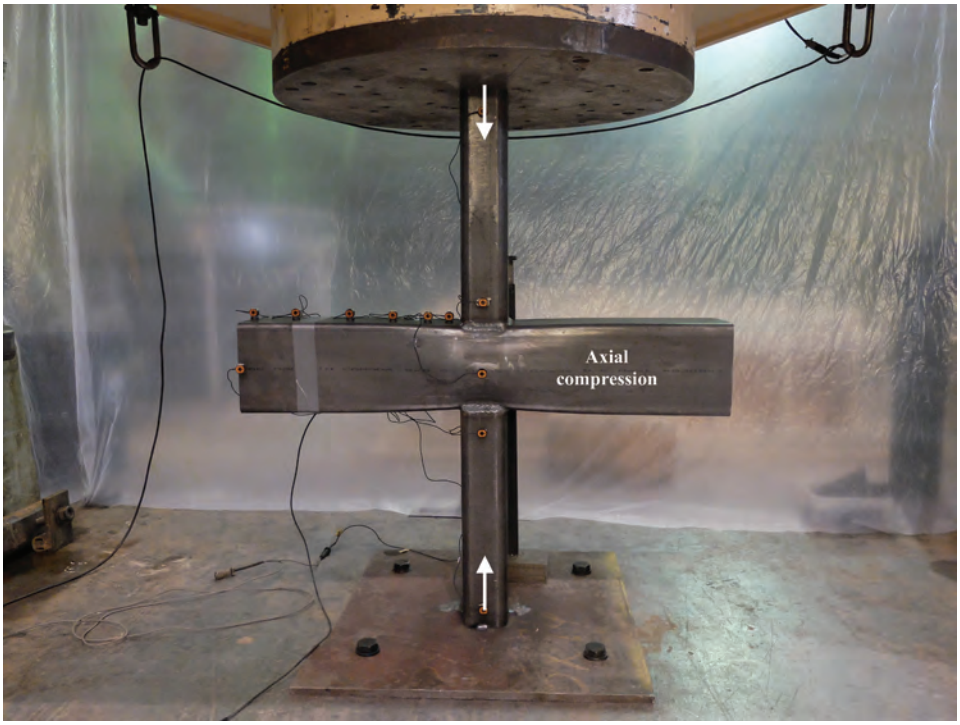

Fig. 4. Testing arrangement for rectangular HSS cross-connections, with failure by web buckling.

Table 5. Actual versus Predicted Ultimate Strengths and Failure Modes for Tests X1 and X2						
	Actual		Predicted			
Test No.	Ultimate Strength (kips)	Observed Failure Mode	Web Local Yielding Eq. (1)	Web Local Crippling Eq. (3)	Web Compression Buckling Eq. (6)	Web Compression Buckling Eqs. (10) and (14)
X1	**128**	Sidewall buckling	150.9	279.0	**105.2**	105.5
X2	**244**	Sidewall buckling	**254.2**	590.6	343.5	214.3

limit state (Lu et al., 1994). Thus, the connection ultimate strength was given by P_a, as shown on the load-displacement curves in Figure 5. To obtain the load-displacement curves in Figure 5, connection displacement was determined from the global vertical displacement of the difference between light-emitting-diode (LED) targets placed slightly above the chord face and the targets positioned at the centroid of the chord, and the branch compression load was provided by the testing machine's load cell. Table 5 compares the predicted ultimate strength and predicted failure mode, by the three limit states, with the observed strength and failure mode. For test X1, the capacity is reasonably predicted for the correct failure mode. For test X2, the capacity is reasonably predicted but for an incorrect failure mode. Both of these connections had a bearing length-to-chord height ratio of 0.50, but different H/t ratios (34.7 and 23.6). These results indicate that a wider review of these limit states—as applied to HSS connections—is warranted.

EVALUATION OF HSS WEB COMPRESSION LIMIT STATES

Although early design provisions have been evaluated (Packer, 1984, 1987), it is timely to apply the current 2016 AISC *Specification* rules to an expanded contemporary database of HSS experiments. Thus, aside from the two laboratory tests described, an additional 76 cross-connection tests from the literature were collated. This total database consists of 44 tests performed at the University of Toronto, 29 in the United Kingdom, and 5 in Spain. Pertinent data for all 78 tests is tabulated in Appendix G of Wei (2019). The group of 78 tests covers chord sidewall slenderness ratios (H/t) from 12.6 to 56.9; bearing lengths ranging from $0.07H$ to $3.72H$; chord compressive stress up to 86% of chord yield stress; branch angles of 45°, 60°, and 90°; and three HSS production processes: cold-formed, cold-formed stress-relieved, and hot-formed. Measured geometric and

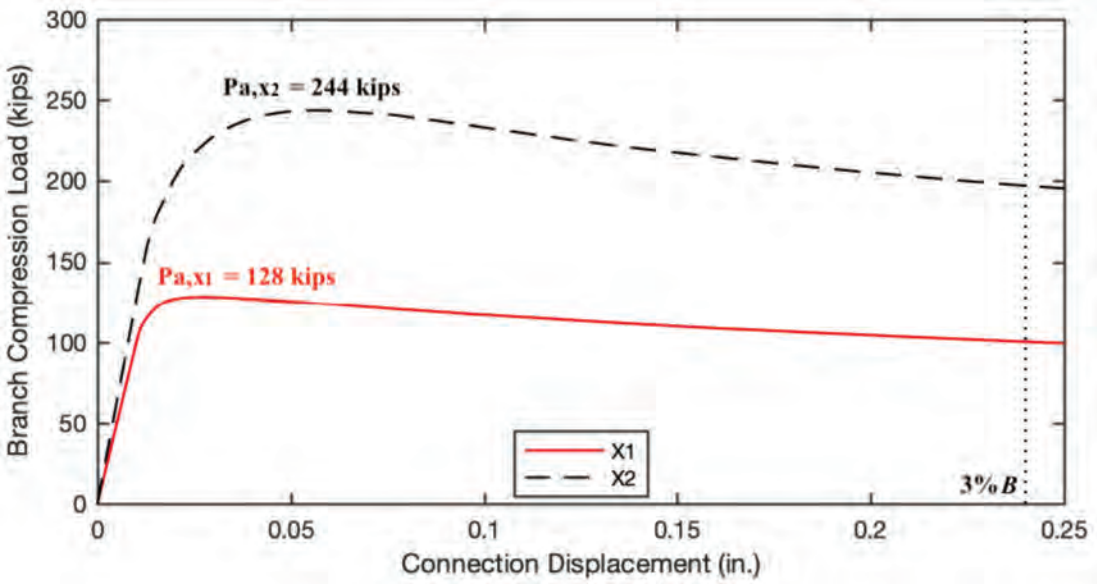

Fig. 5. Connection load-displacement curves for tests X1 and X2.

mechanical properties of the test specimens were used. Based on the configuration of individual connection tests, the database has been further divided into two categories: welded rectangular HSS to rectangular HSS connections and welded plate to rectangular HSS connections.

Welded Rectangular HSS to Rectangular HSS Connections

In this section, an evaluation is made of the current design provisions against 53 welded rectangular HSS to rectangular HSS cross-connections. When the bearing length of the load, $H_b/\sin\theta$, is less than or equal to the total depth of the chord member, H, the three web compression limit states (local yielding of the chord sidewalls, local crippling of the chord sidewalls, and buckling of the chord sidewalls) are represented by Equation 1, Equation 3, and Equation 6 respectively, as discussed earlier.

The correlation between actual experimental test results and predicted connection strengths is shown in Figure 6. Ultimate strengths P_n and P_a are used in the correlation plots, where P_n represents the connection theoretical capacity calculated from the limit states and P_a represents the actual experimental test results recorded by the researchers, both expressed as a force in the branch. Although the mean of this ratio is 1.37, the scatter is huge (COV = 0.45). A number of tests are overestimated, while some tests are significantly underestimated by the limit state of chord sidewall buckling. The large variability shown by chord sidewall buckling predictions indicates that the interior web compression buckling equation, Equation 6—when applied to rectangular HSS-to-HSS connections—is generally a poor predictor of the strength for this limit state. As noted earlier, Equation 6 originates from point-load tests on wide-flange section webs. In addition, none of the connection tests is governed by local crippling of the chord sidewalls, represented by Equation 3, indicating that this is not a viable failure mode over this range of data.

When the bearing length of the load is greater than the total depth of the chord member, each chord sidewall needs to be designed as a column with a slenderness ratio of KL/r. As discussed earlier, instead of using Equation 6, the nominal flexural buckling strength can be calculated using AISC *Specification* Section E3:

$$P_n = F_{cr} A_g \tag{11}$$

and the "column" cross-sectional area of one web can be calculated as:

$$A_g = \left(7.5t + \frac{H_b}{\sin\theta}\right) t \tag{12}$$

AISC *Specification* Section E3 applies the full gross cross-sectional area, A_g, to compression members with nonslender elements, as defined in Section B4.1; however, none of the cases included in Table B4.1a of the *Specification* directly correspond to a laterally compressed rectangular HSS sidewall. Hence, the full gross cross-sectional area, A_g, is always used in the sidewall buckling equation. The critical stress, F_{cr}, is determined based on the slenderness ratio of KL/r. The *Specification* and Commentary do not clearly state which value of the effective length factor, K, to use, and designers could adopt $K = 1.0$ to be conservative. Because $F_{cr} \le F_y$, the limit state of local yielding of the chord sidewalls is thus incorporated into the nominal flexural buckling strength by:

$$P_n = \frac{2F_{cr}t}{\sin\theta}\left(7.5t + \frac{H_b}{\sin\theta}\right) Q_f \tag{13}$$

where Q_f is a reduction factor to account for the effect of normal stress in the chord. All 16 connection tests with bearing length of the load greater than the total depth of the chord member were governed by the limit state of flexural buckling of the chord sidewalls, represented by Equation 13, and the correlation between actual experimental test results and predicted connection strengths, using $K = 1.0$, is shown in Figure 7.

With the two bearing length situations combined, correlation between the entire group of 53 welded rectangular HSS-to-HSS cross-connection tests is plotted in Figure 8. The mean ratio of actual/predicted capacity is 1.41 with a very large scatter (COV of 0.46). When the bearing length of the load is greater than the total depth of the chord member, web buckling failure predictions given by Equation 13 using $K = 1.0$ are conservative for a considerable number of the test results. In this case, 1 out of 53 tests had a ratio of actual/predicted capacity greater than 2.6, which did not fit into Figure 8(a). This correlation suggests that the end fixity of the sidewall "column" is more likely to be fixed-fixed rather than pin-ended for a chord member with branches welded to either side, which seems logical considering the large flare bevel groove welds at either end of the chord member web. This implies that the effective length factor, K, can better be taken as 0.65 instead of 1.0.

For these 53 welded rectangular HSS-to-HSS cross-connections, 42 of them have the failure mode recorded (although there may be misinterpretations of the initial failure mode by some researchers). Nine of the 42 connections had the failure mode incorrectly predicted when compared against the observed actual test failure mode (Wei, 2019). All nine of these incorrect predictions were a result of high predicted sidewall buckling strength.

Welded Plate to Rectangular HSS Connections

Unlike the welded rectangular HSS-to-HSS cross-connection tests, the load bearing length of all 25 welded plate to rectangular HSS cross-connection tests is less than the total

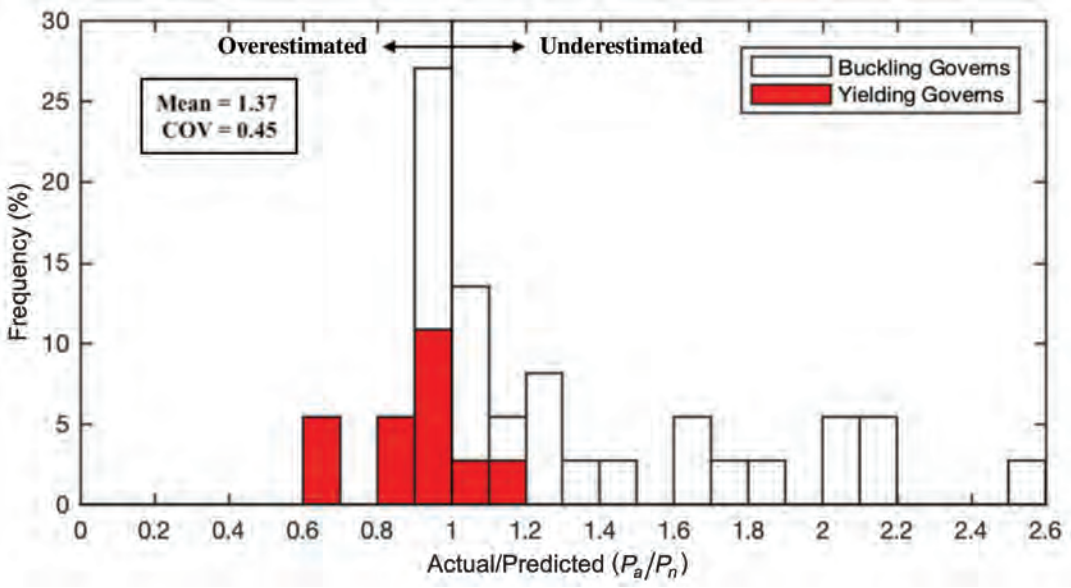

(a)

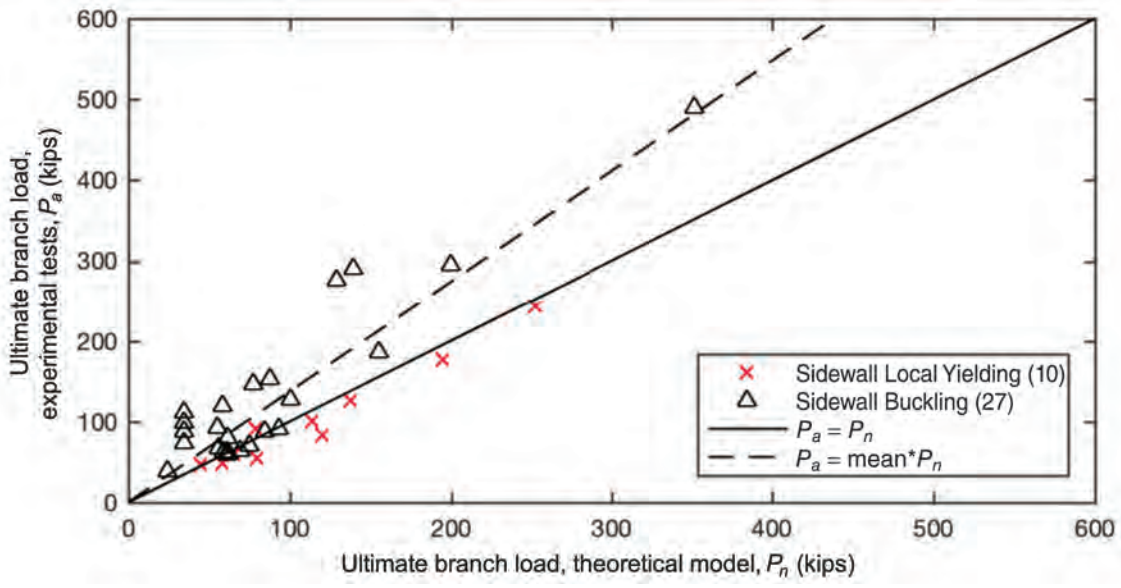

(b)

Fig. 6. Correlation between 37 welded rectangular HSS to rectangular HSS connection tests with bearing length ≤ H *and the 2016 AISC* Specification.

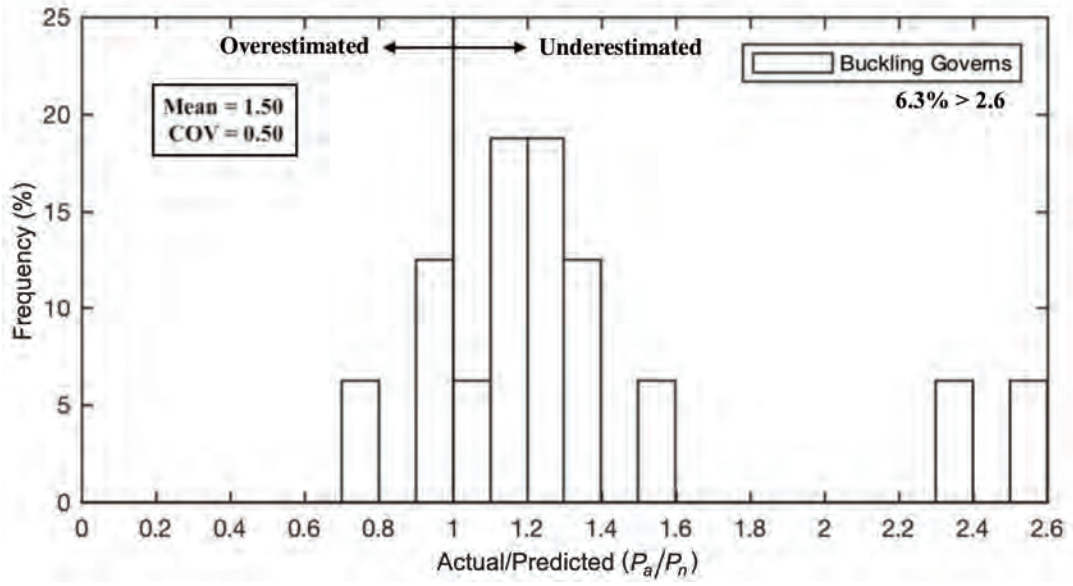

(a)

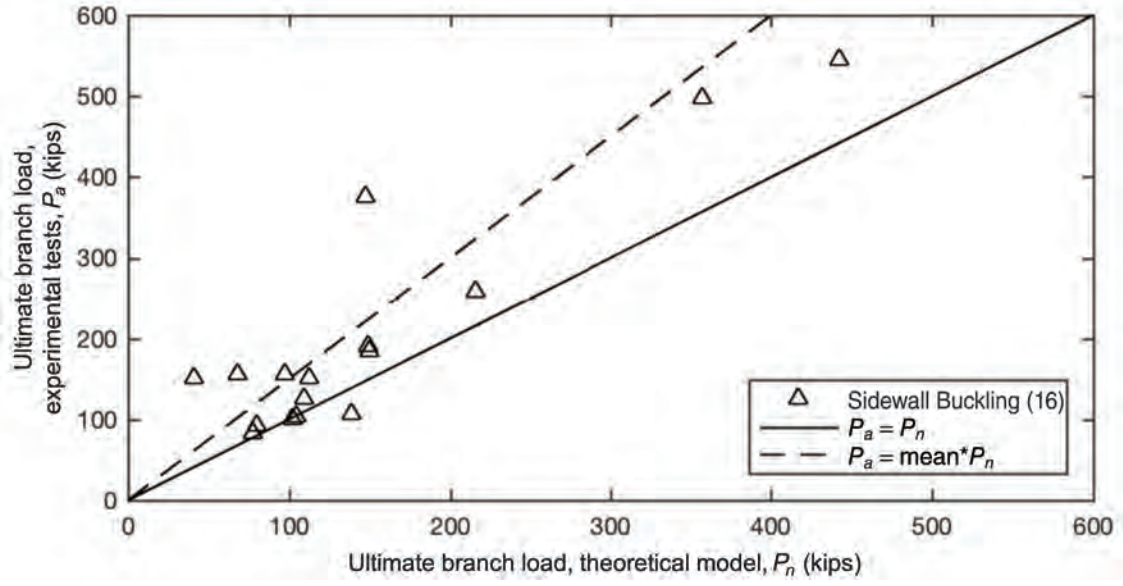

(b)

Fig. 7. Correlation between 16 welded rectangular HSS to rectangular HSS connection tests with bearing length > H *and 2016 AISC* Specification*, using* K = *1.0.*

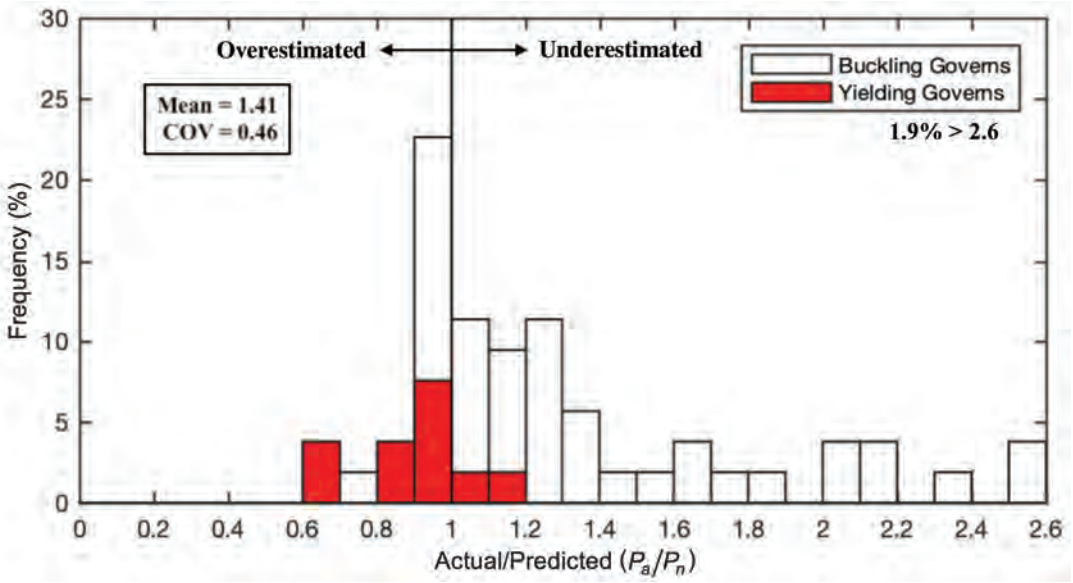

(a)

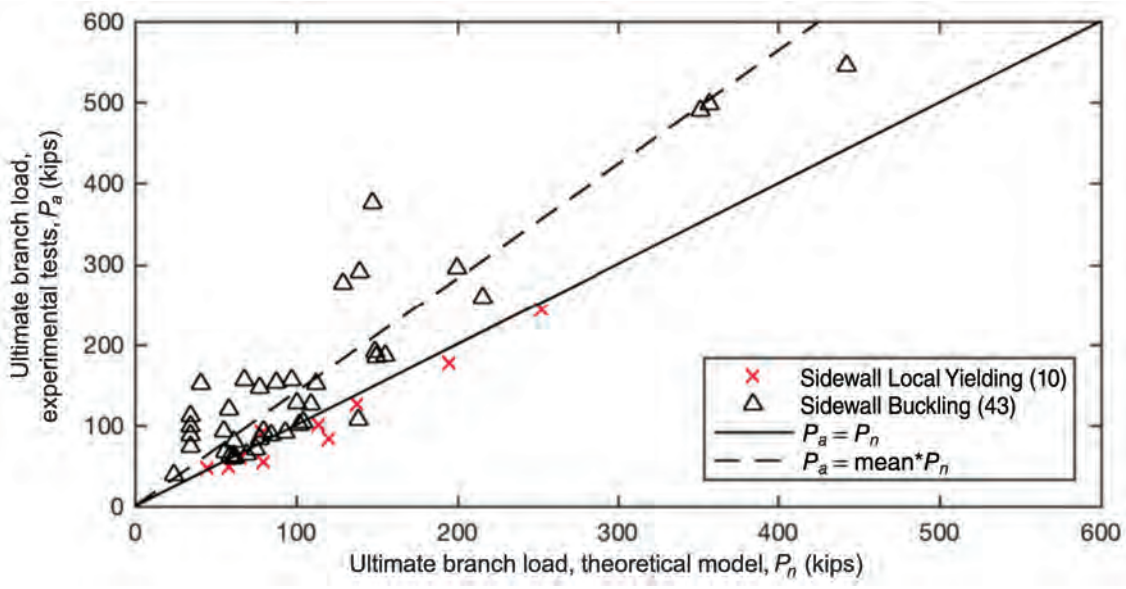

(b)

Fig. 8. Correlation between 53 welded rectangular HSS to rectangular HSS connection tests and the AISC Specification.

depth of the chord member. Thus, the web compression limit states are represented by Equation 1, Equation 3, and Equation 6. In this category, the web local yielding limit state governed the predicted strength of all cases, with only one exception. The actual-to-predicted strength distribution, shown in Figure 9(a), is much better compared to that of welded rectangular HSS-to-HSS connection tests. The mean is slightly greater than unity (1.15) with a relatively low spread of data, indicated by a COV of 0.18. Figure 9(b) shows a somewhat more conservative correlation by taking the predicted branch capacity as simply the vertical force component. These plots indicate the excellent applicability of the existing web local yielding model to HSS webs.

In Figure 9, the one test for which buckling governed had $H_b/H = 0.20$ and $H/t = 57$. Because $H_b/H < 0.25$, the breakpoint between web yielding and web buckling established by Kuhn et al. (2019), one might expect web yielding to govern. However, the 0.25 value was determined on the basis of numerical research on HSS up to $H/t = 50$ (Kuhn et al., 2019), so there may be less reliability in this breakpoint at $H/t > 50$. Nevertheless, in Figure 9 the actual strength far exceeds the predicted strength for this test and is conservative.

ALTERNATE MODELS

From the evaluation of existing test results for full-width, welded rectangular HSS cross-connections, it was shown that the 2016 AISC *Specification* web crippling equation and the web buckling equation, which are based on specific tests on I-section webs, either never govern or result in a large scatter in the predicted strengths when applied to the chord sidewall of rectangular HSS. One of the most influential parameters, bearing length $H_b/\sin\theta$, is absent from the web buckling equation. Even for connections where the strength prediction is governed by a sidewall flexural buckling equation, represented by Equation 13, the assumption of pinned-pinned end fixity ($K = 1.0$) leads to generally conservative estimates. Hence, the web compression limit states for rectangular HSS connections could be modified to one of the following.

Model 1

According to a recent numerical study by Kuhn et al. (2019), a failure mode transition from web local yielding to web buckling was observed at a critical bearing length $(H_b/\sin\theta) = 0.25H$. For bearing lengths greater than $0.25H$, the sidewall compression strength was well-predicted using the column flexural buckling approach, over a practical H/t range associated with manufactured HSS. Thus, the first proposed modification is to require HSS sidewalls to be considered as columns (and analyzed using AISC *Specification* Section E3) for bearing lengths greater than $0.25H$ [rather than the current $1.0H$, as indicated below Equation 6 in Table 1]. With this modification, the capacity of 37 welded rectangular HSS-to-HSS connections with bearing length ($H_b/\sin\theta$) ranging from $0.25H$ to H, which are originally estimated as per Table 1, can now be predicted by Equation 13. A second proposed modification is to adopt an effective length factor of $K = 0.65$ instead of 1.0. Combined with the other 16 tests, the correlation between actual experimental test results and predicted connection strengths using Equation 13 is presented in Figure 10(a) to evaluate the effectiveness of these modifications.

A clear improvement can be observed by a comparison of Figure 10(a) with Figure 8(a). Although the COV of 0.27 is still not low, it is significantly reduced from the value of 0.46 obtained previously, which indicates that the sidewall flexural buckling equation, Equation 13, is a better strength predictor of connections with bearing length $(H_b/\sin\theta) > 0.25H$ when compared to web buckling Equation 6. Moreover, for connections with inclined branches (i.e., when $\theta < 90°$), there is a trend for the connection strengths to be overpredicted. Packer (1984) has already noted that the connection strength increase (measured as a force in the branch) is less than associated with $1/\sin\theta$. The effect of branch member inclination requires more study but, in the meantime, if one takes the predicted branch capacity as simply the vertical force component, the more-conservative correlation shown in Figure 10(b) is the result. In Figure 10, the connection capacity prediction is based on a column-buckling model, which incorporates both sidewall local yielding (squashing) and flexural buckling; hence, no legend (buckling governs/yielding governs) is given in this figure.

A simple reliability analysis (Fisher et al., 1978; Ravindra and Galambos, 1978) can be applied to the statistics (or model parameters) in Figure 10(b) in which a resistance factor, ϕ, is calculated using a target safety/reliability index of 3.0 and a coefficient of separation of 0.55. Furthermore, one can introduce statistical parameters to model geometric variations [as recommended by AISI (2016)] and typical material strength variations for ASTM A500 Grade B/C yield strength [as determined by Liu (2016)], the result of which is $\phi = 0.95$. Because a value of $\phi_c = 0.90$ is used in AISC *Specification* Section E1, which is lower, adequate safety/reliability is provided by Model 1 for welded rectangular HSS-to-HSS cross-connections.

For connections with a bearing length $(H_b/\sin\theta) \le 0.25H$ (all 25 welded plate to rectangular HSS connections), the capacity can be predicted by Equation 1 alone since the web local yielding limit state governed the predicted strength of all 25 cases, with only one exception. Applying this single limit state check to connections in this bearing length range leads to a mean value of 1.14 and a COV of 0.17, which are almost identical to what was obtained in Figure 9(a). If one takes the predicted branch capacity as simply the vertical

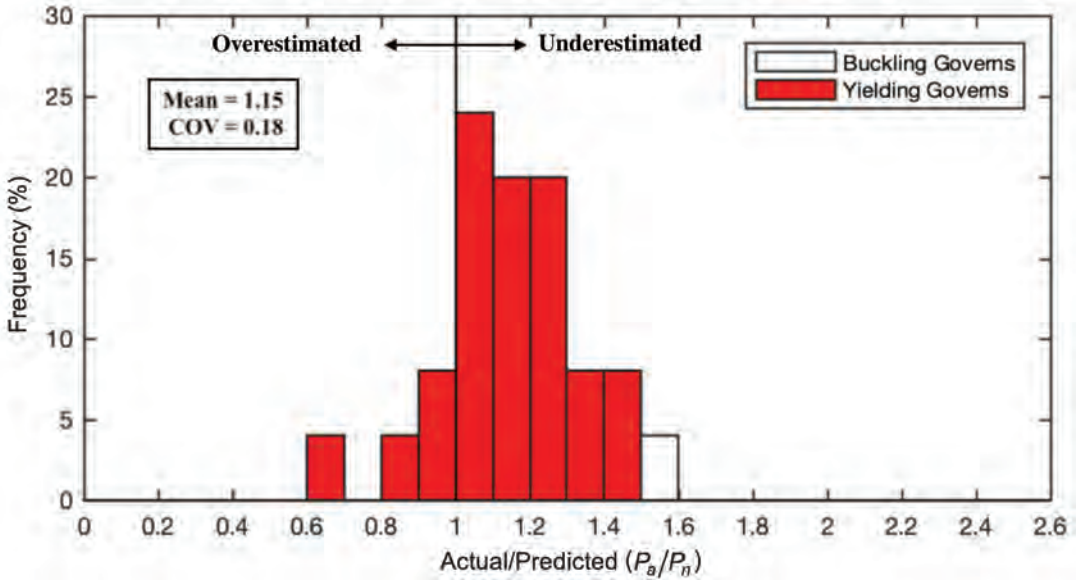

(a) Using Equation 1

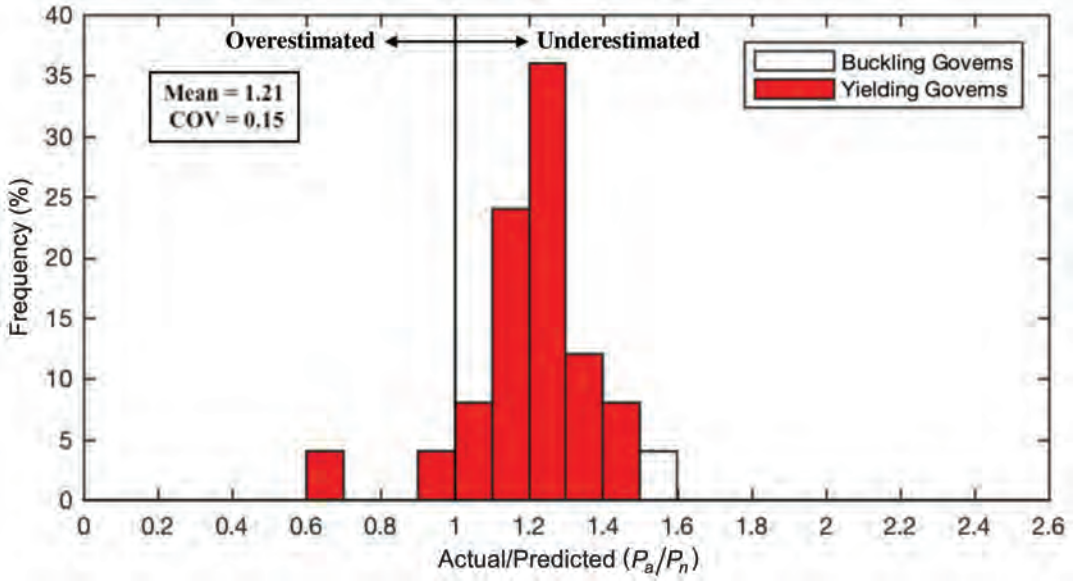

*(b) Using Equation 1 but deleting the first sin*θ *term (below* $2F_yt$*)*

Fig. 9. Correlation between 25 welded plate to rectangular HSS connection test and the 2016 AISC Specification.

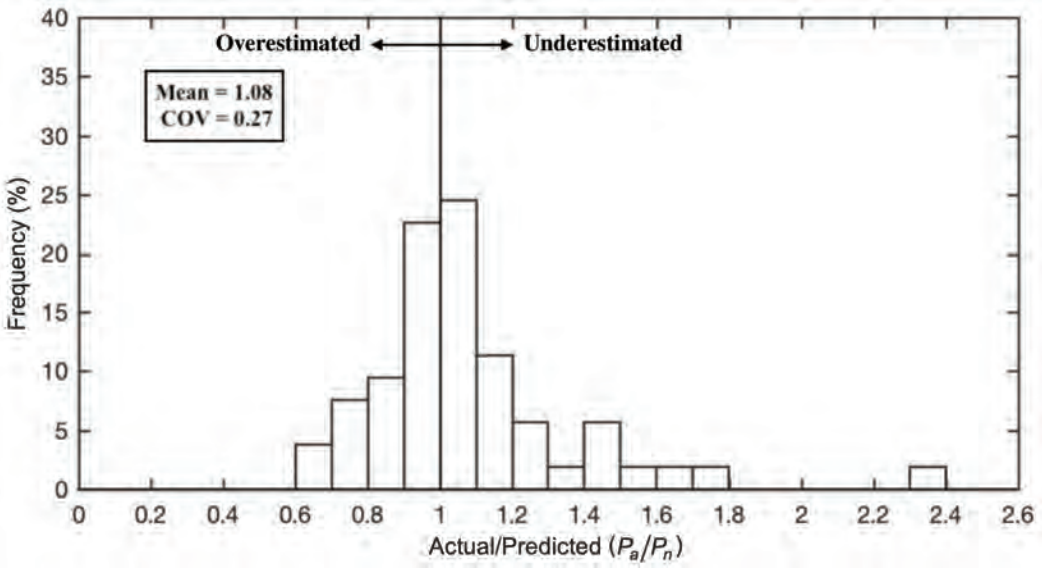

(a) Using Equation 13

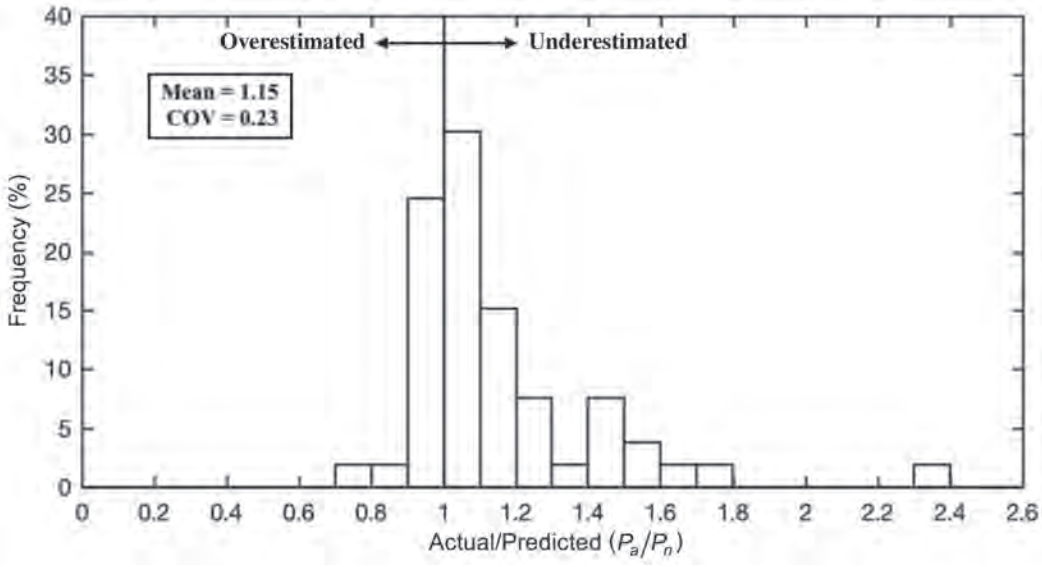

*(b) Using Equation 13 but deleting the first sin*θ *term (below* $2F_{cr}t$*)*

Fig. 10. Correlation between 53 welded rectangular HSS to rectangular HSS connection tests and Equation 13 with K = *0.65.*

force component a mean value of 1.19 and a COV of 0.15 result, which are almost identical to what was obtained in Figure 9(b). Performing the same reliability analysis as described above, but with model parameters of mean = 1.19 and COV = 0.15, one obtains $\phi = 1.09$. Because a value of $\phi = 1.00$ is used in AISC *Specification* Section J10.2, which is lower, adequate safety/reliability is provided by Model 1 for welded plate to rectangular HSS connections.

To design a full-width welded rectangular HSS-to-HSS cross-connection, the AISC *Specification* requires designers to check three web compression limit states: local yielding of the chord sidewalls, local crippling of the chord sidewalls, and buckling of the chord sidewalls. With this method, the predicted connection capacity can be based on either Equation 1 or Equation 13 with $K = 0.65$, depending on the connection bearing length. A recommended adjustment to these equations, for inclined branches with $\theta < 90°$, is to take the predicted branch capacity as the branch force vertical component. Maintaining the checks for all three limit states, but using the preceding recommendations, will still result in reliable predictions of connection capacity for the limit state that governs.

Model 2

Another simplified method to the foregoing is also possible. As discussed previously, Kuhn et al. (2019) advocated the use of Equation 10 for a reduction factor to be applied to yield stress for column buckling, χ, as it was noticed that most steel codes have a cold-formed column buckling curve that is almost linear when plotted over a practical chord sidewall slenderness range ($H/t \leq 50$) for fixed-fixed end conditions. The AISC *Specification* buckling curve is no exception, as presented in Figure 3. Thus, to simplify the process of calculation, the critical stress, F_{cr}, can be replaced by χF_y to give a sidewall compression strength of:

$$P_n = \frac{2\chi F_y t}{\sin\theta}\left(7.5t + \frac{H_b}{\sin\theta}\right)Q_f \tag{14}$$

Of the 53 tests, 47 lie within the chord sidewall slenderness range of $H/t \leq 50$. The correlation between actual experimental test results and predicted connection strengths using Equation 14 is shown in Figure 11(a) and, as expected, a similar relationship to Model 1 is obtained. The numerical research of Kuhn et al. (2019) was based only on 90° connections, so it would be logical to again investigate (as in Model 1) the correlation with experiments by taking the predicted branch capacity as simply the vertical force component. This results in the excellent correlation shown in Figure 11(b). In Figure 11, the connection capacity prediction is based on a single limit state model; hence, no legend (buckling governs/yielding governs) is given in this figure.

For welded plate to rectangular HSS connections or welded rectangular HSS-to-HSS connections with bearing length $(H_b/\sin\theta) \leq 0.25H$, it is recommended for Model 2 that the buckling reduction factor, χ, be taken as 1.0. As connections within this range are very likely governed by sidewall local yielding, the correlation is again very similar to that shown in Figure 9.

CONCLUSIONS

AISC *Specification* Section J10 (AISC, 2016) provisions for concentrated compression forces on webs have been applied to the case of transversely compressed rectangular HSS members. These provisions have then been evaluated against 78 laboratory tests, taking the form of welded interior plate-to-HSS cross-connections and welded interior HSS-to-HSS cross-connections. The web local yielding limit state, represented by Equation 1 in Table 1, has been found to be very applicable to HSS. The web local crippling limit state, represented by Equation 3 in Table 1, has been found to never govern for the range of HSS examined (specified yield strengths up to 50 ksi and sidewall slenderness values up to 57). It has been shown that, for the web compression buckling limit state, represented by Equation 6 in Table 1, greater prediction accuracy can be obtained if a column buckling model is used when bearing lengths are greater than 0.25 of the chord depth. It is thus recommended (as a modification to AISC *Specification* Section J10.5 Commentary) that the HSS member web be designed as a compression member, in accordance with AISC *Specification* Chapter E, when l_b or $(H_b/\sin\theta) > 0.25H$. Moreover, when doing so, the compression member (each web) can be taken to have a cross-sectional area given by Equation 12 and an effective length factor of $K = 0.65$. The influence of branch member inclination on connection capacity is not conclusive, so it is recommended that—in the case of inclined branches with $\theta < 90°$—one conservatively takes the predicted branch capacity, for all failure modes, as simply the vertical force component. Table 6, which can be compared to Table 1, provides a summary of the foregoing recommendations, applied to interior HSS connections. The limit state of web local crippling should be redundant for normal HSS sizes, but it is included in Table 6 for completeness and also in the design example that follows.

This review has studied connections that were not prone to out-of-plane stability. This will be the usual case when an HSS main member is subject to transverse compression because lateral restraint is generally provided (e.g., at reaction or load points of trusses and beam-to-column moment connections). It is conceivable that lateral instability of the chord member could arise with a lack of symmetry due to misalignment or with long compression-loaded branch members; in such cases, this should be incorporated in modeling structural behavior of the system.

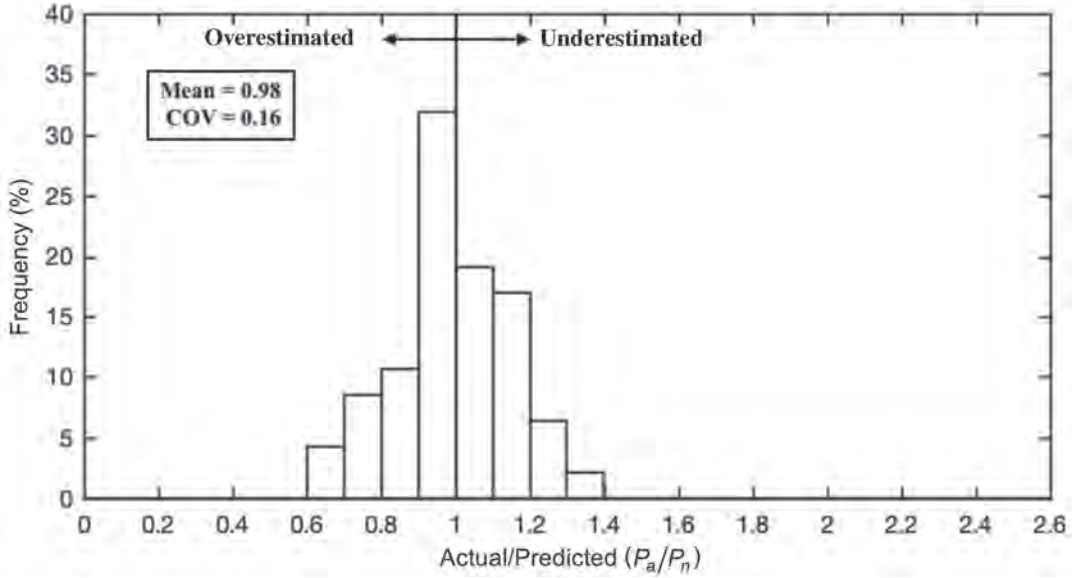

(a) Using Equation 14

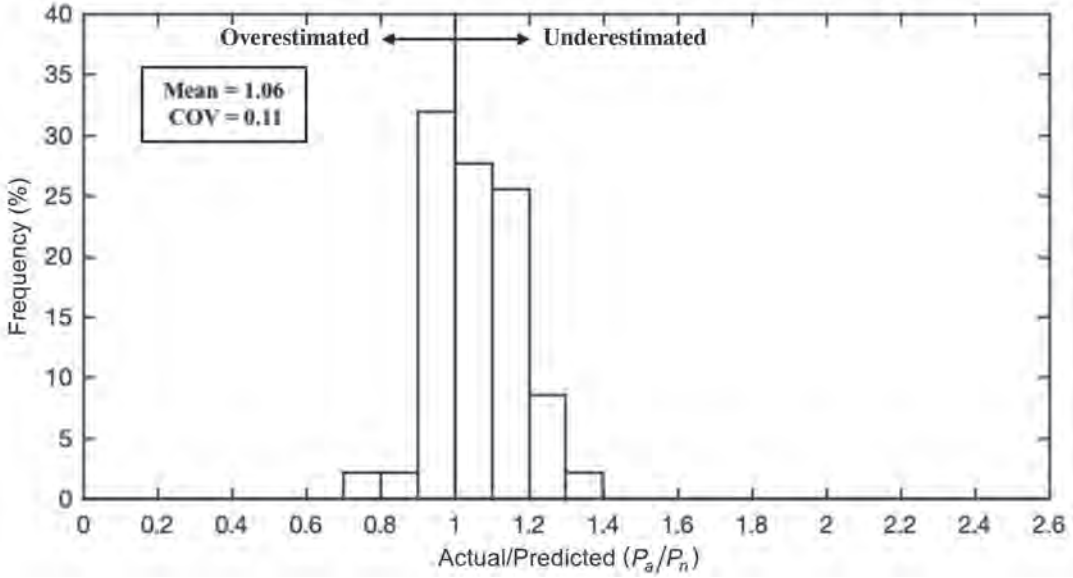

(b) Using Equation 14 but deleting the first sinθ *term (below* $2\chi F_y t$*)*

Fig. 11. Correlation between 47 welded rectangular HSS to rectangular HSS connection tests and Equation 14, with $H/t \leq 50$.

Table 6. Recommended Nominal (and Available) Strengths of Web Compression Limit States for Rectangular HSS Connections		
Limit State	**HSS-to-HSS Connection, P_n (kips)**	**ϕ (Ω)**
Web local yielding, interior	for $l_{end} > H$ $2F_y t\left(7.5t + \frac{H_b}{\sin}\right)$ (15)	1.00 (1.50)
Web local crippling, interior	for $l_{end} \geq H/2$ $\frac{1.6t^2}{\sin\theta}\left(1+\frac{\frac{3H_b}{\sin\theta}}{H}\right)\sqrt{EF_y}Q_f$ (16)	0.75 (2.00)
Web compression buckling, interior, and $l_b \leq 0.25H$	for $l_{end} \geq H/2$ and $H_b/H\sin\theta \leq 0.25$ $\left(\frac{48t^3}{H-3t}\right)\sqrt{EF_y}Q_f$ (17)	0.90 (1.67)
Web compression buckling, interior, and $l_b > 0.25H$	for $l_{end} \geq H/2$ and $H_b/H\sin\theta > 0.25$ Use AISC *Specification* Equations E3-1, E3-2, and E3-3 with $K = 0.65$, L_c/r from Equation 8, and A_g (for each sidewall) from Equation 12	0.90 (1.67)

DESIGN EXAMPLE

Given:

Determine the adequacy of the welded rectangular HSS-to-HSS 90° cross-connection shown in Figure 12 subjected to the loads indicated. The branch members are oriented such that the chord is loaded across its full width, and the loads shown consist of 50% dead load and 50% live load. Assume the welds are noncritical and that there is zero force in the chord member.

From AISC *Manual* (AISC, 2017) Table 2-4, the material properties are as follows:

All members
ASTM A500 Grade C
F_y, $F_{yb} = 50$ ksi
F_u, $F_{ub} = 62$ ksi

From AISC *Manual* Table 1-11 and Table 1-12, the HSS geometric properties are as follows:

HSS 8×8×⅜
$A = 10.4$ in.^{2}
$B = 8.00$ in.
$H = 8.00$ in.
$t = 0.349$ in.

HSS 8×4×½
$A_b = 9.74$ in.^{2}
$B_b = 8.00$ in.
$H_b = 4.00$ in.
$t_b = 0.465$ in.

Solution:

Required strength (expressed as a force in the branch)

From ASCE/SEI 7 (ASCE, 2016) Chapter 2, the required strength of the connection is:

LRFD	ASD
P_u = 1.2 (50.0 kips) + 1.6 (50.0 kips) = 140 kips	P_a = 50.0 kips + 50.0 kips = 100 kips

The strength of a matched-width ($\beta = 1.0$), welded, rectangular HSS to rectangular HSS cross-connection, under branch axial compression, can be determined from the limit states of web local yielding, web local crippling, and web compression buckling.

$$\beta = \frac{8.00 \text{ in.}}{8.00 \text{ in.}} = 1.00$$

Limit State of Web Local Yielding

From Equation 15 in Table 6,

$$P_n = 2F_y t\left(7.5t + \frac{H_b}{\sin\theta}\right) \tag{15}$$

$$= 2(50 \text{ ksi})(0.349 \text{ in.})\left[7.5(0.349 \text{ in.}) + \frac{4.00 \text{ in.}}{\sin 90°}\right]$$

$$= 231 \text{ kips}$$

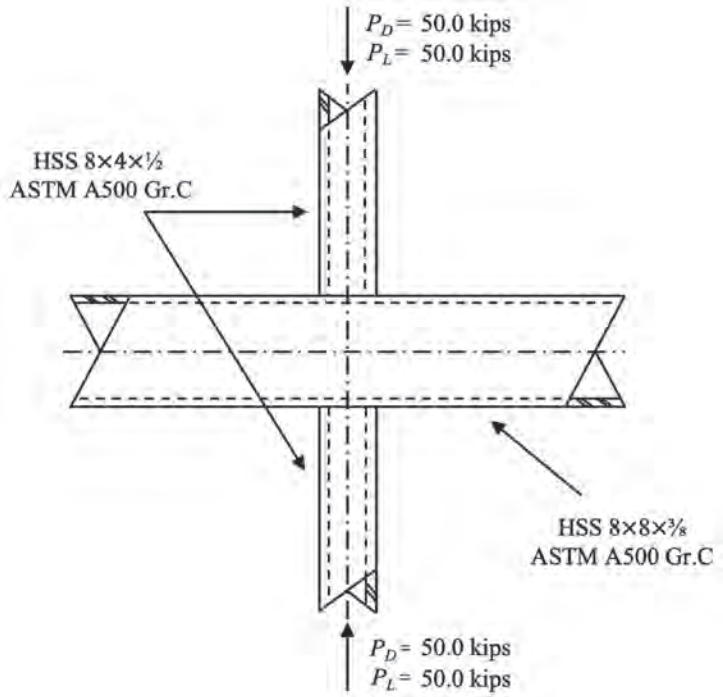

Fig. 12. Rectangular HSS-to-HSS cross-connection subjected to branch axial compression.

By applying the resistance factor of $\phi = 1.00$, and the safety factor of $\Omega = 1.50$, for this limit state (AISC *Specification* Section J10.2), the available strength (ϕP_n or P_n/Ω) is:

LRFD	ASD
$\phi P_n = 1.0(231 \text{ kips})$ $= 231 \text{ kips}$ $231 \text{ kips} > 140 \text{ kips}$ **o.k.**	$\frac{P_n}{\Omega} = \frac{231 \text{ kips}}{1.50}$ $= 154 \text{ kips}$ $154 \text{ kips} > 100 \text{ kips}$ **o.k.**

Limit State of Web Local Crippling

From Equation 16 in Table 6,

$$P_n = 1.6t^2\left(1+\frac{\frac{3H_b}{\sin\theta}}{H}\right)\sqrt{EF_y}Q_f \tag{16}$$

$Q_f = 1.0$ for a chord with no load, or a tension force, in accordance with AISC *Specification* Table K3.2.

$$P_n = 1.6(0.349 \text{ in.})^2\left[1+\frac{\frac{3(4.00 \text{ in.})}{\sin 90^\circ}}{8.00 \text{ in.}}\right]\sqrt{(29{,}000 \text{ ksi})(50 \text{ ksi})}(1.0)$$

$$= 587 \text{ kips}$$

By applying the resistance factor of $\phi = 0.75$, and the safety factor of $\Omega = 2.00$, for this limit state (AISC *Specification* Section J10.3), the available strength is:

LRFD	ASD
$\phi P_n = 0.75(587 \text{ kips})$ $= 440 \text{ kips}$ $440 \text{ kips} > 140 \text{ kips}$ **o.k.**	$\frac{P_n}{\Omega} = \frac{587 \text{ kips}}{2.00}$ $= 294 \text{ kips}$ $294 \text{ kips} > 100 \text{ kips}$ **o.k.**

Limit State of Web Compression Buckling

$H_b/\sin\theta = 4.00 \text{ in.} > 0.25H = 0.25(8.00 \text{ in.}) = 2.00 \text{ in.}$

Hence, from Table 6, the member webs will be designed as compression members in accordance with AISC *Specification* Chapter E, using $K = 0.65$.

Critical Buckling Stress, F_{cr}

Calculate the effective slenderness ratio (L_c/r) using Equation 8, with $K = 0.65$, to determine applicable equation:

$$\frac{KL}{r} = \frac{L_c}{r} = 3.46K\left(\frac{H}{t}-3\right)\sqrt{\frac{1}{\sin\theta}} \tag{8}$$

$$= 3.46(0.65)\left(\frac{8.00 \text{ in.}}{0.349 \text{ in.}}-3\right)\sqrt{\frac{1}{\sin 90^\circ}}$$

$$= 44.8$$

$$4.71\sqrt{\frac{E}{F_y}} = 4.71\sqrt{\frac{29{,}000 \text{ ksi}}{50 \text{ ksi}}}$$
$$= 113.4$$

Because $\frac{KL}{r} < 4.71\sqrt{\frac{E}{F_y}}$, AISC *Specification* Equation E3-2 applies:

$$F_{cr} = \left(0.658^{\frac{F_y}{F_e}}\right)F_y \qquad \text{(Spec. Eq. E3-2)}$$

where

$$F_e = \frac{\pi^2 E}{\left(\frac{L_c}{r}\right)^2}$$
$$= \frac{\pi^2 (29{,}000 \text{ ksi})}{(44.8)^2}$$
$$= 143 \text{ ksi}$$

Hence,

$$F_{cr} = \left(0.658^{\frac{50 \text{ ksi}}{143 \text{ ksi}}}\right)(50 \text{ ksi})$$
$$= 43.2 \text{ ksi}$$

Flexural Buckling of the Chord Sidewalls

The nominal compressive strength of the two sidewalls, by flexural buckling, is given by AISC *Specification* Equation E3-1:

$$P_n = F_{cr}A_g \qquad \text{(Spec. Eq. E3-1)}$$

where A_g for one sidewall is given by Equation 12. For two sidewalls,

$$A_g = 2\left(7.5t + \frac{H_b}{\sin\theta}\right)t \qquad (12)$$
$$= 2\left[7.5(0.349 \text{ in.}) + \frac{4.00 \text{ in.}}{\sin 90°}\right](0.349 \text{ in.})$$
$$= 4.61 \text{ in.}^2$$

Therefore, the nominal strength of the two sidewalls in flexural buckling is:

$$P_n = (43.2 \text{ ksi})(4.61 \text{ in.}^2)$$
$$= 199 \text{ kips}$$

By applying the resistance factor of $\phi_c = 0.90$, and the safety factor of $\Omega_c = 1.67$, for this limit state (AISC *Specification* Section E1), the available strength is:

LRFD	ASD
$\phi_c P_n = 0.90\ (199\ \text{kips})$ $= 179\ \text{kips}$ $179\ \text{kips} > 140\ \text{kips}$ **o.k.**	$\frac{P_n}{\Omega_c} = \frac{199\ \text{kips}}{1.67}$ $= 119\ \text{kips}$ $119\ \text{kips} > 100\ \text{kips}$ **o.k.**

As expected, because the bearing length is greater than $0.25H$, the connection resistance by web compression buckling governs. The connection shown in Figure 12 has an identical configuration to Specimen X2, which, as indicated in Table 5, failed by sidewall buckling.

ACKNOWLEDGMENTS

Financial support for this project was provided by the Natural Sciences and Engineering Research Council of Canada (NSERC). Hollow structural sections used for two experiments reported herein were donated by Atlas Tube, Harrow, Ontario.

SYMBOLS

A Cross-sectional area of rectangular HSS chord member, in.^{2}

A_b Cross-sectional area of rectangular HSS branch member, in.^{2}

A_g Cross-sectional area of element, in.^{2}

B Overall width of rectangular HSS chord member, perpendicular to the plane of the connection, in.

B_b Overall width of rectangular HSS branch member or plate, perpendicular to the plane of the connection, in.

COV Coefficient of variation

E Modulus of elasticity of HSS member, ksi

F_{cr} Critical stress of HSS chord member, ksi

F_u Ultimate tensile strength of HSS chord member, ksi

F_{ub} Ultimate tensile strength of branch member, ksi

F_y Yield stress of HSS chord member, ksi

F_{yb} Yield stress of branch member, ksi

F_{yw} Yield stress of web material, ksi

H Overall height of rectangular HSS chord member, perpendicular to the plane of the connection, in.

H_b Overall height of rectangular HSS branch member or plate, perpendicular to the plane of the connection, in.

K Effective length factor

L_c Effective length of member, in.

P Axial force, kips

P_D Axial force due to dead load, kips

P_L Axial force due to live load, kips

P_a Actual connection ultimate load, kips; required axial strength using ASD load combinations, kips

$P_{a,X1}$ Actual connection ultimate load of specimen X1, kips

$P_{a,X2}$ Actual connection ultimate load of specimen X2, kips

P_n Nominal connection strength, kips

P_u Required axial strength in tension or compression, using LRFD load combinations, kips

Q_f Chord-stress interaction parameter

R_n Nominal strength, kips

d Full nominal depth of member, in.

h Clear distance between flanges less the fillet or corner radius, in.

k Distance from outer face of flange to web toe of fillet for I-section, in.; outside corner radius for rectangular HSS section, in.

l_b Bearing length of the load, measured parallel to the axis of the HSS member, in.

l_{end} Distance from the near side of the connecting branch or plate to end of member, in.

t Wall thickness of rectangular HSS chord member, in.

t_b Wall thickness of rectangular HSS branch member, in.

t_f Thickness of flange, in.

t_w Thickness of web, in.

Ω Safety factor

β Ratio of branch width to chord width, perpendicular to the plane of the connection

χ Reduction factor for (column) buckling

ε_{rup} Strain at rupture

ε_y Strain at yield

τ Ratio of branch wall thickness to chord wall thickness

γ Chord slenderness; the ratio of one-half the width to wall thickness for rectangular HSS

η Load length parameter; the ratio of the length of contact of the branch with the chord in the plane of the connection to the chord width

ϕ Resistance factor

θ Acute angle between the branch and chord, degrees

REFERENCES

AISC (2010), ANSI/AISC 360-10, *Specification for Structural Steel Buildings*, American Institute of Steel Construction, Chicago, Ill.

AISC (2016), ANSI/AISC 360-16, *Specification for Structural Steel Buildings*, American Institute of Steel Construction, Chicago, Ill.

AISC (2017), *Steel Construction Manual*, 15th Ed., American Institute of Steel Construction, Chicago, Ill.

AISI (2016), AISI S100-16, *North American Specification for the Design of Cold-Formed Steel Structural Members*, American Iron and Steel Institute, Washington, D.C.

ASCE (2016), *Minimum Design Loads and Associated Criteria for Buildings and Other Structures*, ASCE/SEI 7-16, American Society of Civil Engineers, Reston, Va.

ASTM (2018), ASTM A500/A500M-18, *Standard Specification for Cold-Formed Welded and Seamless Carbon Steel Structural Tubing in Rounds and Shapes*, American Society for Testing and Materials, West Conshohocken, Pa.

CEN (2005), *Eurocode 3: Design of Steel Structures—Part 1-8: Design of Joints*, EN 1993-1-8:2005, European Committee for Standardization, Brussels, Belgium.

CSA (2013), CSA G40.20-13/G40.21-13, *General Requirements for Rolled or Welded Structural Quality Steel/ Structural Quality Steel*, Canadian Standards Association, Toronto, Canada.

Davies, G. and Packer, J.A. (1987), "Analysis of Web Crippling in a Rectangular Hollow Section," *Proceedings of the Institution of Civil Engineers*, Part 2, Vol. 83, pp. 785–798.

Fisher, J.W., Ravindra, M.K., Kulak, G.L., and Galambos, T.V. (1978), "Load and Resistance Factor Design Criteria for Connectors," *Journal of the Structural Division,* ASCE*,* Vol. 104, No. 9, pp. 1,427–1,441.

IIW (2012), *Static Design Procedure for Welded Hollow Section Joints—Recommendations*, 3rd Ed., IIW Doc. XV-1402-12, International Institute of Welding, Paris, France.

ISO (2013), *Static Design Procedure for Welded Hollow Section Joints—Recommendations,* ISO 14346, International Organization for Standardization, Geneva, Switzerland.

Kuhn, J., Packer, J.A., and Fan, Y. (2019), "Rectangular Hollow Section Webs under Transverse Compression," *Canadian Journal of Civil Engineering*, Vol. 46, pp. 810–827.

Liu, J. (2016), "Updates to Expected Yield Stress and Tensile Strength Ratios for Determination of Expected Member Capacity in the 2016 AISC Seismic Provisions," *Engineering Journal,* AISC*,* Vol. 53, No. 4, pp. 215–227.

Lu, L.H., de Winkel, G.D., Yu, Y., and Wardenier, J. (1994), "Deformation Limit for the Ultimate Strength of Hollow Section Joints," *Sixth International Symposium on Tubular Structures*, Melbourne, Australia, pp. 341–347.

Newlin, D.E. and Chen, W.F. (1971), "Strength and Stability of Column Web in Welded Beam-to-Column Connections," Fritz Engineering Laboratory Report No. 333.14, Lehigh University, Bethlehem, Pa.

Packer, J.A. (1984), "Web Crippling of Rectangular Hollow Sections," *Journal of Structural Engineering*, ASCE, Vol. 110, No. 10, pp. 2,357–2,373.

Packer, J.A. (1987), "Review of American RHS Web Crippling Provisions," *Journal of Structural Engineering*, ASCE, Vol. 113, No. 12, pp. 2,508–2,513.

Packer, J.A., Wardenier, J., Zhao, X.-L., van der Vegte, G.J., and Kurobane, Y. (2009), *Design Guide for Rectangular Hollow Section (RHS) Joints under Predominantly Static Loading,* CIDECT Design Guide No. 3, 2nd Ed., CIDECT, Geneva, Switzerland.

Ravindra, M.K. and Galambos, T.V. (1978), "Load and Resistance Factor Design for Steel," *Journal of the Structural Division*, ASCE, Vol. 104, No. 9, pp. 1,337–1,353.

Roberts, T.M. (1981), "Slender Plate Girders subject to Edge Loading," *Proceedings of the Institution of Civil Engineers*, Part 2, Vol. 71, No. 3, pp. 805–819.

Wei, F. (2019), "Experimental Study of Laterally Offset RHS X-Connections in Branch Axial Compression," M.A.Sc. Thesis, University of Toronto, Toronto, Canada.

Critical Temperature of Axially Loaded Steel Members with Wide-Flange Shapes Exposed to Fire

ANA SAUCA, RACHEL CHICCHI, CHAO ZHANG, and LISA CHOE

ABSTRACT

This paper presents closed-form equations that were developed to evaluate critical temperatures of structural steel compression and tension members exposed to fire. The deterministic approach involved a parametric study using finite element simulations in order to identify influencing factors—for example, mechanical properties of steel, member slenderness, and axial load ratios. Statistical models were employed to develop closed-form equations representing the best fit of numerical results. A comparison with experimental column test data indicates that the proposed equation for compression members provides a conservative lower bound (16% lower on average) relative to the test data at load ratios greater than 0.3. A sensitivity study was also performed to further explore uncertainty in predicted critical temperatures due to variability of axial load ratios. For both compression and tension members, the ambient-temperature yield stress of steel, F_y, has a great impact on determination of axial load ratios, subsequently influencing the overall accuracy of the critical temperature estimated by the proposed equations. The applicability of the proposed equations is limited to wide-flange steel members that are simply supported, concentrically loaded, and exposed to uniform heating.

Keywords: critical temperature, structural steel, compression, tension, fire.

INTRODUCTION

Background

In the United States, fire resistance design of load-carrying steel members (beams and columns) in steel-framed buildings is mainly achieved through compliance with prescriptive provisions in the International Building Code (ICC, 2009). In this approach, fireproofing insulation is applied to exposed steel so that the steel does not exceed the critical temperature under standard fire conditions for a minimum specified duration (known as a fire-resistant rating). According to the American Society for Testing and Materials (ASTM) E119 standard (ASTM, 2019), the critical temperature of exposed steel members in a standard fire test is 1000°F (538°C) for columns and 1100°F (593°C) for beams, determined as the average temperature of all measurement points. However, these limiting temperatures seldom account for the effects of imposed load levels, semi-rigid support conditions, and both member and section slenderness.

Prescriptive methods have provided little information regarding the high-temperature strength and associated failure modes of steel members exposed to fire. As an alternative engineering approach, AISC *Specification* Appendix 4 (AISC, 2016b) provides high-temperature member strength equations for the limit states of flexural buckling and lateral-torsional buckling. To calculate member strengths at elevated temperature, users need to define the temperature of interest as an input, which must be greater than 392°F (200°C), based on heat transfer analyses or engineering judgments. These equations are less practical for solving the critical temperature at which the member demand exceeds its capacity because iteration with increasing temperatures is required (Sauca et al., 2019).

In Europe, the evaluation of critical temperatures of axially loaded steel members was of interest beginning in the late 1970s. Kruppa (1979) defined "critical" or "collapse" temperature as the temperature at which the structure cannot assume its function and proposed a critical temperature equation for steel columns using the temperature-dependent axial stress and buckling coefficient. Rubert and Schaumann (1988) used finite element models for calculating critical temperature of steel columns. The analytical results were compared with 50 full-scale column tests and showed good correlation at temperatures in the range of 390°F (200°C) to 1300°F (700°C) and utilization (demand-to-capacity) ratios of 0.2 to 0.6.

Neves (1995) further explored the critical temperature of restrained steel columns analytically, with three column slenderness values (40, 80, and 120) and eccentricity of the

Ana Sauca, Post-doc Research Engineer, Danish Institute of Fire and Security Technology, Denmark. Email: AS@dbigroup.dk

Rachel Chicchi, Assistant Professor, University of Cincinnati, Cincinnati, Ohio. Email: rachel.chicchi@uc.edu

Chao Zhang, Guest Researcher, National Institute of Standards and Technology, Gaithersburg, Md. Email: chao.zhang@nist.gov

Lisa Choe, Research Structural Engineer, National Institute of Standards and Technology, Gaithersburg, Md. Email: lisa.choe@nist.gov (corresponding)

Paper No. 2019-21

applied load. Due to the variety of parameters being considered, a critical temperature equation was not proposed. Similarly, Franssen (2000) applied an arc-length numerical technique to calculate the collapse temperature of columns. Wang et al. (2010) evaluated the critical temperature of restrained steel columns using a finite element ABAQUS model (Smith, 2009) with two-dimensional beam elements. Their study indicated that the section geometry had very limited effects on the column critical temperature, and the critical temperature of a restrained column can be obtained by making a reduction in corresponding values of columns without axial restraint.

The European standards provide critical temperature equations or tabulated data for steel members. For steel members "without instability phenomena" (e.g., tension or flexural yielding), the critical temperature is only a function of a utilization ratio for fire conditions (CEN, 2005). This equation is very similar to an inverse of the temperature-dependent yield strength of structural steel. For steel columns, however, only tabulated forms (e.g., Vassart et al., 2014; BSI, 2005) are available to evaluate critical temperatures, depending upon the member slenderness and utilization ratio. Despite all the limitations (i.e., applicability only under standard fires, uniform distribution of temperatures across the section and length, and simplified boundary conditions), the critical temperature method would remain as a useful tool to evaluate the fire resistance of load-carrying steel members (Milke, 2016).

Objectives, Scope, and Limitations

The significance of the critical temperature method lies in its simplicity and the useful information obtained about a structural member exposed to varying temperatures during a fire event. To date, however, a critical temperature method is not available in AISC *Specification* Appendix 4 (AISC, 2016b). The objective of the study presented herein was to develop closed-form solutions that can be used to evaluate critical temperatures of axially loaded steel members exposed to fire. The methodology adopted in this study included (1) a parametric study using 900 finite element models to identify the influencing variables for determination of critical temperatures of steel members at elevated temperatures, (2) three-dimensional regression analyses to develop a closed-form equation that represents the best fit of numerical results with given ranges of the parameters considered in this study, (3) comparison of the critical temperature predicted using the proposed equation with test data in literature, and (4) a sensitivity study to estimate uncertainty in critical temperatures computed using proposed equations.

The scope of this study focused on the critical temperature of structural steel tension and compression members with wide-flange rolled shapes. The parameters influencing critical temperatures were evaluated, including various axial load levels, steel grades, and section compactness and member slenderness at ambient temperature. The use of proposed equations presented herein should be limited to wide-flange steel members simply supported, concentrically loaded, and exposed to uniform heating. Future work will include the effects of thermal restraints as well as thermal gradients through the section depth and along the member length.

NUMERICAL ANALYSES

Test Bed

The critical temperature of axially loaded steel columns with wide-flange rolled shapes was evaluated using the finite element method (FEM). In this study, a total of 900 FEM models were analyzed in combination with various ranges of parameters summarized in Table 1. Five different wide-flange rolled shapes, including W8×31, W10×68, W14×22, W14×90, and W14×211, were used in this study. With the exception of the W14×22, all other shapes are compact for compression at ambient temperature. In addition, two American standard grades of structural steel shapes, including $F_y = 50$ ksi and $F_y = 36$ ksi, are considered, where F_y is the minimum specified yield stress. Effective slenderness ratios, L_c/r, range from 20 to 200, and applied load ratios vary from 0.1 to 0.9. The load ratio is defined as the axial demand at elevated temperatures, P_u, normalized by the nominal capacity at ambient temperature, P_{na}. The demand for fire condition can be determined from the load combination for extraordinary events, 1.2 × dead load + 0.5 × live load + A_T, where A_T is the force and deformation induced by fire effects (ASCE, 2016). In this study, all investigated members were assumed to be simply supported, concentrically loaded, and exposed to uniform heating; therefore, the magnitude of A_T was assumed to be zero. The nominal capacity at ambient temperature, P_{na}, can be calculated using AISC *Specification* Section E3.

Numerical models of columns were developed using three-dimensional shell elements. Each model was discretized into 50 elements along the member length and 8 elements each for the flange and the web. The FEM solution with this element size was converged with the maximum error of about 2%, based on the mesh density study presented in Sauca et al. (2019). Linear kinematic constraints were applied to both the flanges and web at each end in order to enforce rigid planar behavior. The column ends were simply supported. An axial force was applied to the centroid of the end section. An initial displacement at midspan was taken as the 1/1000 of the column length to simulate global imperfections (initial sweep). Local geometrical imperfections were implemented by scaling a sinusoidal deformation of the cross sections using elastic buckling analyses. The

Table 1. Test Parameters Used in Numerical Analyses			
Shape	F_y	L_c/r	P_u/P_{na}
W8×31 W10×68 W14×22 W14×90 W14×211	36 ksi (250 MPa) 50 ksi (350 MPa)	20 to 200 (increment: 20)	0.1 to 0.9 (increment: 0.1)

scaled value was taken as the larger of a web out-of-flatness equal to the ratio of the section depth over 150 (Kim and Lee, 2002) or a tilt in the compression flanges taken as the ratio of the flange width over 150 (Zhang et al., 2015). No residual stresses were applied because their influence is limited at elevated temperature (Vila Real et al., 2007). The Eurocode 3 (CEN, 2005) temperature-dependent stress-strain relationship was employed, whereas no thermal creep model was incorporated explicitly.

In order to estimate critical temperatures of columns using FEM models, an axial load as a fraction of P_{na} was applied at ambient temperature, and then the member temperature was increased monotonically until force equilibriums could not be achieved. The maximum value of temperature achieved from each FEM model was defined as a critical temperature.

Numerical Results

Figure 1 shows the critical temperature, T_{cr}, of steel columns predicted using the finite element models with F_y = 50 ksi (350 MPa), where the dotted lines indicate the linear regression of these predicted results. Figure 1(a) shows the average critical temperature of columns as a function of a load ratio. The error bars indicate the standard deviation of the results varying with five different shapes and all slenderness ratios (L_c/r = 20 to 200) at the same load level. Figure 1(b) shows the relationship of the average critical temperature of all five columns versus the slenderness ratio at four different load ratios (P_u/P_{na}) of 0.1, 0.3, 0.6, and 0.9. As shown, the critical temperature appears to be linearly decreasing with both increasing load ratios and increasing slenderness ratios. However, the critical temperature is less sensitive to the member slenderness at the same load level. Some statistical results and discussions on the effect of member slenderness and applied load levels are as follows.

- *Member slenderness:* The reduction in critical temperatures with increasing slenderness ratios is influenced by the applied load level. At load ratios smaller than 0.5, the critical temperature is reduced by about 10% between the slenderness ratio of 20 and 200. At higher load ratios, the critical temperature can reduce by 30% to 60% for the L_c/r ratio of 20 to 200. This reduction is not proportional to load ratios.
- *Applied load level:* The critical temperature is affected by the magnitude of applied loads. The reduction in critical temperature can reach nearly 80% between the load ratio of 0.1 and 0.9 and 20% on average at each increment of 0.1. Larger scatter of the results is observed for the models with the load ratio between 0.5 and 0.8, as shown by the error bars in Figure 1(a), due to variation in member slenderness. The critical temperature versus applied load relationship shows a very good linear fit, similar to an empirical relationship presented in Choe et al. (2011).

Figure 2 shows critical temperatures of steel columns relative to load ratio with (1) all five shapes and two different steel grades and (2) W14×22 and W14×90 columns with F_y = 50 ksi. Both graphs considered the slenderness ratios of 20, 40, and 100. Some discussions on the effect of the ambient yield stress, F_y, and the section compactness are as follows.

- *Ambient yield strength:* The variation in critical temperatures predicted using two different steel grades (36 ksi versus 50 ksi) is about 1% on average. This is to be expected as the buckling behavior of columns with the slenderness ratio greater than 40 (i.e., medium-length to slender columns) is mainly affected by low strain levels (less than 0.05% strain) and temperature-dependent elastic modulus (Choe et al., 2017).
- *Section geometry:* Between two different wide-flange shapes, the variation in critical temperatures is over 10% for short columns subjected to large axial loads (i.e., a slenderness ratio less than 60 and a load ratio greater than 0.6). The critical temperature variation for slender columns subjected to small axial loads is below 5%.

PROPOSED CLOSED-FORM EQUATION

Compression Members

The numerical results from 900 finite-element models were used to develop a closed-form equation that predicts critical temperatures of steel columns as a function of member slenderness and load ratio. The three-dimensional linear polynomial model, as shown in Figure 3, was employed

based on the results from the parametric study presented previously. Equations 1 and 2 show the resulting best linear fit equation in °C and °F, respectively, with the *R*-square value of 0.97.

$$T_{cr} = 858 - 0.455\frac{L_c}{r} - 722\frac{P_u}{P_{na}} \quad \text{in °C} \tag{1}$$

$$T_{cr} = 1580 - 0.814\frac{L_c}{r} - 1300\frac{P_u}{P_{na}} \quad \text{in °F} \tag{2}$$

Figure 4 shows a comparison of critical temperatures calculated using the proposed equation with those estimated using various methods, including FEM models, the ASTM E119 limiting temperature of columns, and the AISC *Specification* Appendix 4 equation. In Figure 4(a), the results of

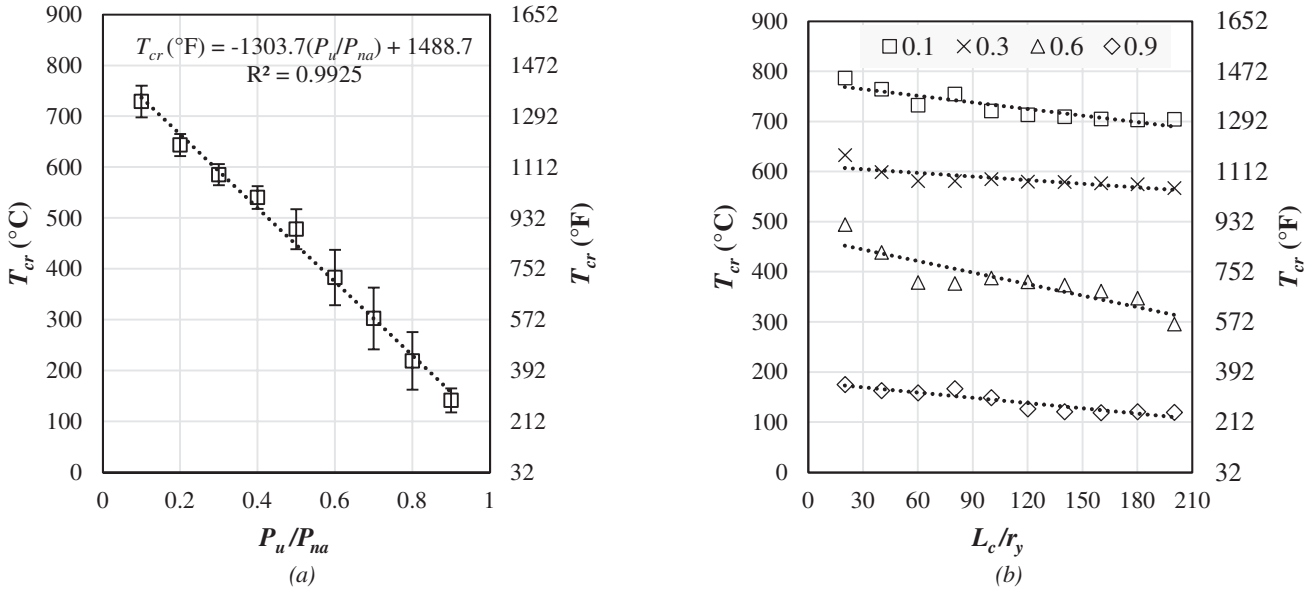

Fig. 1. Average critical temperatures for columns predicted using FEM models of five shapes with F_y *= 50 ksi as a function of (a) load ratio (*P_u/P_{na}*) and (b) member slenderness (*L_c/r_y*).*

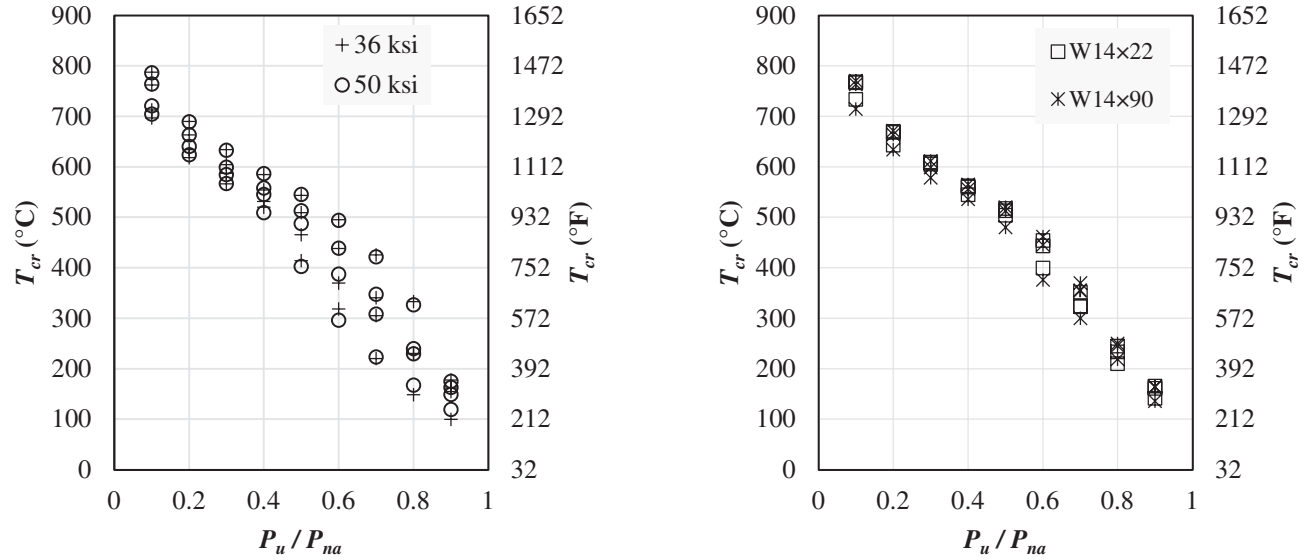

(a) All five shapes with F_y *= 36 ksi and 50 ksi* *(b) W14×22 and W14×90 shapes with* F_y *= 50 ksi*

Fig. 2. Predicted critical temperatures of columns with slenderness ratios of 20, 40, and 100.

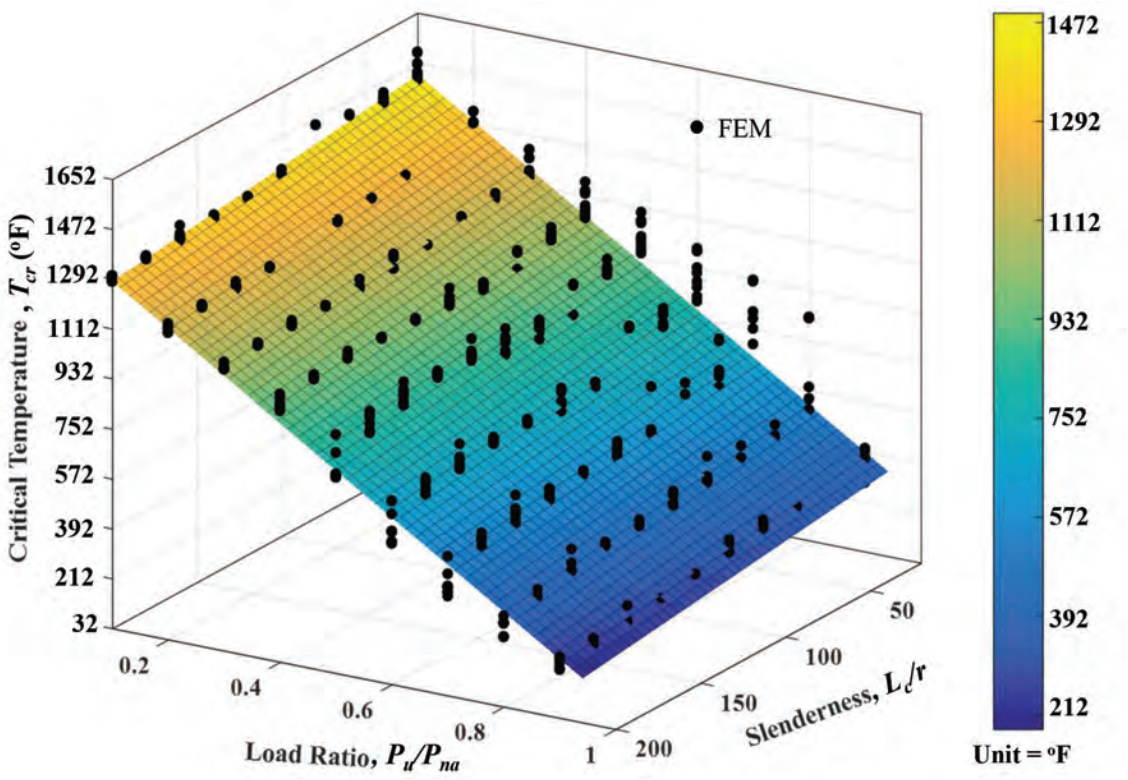

Fig. 3. A three-dimensional linear curve fit of 900 FEM models of columns.

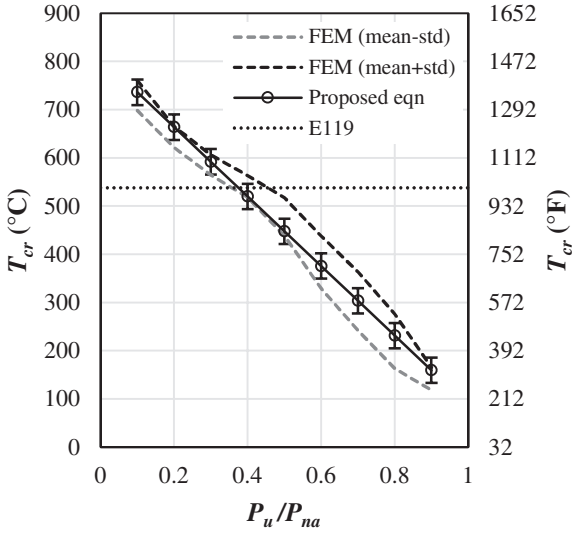

(a) FEM results and ASTM E119 limiting temperature

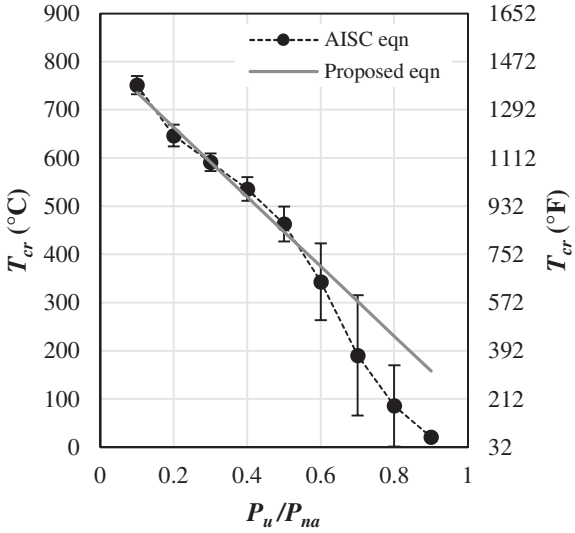

(b) AISC Specification *Appendix 4 equation results*

Fig. 4. Comparisons of the proposed column equation.

FEM models are presented with two lines: the upper bound as mean values plus standard deviations (std) and the lower bound as mean values minus standard deviations. The standard deviation incorporates the total variation in the FEM data resulting from the range in parameters described in Table 1 at each load level. The error bars plotted with the critical temperature predicted using Equation 1 indicate the standard deviation due to slenderness ratio ranges from 20 to 200. Overall, the proposed equation compares reasonably well with the FEM results. With this equation, the load-bearing capacity of steel columns is approximately 40% of the ambient capacity at the ASTM E119 limiting temperature of 1000°F (540°C).

Figure 4(b) gives a comparison with critical temperatures estimated using the AISC *Specification* Appendix 4 flexural buckling strength equation, Equation A-4-2. A detailed description of computation methods, which required an iteration process, is presented in Sauca et al. (2019). The error bars in this figure indicate the standard deviation resulted from a variety of steel shapes and slenderness ratios considered in this study. For columns with load ratios less than 0.6, the proposed equation also adequately predicts critical temperatures, with 2% difference on average. At load ratios equal to or greater than 0.6, however, the proposed equation may overestimate critical temperatures estimated using AISC *Specification* Equation A-4-2.

The efficacy of Equation 1 was examined by comparing predicted critical temperatures with observed critical temperatures from previous experimental studies (Franssen et al., 1996; Ali et al., 1998; Choe et al., 2011) of steel columns that had similar properties used for the present study. Test data used for this comparison included 36 wide-flange, hot-rolled column specimens that had simply supported boundary conditions and were concentrically loaded (i.e., an eccentricity of axial loading was less than the 1/1000 of the column length) at elevated temperatures. In this data set, the ambient-temperature yield stress ranged from 32 ksi (220 MPa) to 60 ksi (400 MPa), and effective slenderness ratios varied from 30 to 137.

Figure 5 shows a comparison of the column test data with predicted critical temperatures using Equation 1 and with the linear regression of the data itself. Overall, the proposed equation provides a conservative lower bound of the test results. For the specimens with load ratios greater than 0.3, the calculated critical temperatures are approximately 16% lower than the measured values on average. For load ratios less than 0.2, Equation 1 slightly overestimates the critical temperature by 4%.

Tension Members

Critical temperatures of uniformly heated steel members in tension have a dependency of high-temperature mechanical properties, such as temperature-dependent yield stress and ultimate tensile strength. This paper also suggests a critical temperature equation for tensile yielding in gross sections of a steel member as a function of imposed tension loads, T_u, at elevated temperature normalized by the nominal capacity, T_{na}, at ambient temperature. As shown in Figure 6, the critical temperature equation is an inverse relationship of the AISC *Specification* temperature-dependent retention factors for yield stress, k_y, essentially the same as the Eurocode 3 (CEN, 2005) retention factors. The logarithmic regression model was employed similar to the Eurocode 3 critical temperature equation for members "without instability phenomena." Equations 3 and 4 show the best fit equation

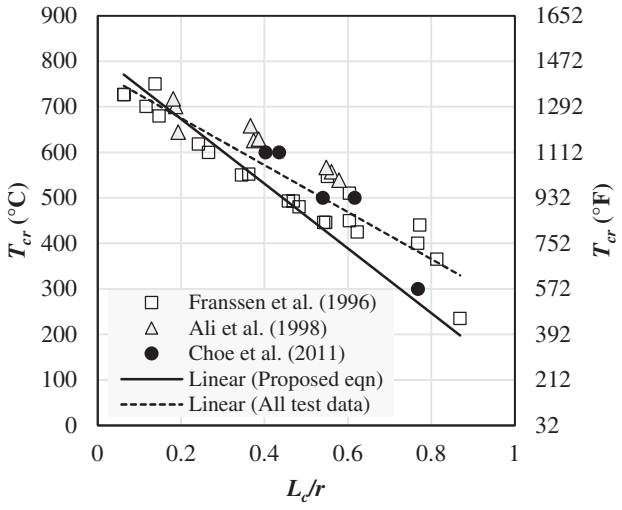

Fig. 5. A comparison of critical temperatures of columns calculated using Equation 1 with experimental test data.

Table 2. Statistical Data for Uncertainties (Takagi and Deierlein, 2007)			
Variable	**Mean**	**CV**	**Std**
F_y	50 ksi (350 MPa)	0.10	5 ksi (35 MPa)
E	29,000 ksi (200 GPa)	0.06	1,740 ksi (12 GPa)
DL	103% unfactored	0.10	a
LL	25% unfactored	0.60	b
a: The standard deviation for *DL* is taken as the mean load × 1.025 × 0.10. b: The standard deviation for *LL* is taken as the mean load × 0.25 × 0.60.			

in °C and °F, respectively, with the *R*-square value of 0.99. For the use of these equations, the load ratio, T_u/T_{na}, must be greater than or equal to 0.01.

$$T_{cr} = 435 - 170\ln\left(\frac{T_u}{T_{na}}\right) \quad \text{in °C} \tag{3}$$

$$T_{cr} = 816 - 306\ln\left(\frac{T_u}{T_{na}}\right) \quad \text{in °F} \tag{4}$$

ESTIMATED UNCERTAINTY OF CLOSED-FORM EQUATIONS

Compression Members

Because the proposed closed-form solution was developed using a deterministic approach, which does not account for uncertainty in estimation of applied load ratios, P_u/P_{na}, sensitivity was examined with variability in mechanical properties of steel (F_y and elastic modulus, E) and the magnitude of design loads (e.g., dead load, *DL,* and live load, *LL*). Although uncertainty in geometric properties are present in the proposed equation, such as column length, L_c, and the radius of gyration, r, this effect was neglected with the assumption that compliance of standard fabrication tolerances specified in the AISC *Code of Standard Practice for Steel Buildings and Bridges* (AISC, 2016a) would not result in notable critical temperature changes. A comparison of the influence of each parameter (F_y, E, *DL*, and *LL*) on the variation in the critical temperature was calculated by considering reasonable upper and lower bounds of each variable. Each parameter was evaluated at the mean ±1 standard deviation (std) that represents 68% confidence intervals. The mean ±2 standard deviations (to represent a 95% confidence interval) were also reported. A normal distribution of each variable was assumed.

Statistical properties of the investigated variables are summarized in Table 2, based on work from Takagi and Deierlein (2007), who proposed the member strength equation for gravity columns at elevated temperature in AISC *Specification* Appendix 4. The mean values and coefficients of variation (CV) were determined from statistical data obtained by Ellingwood et al. (1980). The percentages

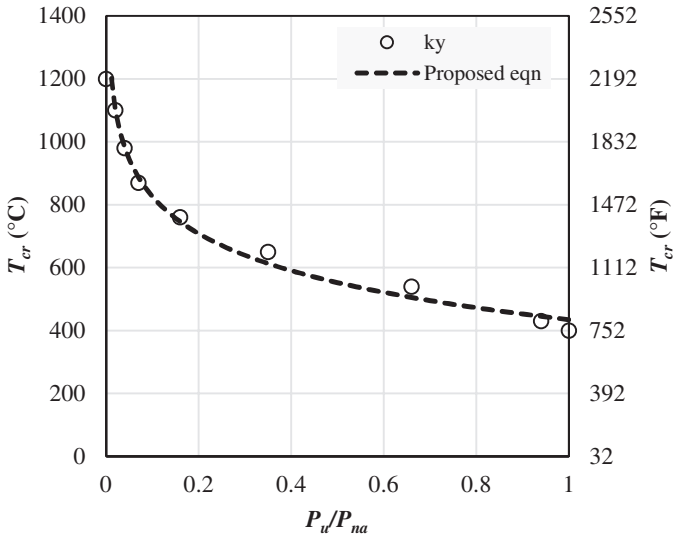

Fig. 6. Critical temperature versus load ratio relationship of tension members.

for *DL* and *LL* were obtained from load surveys using probabilistic load models. They represent the mean values of the unfactored design loads for dead and live loads relative to the nominal design loads in the American National Standard A58. The standard deviation (std) for each variable was calculated as the mean times the coefficient of variation (CV), as shown in Table 2. Ambient temperature values of F_y and E were used to calculate the mean and CV values due to a lack of statistical data on their high-temperature values.

A range of columns used in this study (W8×31, W14×90, and W14×211 with $F_y = 50$ ksi) were examined for sensitivity. The change in critical temperature due to uncertainty of 1 standard deviation is consistent across all compact column shapes, so the results presented represent all of the compact shapes listed above. Figure 7 shows the change in critical temperature for the W14×211 column with $L_c/r = 40$ and $L_c/r = 80$ due to uncertainty in F_y. The solid line represents the critical temperatures determined using the proposed closed-form equation [Equation (1)]. The dashed lines represent the critical temperatures calculated with F_y adjusted by a positive and negative standard deviation. The uncertainty in the critical temperature estimated using the propose equation is more pronounced at lower L_c/r ratios and at higher load ratios where Euler buckling does not likely occur. At higher L_c/r levels, where elastic buckling of the column would dominate, the impact of a change in F_y, appears to be minimal and becomes negligible for L_c/r ratios of 120 and greater. At a load ratio (P_u/P_{na}) of 0.6, the uncertainty in estimated critical temperatures is about 20% at $L_c/r = 40$ and about 10% at $L_c/r = 80$ due to ±1 std of F_y. These percentages represent the ratio of change in critical temperature due to uncertainty relative to the closed-form proposed equation without uncertainty.

Figure 8 shows the variation in estimated critical temperature for the W14×211 column with $L_c/r = 40$ and $L_c/r = 120$

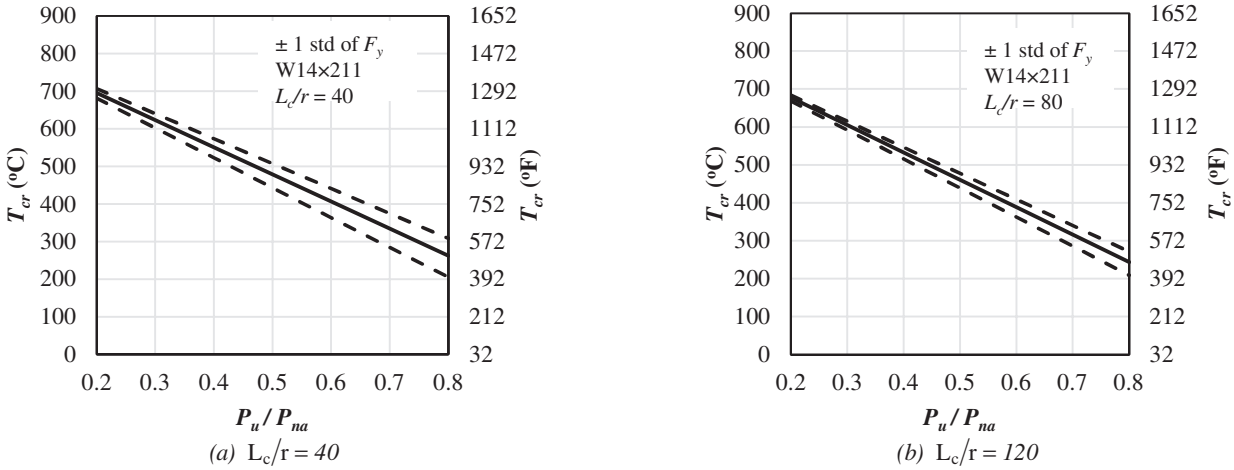

Fig. 7. Sensitivity of calculated critical temperatures of a W14×211 column due to uncertainty in F_y.

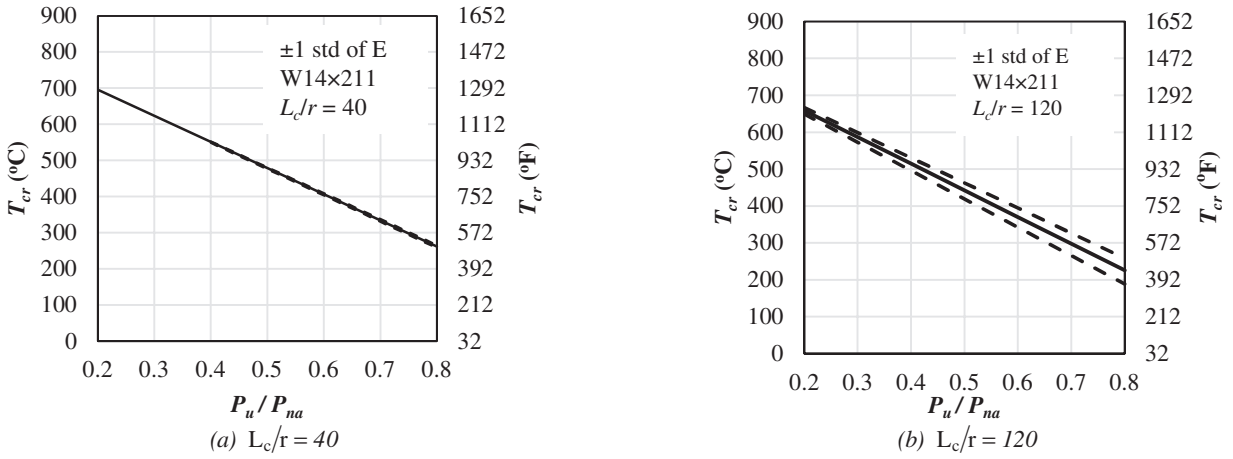

Fig. 8. Sensitivity of calculated critical temperatures of a W14×211 column due to uncertainty in E.

due to uncertainty in the elastic modulus, E, in the calculation of P_{na}. The uncertainty in estimated critical temperature is most pronounced at both higher slenderness and higher load ratios where elastic buckling likely governs. In this study, the maximum uncertainty is observed for slender columns ($L_c/r \geq 120$) and the applied load ratio of 0.8. For these columns, the uncertainty in critical temperatures can be as large as 30%. However, for stockier columns ($L_c/r \leq 40$), this uncertainty in critical temperatures associated with ±1 std of E becomes very minor, less than 3%.

Sensitivity due to uncertainty in applied loads under fire conditions (P_u) was determined by considering three different *DL/LL* ratios selected based on engineering judgment. The first *DL/LL* ratio was 0.65, which was determined by assuming a dead load of 65 psf and a live load of 100 psf. The second *DL/LL* ratio of 1.3 was calculated using the same dead load of 65 psf but a live load of only 50 psf. The 65-psf dead load was selected based on the assumption of 50 psf for the composite slab plus 15 psf for superimposed dead loads such as ceilings and ductwork and piping for utilities. The live load values of 50 psf and 100 psf represent average and high levels of live loading, respectively. According to ASCE/SEI 7 (2016), 50 psf represents live loads for office spaces, while 100 psf represents lobbies and other assembly areas. The final *DL/LL* ratio that was used was 0.33. This ratio is given in the AISC *Specification* Section A1 Commentary (AISC, 2016b) as the ratio that results in the same reliability between the ASD and LRFD design methods. Using these ratios, the dead and live loads on the column were determined by assuming that the demand-to-capacity ratio for each column at ambient conditions is equal to 1.0 for the ambient load combination, $1.2DL + 1.6LL$. Converting to the fire load combination ($1.2DL + 0.5LL$), this equates to a P_u/P_{na} ratio of approximately 0.4, 0.5, and 0.6 for *DL/LL* ratios of 0.33, 0.65, and 1.3, respectively. Figure 9(a) shows the change in critical

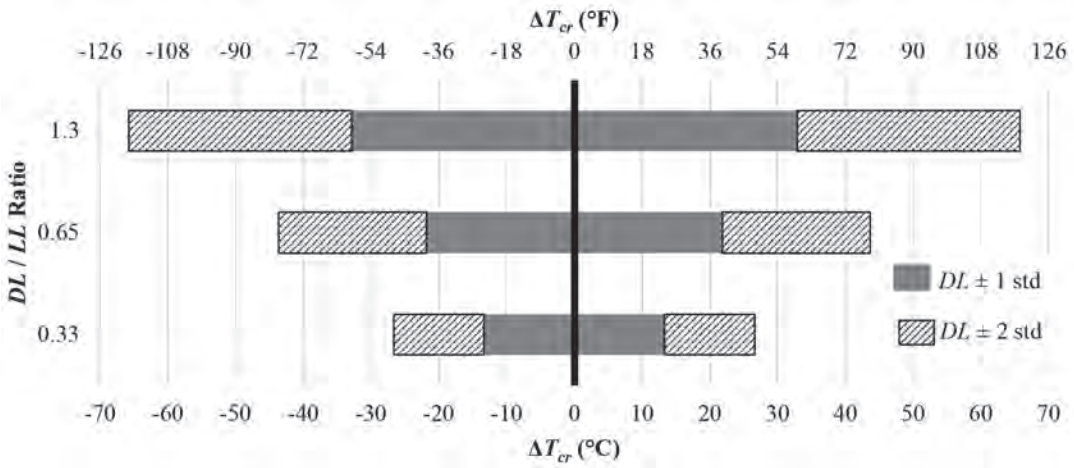

(a) Dead load (DL)

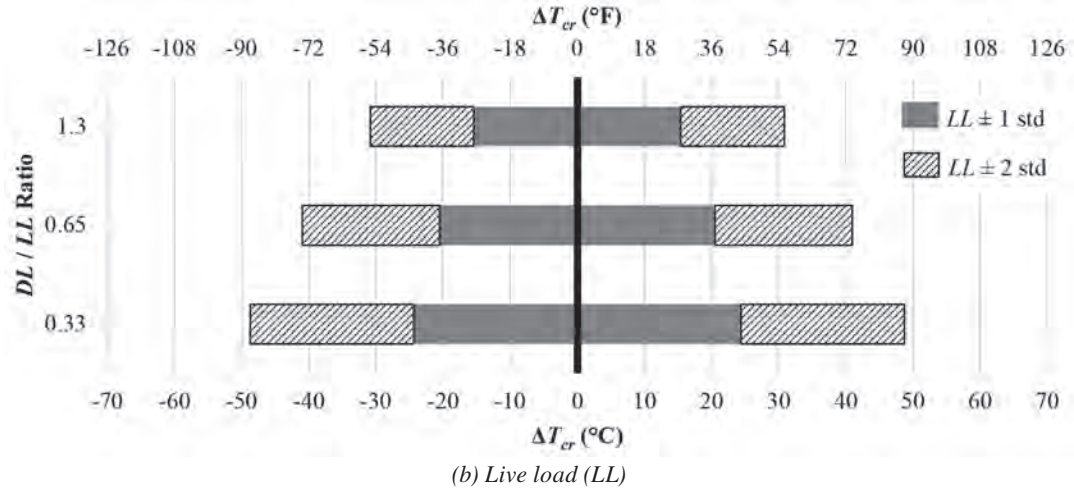

(b) Live load (LL)

Fig. 9. Sensitivity of the change in critical temperature due to uncertainty. Note: ΔT_{cr} *is presented (not* T_{cr}*);* $\Delta T_{cr}(°F) = 9/5[\Delta T_{cr}(°C)]$.

temperature due to uncertainty in dead load, while Figure 9(b) represents the change in critical temperature due to live load uncertainty. These results show that critical temperatures are more influenced by a higher *DL/LL* ratio for dead load variability and a lower *DL/LL* for live load variability. These critical temperature changes (ΔT_{cr}) are independent of the L_c/r ratio of the column. The maximum change in critical temperature due to uncertainty of 1 standard deviation in *DL* and *LL* is 59°F and 44°F, respectively.

Tension Members

The same variables (F_y, *DL*, and *LL*) were studied for tension members to determine the sensitivity of the closed-form equation. There is no sensitivity in the equation to a change in modulus of elasticity (E). A W14×22 shape was chosen to demonstrate the sensitivity. Figure 10 summarizes the sensitivity by showing the change in critical temperate for ±1 std and ±2 std of each parameter, estimated using CV values in Table 2. The same *DL/LL* ratios of 0.33, 0.65, and 1.3 were also used. This comparison shows that the greatest change in critical temperatures is due to a change in the yield stress of the material. At 1 standard deviation, the change in temperature is −32°F to 29°F, and at 2 standard deviations, it is −68°F to 56°F. The variation in *DL* with a high *DL/LL* ratio produces the second highest sensitivity.

SUMMARY AND CONCLUSIONS

This paper presents the development of closed-form solutions to evaluate critical temperatures of axially loaded steel members exposed to fire. For compression members, a total of 900 FEM models were analyzed in combination with various ranges of parameters, including five different wide-flange rolled shapes made of two American standard grades of structural steel, member slenderness ratios from 20 to 200, and applied load ratios varying from 0.1 to 0.9. Load ratios represent the axial demand at elevated temperatures, P_u, normalized by the nominal capacity at ambient temperature, P_{na}.

The parametric study indicates that the most influential parameters for critical temperature of columns are member slenderness and applied load ratios. A closed-form equation predicting critical temperatures of steel columns with these two factors is proposed based on curve-fitting of the FEM results using the three-dimensional linear polynomial model. With this equation, the load-bearing capacity of steel columns is approximately 40% of the ambient capacity at the ASTM E119 limiting temperature of 1000°F (540°C). At load ratios less than 0.6, the proposed equation accurately predicts critical temperatures determined using the high-temperature flexural buckling strength equation in AISC *Specification* Appendix 4, whereas it may overestimate critical temperatures (10% difference or greater) at load ratio greater than or equal to 0.6. The proposed equation also provides a conservative lower bound (16% lower on average) of the published test data for the specimens with load ratios greater than 0.3. This result considers column failure by flexural buckling at elevated temperature.

A critical temperature equation for tension members is also proposed using the logarithmic regression model for the case with tensile yielding only. This equation is essentially the same as an inverse relationship of the AISC

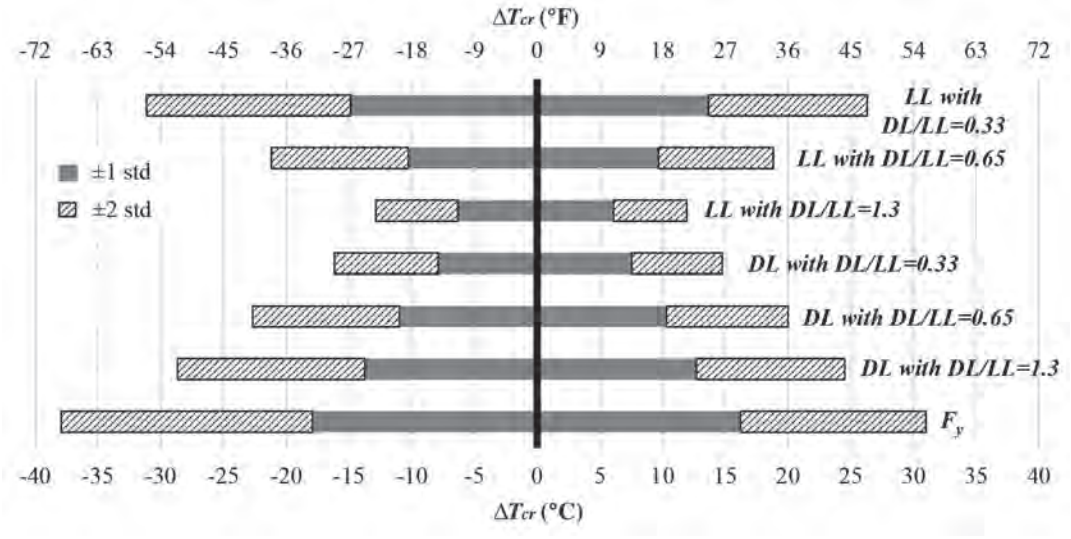

Fig. 10. Sensitivity of the change in critical temperature of tension members due to uncertainty in parameters. Note: ΔT_{cr} is presented (not T_{cr}); $\Delta T_{cr}(°F) = 9/5[\Delta T_{cr}(°C)]$.

Specification temperature-dependent retention factors for yield stress.

A sensitivity study was performed to estimate the uncertainty in critical temperatures predicted using the proposed equations due to the variability in axial load ratios. The results show that these critical temperatures depend on the ambient temperature F_y and E as well as design loads (*DL* and *LL*). The variation in F_y is the most influential factor among other uncertain variables for critical temperatures of both compression and tension members. The influence of F_y uncertainty is apparent in stout columns with a low slenderness ratio. All results show that variations in critical temperature are relatively minor for uncertainty of 1 standard deviation, particularly for typical columns, which are assumed to have load ratios of approximately 0.6 and L_c/r ratios of approximately 40 to 60. Consideration of material sensitivity should be implemented for load ratios beyond 0.6.

The findings and equations from this study are limited to the range of parameters included in the numerical evaluation. Future studies will be conducted to further incorporate probabilistic analyses into the current deterministic approach, accounting for the effects of thermal restraints as well as thermal gradients through the section depth and along the member length.

ACKNOWLEDGMENT

Valuable comments and input on this work were provided by the AISC Committee on Specifications Task Committee 8, Design for Fire.

DISCLAIMERS

Certain commercial entities, equipment, products, software, or materials are identified in this paper in order to describe a procedure or concept adequately. Such identification is not intended to imply recommendation or endorsement by the National Institute of Standards and Technology, nor is it intended to imply that the entities, products, software, materials, or equipment are necessarily the best available for the purpose.

REFERENCES

Ali, F.A., Shepherd, P., Randall, M., Simms, I.W., O'Connor, D.J., and Burgess, I. (1998), "The Effect of Axial Restraint on the Fire Resistance of Steel Columns," *Journal of Construction Steel Research,* Vol. 46, pp. 305–306.

AISC (2016a), *Code of Standard Practice for Steel Buildings and Bridges*, ANSI/AISC 303-16, American Institute of Steel Construction, Chicago, Ill.

AISC (2016b), *Specification for Structural Steel Buildings*, ANSI/AISC 360-16, American Institute of Steel Construction, Chicago, Ill.

ASCE (2016), *Minimum Design Loads and Associated Criteria for Buildings and Other Structures*, ASCE/SEI 7-16, American Society of Civil Engineers, Reston, Va.

ASTM (2019), *Standard Methods of Fire Test of Building Construction and Materials*, ASTM E119-19, ASTM International, West Conshohocken, Pa.

BSI (2005), *UK National Annex to Eurocode 3. Design of Steel Structures. General Rules. Structural Fire Design*, BS NA EN 1993-1-2, United Kingdom.

Choe, L., Varma, A.H., Agarwal, A., and Surovek, A. (2011), "Fundamental Behavior of Steel Beam Columns and Columns under Fire Loading: Experimental Evaluation," *Journal of Structural Engineering,* Vol. 137, pp. 954–966.

Choe, L., Zhang, C., Luecke, W.E., et al. (2017), "Influence of Material Models on Predicting the Fire Behavior of Steel Columns," *Fire Technology*, Vol. 53, pp. 375–400, https://doi.org/10.1007/s10694-016-0568-4.

CEN (2005), *Eurocode 3: Design of Steel Structures—Part 1-2: General Rules—Structural Fire Design*, Standard EN 1993-1-2, European Committee for Standardization, Luxembourg.

Ellingwood, B., Galambos, T.V., MacGregor, J.G., and Cornell, C.A. (1980), "Development of a Probability-Based Load Criterion for American National Standard A58," National Bureau of Standards Special Publication No. 577, Washington, D.C.

Franssen, J.M., Schleich, J.B., Cajot, L.G., and Azpiazu, W. (1996), "A Simple Model for the Fire Resistance of Axially-Loaded Members—Comparison with Experimental Results," *Journal of Construction Steel Research*, Vol. 37, pp. 175–204.

Franssen, J.M. (2000), "Failure Temperature of a System Comprising a Restrained Column Submitted to Fire," *Fire Safety Journal*, Vol. 34, No. 2, pp. 191–207.

ICC (2009), *International Building Code*, International Code Council, Falls Church, Va.

Kim, S. and Lee, D. (2002), "Second-Order Distributed Plasticity Analysis of Space Steel Frames," *Engineering Structures*, Vol. 24, pp. 735–744.

Kruppa, J. (1979), "Collapse Temperature of Steel Structures," *Journal of the Structural Division*, ASCE, Vol. 105, No. ST9, September.

Milke, J.A. (2016), "Analytical Methods for Determining Fire Resistance of Steel Members," In: Hurley M.J. et al. (eds.), *SFPE Handbook of Fire Protection Engineering*, Springer, New York, N.Y., https://doi.org/10.1007/978-1-4939-2565-0_53.

Neves, I.C. (1995), "The Critical Temperature of Steel Columns with Restrained Thermal Elongation," *Fire Safety Journal*, Vol. 24, pp. 211–227.

Rubert, A. and Schaumann, P. (1988), "Critical Temperatures of Steel Columns Exposed to Fire," *Fire Safety Journal*, Vol. 13, pp. 39–44.

Sauca, A., Zhang, C., Seif, M., and Choe, L. (2019), "Axially Loaded I-Shaped Steel Members: Evaluation of Critical Temperature Using ANSI/AISC-360 Appendix 4 and Finite Element Model," *Proceedings of the Annual Stability Conference*, Structural Stability Research Council, St. Louis, Mo., April 2–5.

Smith, M. (2009), *ABAQUS/Standard User's Manual, Version 6.9*, Simulia, Providence, R.I.

Takagi, J. and Deierlein, G.G. (2007), "Collapse Performance Assessment of Steel-Frames Buildings under Fires," John A. Blume Earthquake Engineering Center Technical Report No. 163.

Vassart, O., Zhao, B., Cajot, L.G., Robert, F., Meyer, U., and Frangi, A. (2014), "Eurocodes: Background & Applications Structural Fire Design," *JRC Science and Policy Reports*, European Union.

Vila Real, P.M.M., Lopes da Silva, N.L.S., and Franssen, J.M. (2007), "Parametric Analysis of the Lateral—Torsional Buckling Resistance of Steel Beams in Case of Fire," *Fire Safety Journal*, Vol. 42, pp. 461–524.

Wang, P., Wang, Y.C., and Li, G.Q. (2010), "A New Design Method for Calculating Critical Temperatures of Restrained Steel Column in Fire," *Fire Safety Journal*, Vol. 45, pp. 349–360.

Zhang, C., Choe, L., Seif, M., and Zhang, Z. (2015), "Behavior of Axially Loaded Steel Short Columns Subjected to a Localized Fire," *Journal of Constructional Steel Research*, Vol. 111, pp. 103–111.

Design for Local Member Shear at Brace and Diagonal-Member Connections: Full-Height and Chevron Gussets

RAFAEL SABELLI and BRANDT SAXEY

ABSTRACT

Large local member shear forces develop in beams in chevron-braced frames due to the delivery of brace forces to beam flanges, which are at a distance from the beam centerline (Fortney and Thornton, 2015, 2017; Hadad and Fortney, 2020). Using the "lower bound theorem" (Thornton, 1984), Sabelli and Arber (2017) developed design methods to address this local member shear by optimizing the internal stress distribution and thus maximizing the resistance utilized in design. This paper further develops those design methods for chevron beams and extends them to gusset connections at columns.

Keywords: gusset plates, braced frames, truss connections.

INTRODUCTION

The "chevron effect" is a term used to describe local beam forces in the gusset region of a chevron (also termed inverted-V) braced frame. These local forces are not captured by beam analysis methods that neglect connection dimensions. Fortney and Thornton (2015, 2017) and Hadad and Fortney (2020) have shown methods of analysis for these forces. This study adds design solutions for addressing high member shear in the connection region, including reinforcement and proportioning for (chevron) gussets within the beam span and for full-height gussets at beam-column-brace connections.

V-braced frames (and their variants) are commonly used in steel structures and are commonly termed "chevron-braced frames." Figure 1 shows three chevron configurations: the inverted-V-braced frame (a), in which two braces connect to the bottom of the beam at its midpoint; the V-braced frame (b), in which two braces connect to the top of the beam at its midpoint; and the two-story, X-braced frame (c), in which four braces connect to the beam at its midpoint, two from above and two from below.

The beams and columns of these frames are typically designed using centerline models, and equilibrium is addressed in the design at the "workpoint" (the intersection of member centerlines). In typical design, a substantial gusset plate is provided at brace connections, and force transfer is accomplished over the length of that plate. Figure 2 shows a frame with such gusset plates. Similar connections

Rafael Sabelli, Director of Seismic Design, Walter P Moore, San Francisco, Calif. Email: rsabelli@walterpmoore.com (corresponding)

Brandt Saxey, Technical Director, CoreBrace, West Jordan, Utah. Email: brandt.saxey@corebrace.com

Paper No. 2020-01R

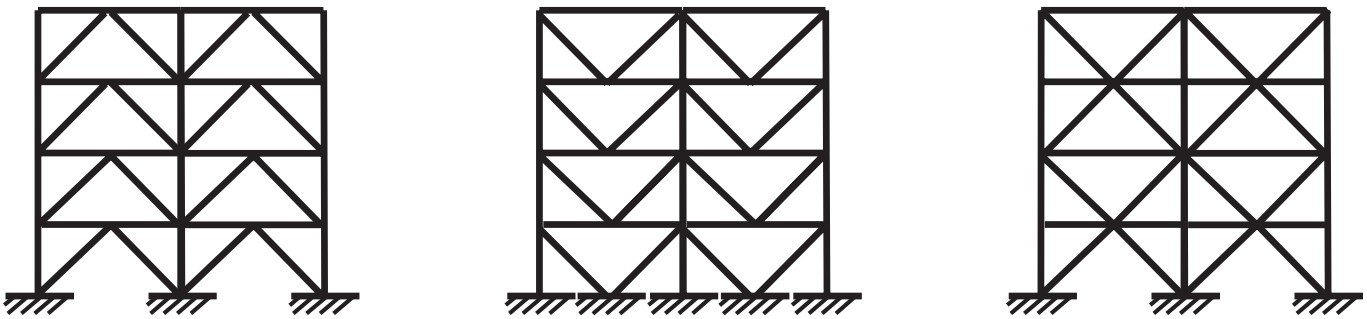

(a) Inverted-V-braced frame *(b) V-braced frame* *(c) Two-story, X-braced frame*

Fig. 1. Chevron-braced frame configurations.

are used in truss construction with web-vertical wide-flange chords (Figure 3).

Work by Fortney and Thornton (2015, 2017) and Hadad and Fortney (2020) highlights the importance of analysis of chevron braced-frame connections. In particular, Fortney and Thornton derive expressions for the local beam shear and moment that result from the distribution of brace forces over the gusset-plate length. These beam forces (in particular, the shear) can result in the need to supplement the beam web with a doubler plate. An example of such a condition is shown in the second edition AISC *Seismic Design Manual* (AISC, 2012). In the third edition *Seismic Design Manual* (AISC, 2018), the example connection utilizes some of the relationships developed by Sabelli and Arber (2017) to eliminate the need for reinforcement.

This study builds on the work of Sabelli and Arber, applying the same concepts developed by Fortney and Thornton, with the aim of providing methods for the design of connections that do not require reinforcement. The methods presented in this paper rely heavily on the "lower bound theorem" as presented by Thornton (1984) for similar connections, demonstrating adequate strength through investigation of an advantageous internal stress distribution in a ductile connection and examining forces at gusset edges and at critical sections.

This study also extends and generalizes the equations developed for chevron connections for use in other conditions, such as columns with full-height gussets (also called "mega-gussets") in which the gusset extends through the beam depth and the beam connects to the gusset rather than to the column (see Figure 4). In addition to transferring brace forces, full-height gusset connections transfer beam forces to the column. Such connections may be accomplished with welded beam flanges (as shown in Figure 4), which provide flexural continuity (and thus additional flexural forces to be transferred by the gusset to the column), or with a connection similar to a single-plate connection (also known as a "shear tab"), which minimizes these flexural forces. Adaptation of these methods to beam-column-brace connections with traditional gussets (Figure 5) is beyond the scope of this paper.

The first part of the paper derives the design equations employing statics and two models of stress distribution along the gusset-flange interface: the Uniform Stress Method, based on Fortney and Thornton (2015), and the Concentrated Stress Method, based on Sabelli and Arber (2017). The former model is simpler, but if that model indicates that reinforcement is required, significant economy can be realized by using the latter. The second portion of the paper is a brief design example that addresses both methods for the design of a chevron connection.

This study addresses both member shear and member moment caused by the local connection forces as these differ from the shears and moments from a simple, centerline model of members. In the authors' experience, the local member shear often controls the connection design (such as by necessitating a minimum gusset length), but the additional member moment caused by the local connection forces does not.

The design equations derived here are based on the static equilibrium of the gusset plate based on the brace axial forces (and beam reactions for the column connection). As such, they are equally applicable to frames designed as part of a ductile seismic system (in which brace forces typically correspond to the brace capacity), and those designed for wind or other cases that do not involve capacity design. Additional considerations for seismic design, such as determination of the appropriate brace force level for which beam yielding should be precluded, are beyond the scope of this paper.

Fig. 2. Typical braced frames with gussets.

Fig. 3. Truss with gussets.

Fig. 4. Full-height gusset brace connection at column.

Fig. 5. Traditional gusset at column.

SYMBOLS, NOMENCLATURE, AND CONVENTIONS

This study employs the following symbols and terms:

D_{clip} Diagonal dimension of reduced critical-diagonal-section length due to $Y_{clip,}$ in. (mm)

D_{crit} Length of critical diagonal section of gusset, in. (mm)

$F_{i,j}$ Brace axial force for brace "j" connecting to gusset "i," kips (N) (sign conventions are per the figures)

F_N Gusset concentrated force at member flange, transverse to member axis, kips (N) (compression is positive)

F_V Gusset shear component parallel to member axis at interface with flange, kips (N)

F_{Xcrit} Force parallel to the member axis acting on critical diagonal section of gusset, kips (N)

F_{Ycrit} Force transverse to member axis acting on critical diagonal section of gusset, kips (N)

F_y Specified minimum yield stress, ksi (MPa)

L_{beam} Beam length (column centerline to centerline), in. (mm)

L_g Gusset length, in. (mm)

L_w Length of weld, in. (mm)

M_{Bm} Beam moment transferred to gusset at column connection, kip-in. (N-mm)

M_{Ch} Chevron moment at face of member due to force F_V (equal and opposite to the distributed moment M_{FV} for concentric workpoints), kip-in. (N-mm)

M_{crit} Moment acting on critical diagonal section of gusset, kip-in. (N-mm)

M_f Moment at gusset-to-flange-interface due to brace forces, kip-in. (N-mm)

M_{FV} Moment in the connection due to force F_V, distributed along gusset length and eccentric to workpoint (equal and opposite to the chevron moment, M_{Ch}, for concentric workpoints), kip-in. (N-mm)

M_g Moment on a gusset section transverse to the member axis, kip-in. (N-mm)

M_M Member moment at workpoint due to loading other than from braces, kip-in. (N-mm).

M_n Nominal member or element flexural strength, kips (N)

M_{max} Maximum member moment (within connection region) due to brace forces, kip-in. (N-mm)

M_{Tot} Total moment acting on beam due to M_{f1} and M_{f2}, kip-in. (N-mm)

N_{Bm} Beam axial force transferred to gusset at column connection, kips (N)

N_g Normal force on a gusset section transverse to the member axis, kips (N)

P_n Nominal member or element axial strength, kips (N)

R_u Required strength, kips (N)

R_z Normal force from moment transfer for Concentrated Stress Method, kips (N)

V_{Bm} Beam connection shear transferred to gusset at column connection, kips (N)

V_{Ch} Chevron shear, equal to the sum of member shear and gusset shear transverse to member axis, kips (N)

V_{ef} Effective member shear strength (deducting demands other than brace connection forces), kips (N)

V_{efTot} Effective member shear strength considering the effects of unbalanced forces from gussets on both sides of the member, kips (N)

V_g Shear on a gusset section transverse to the member axis, kips (N)

V_M Member shear due to loading other than from braces, kips (N)

V_{ma} Member shear (outside connection region), kips (N)

V_{mc} Member shear (within connection region), kips (N)

V_n Nominal member or element shear strength, kips (N)

W Width of brace-to-gusset connection used to locate critical diagonal section, in. (mm)

X_{crit} Dimension parallel to the member axis used to locate critical diagonal section, in. (mm)

Y_{clip} Dimension transverse to member axis of gusset corner clip, in. (mm)

d_m Member depth, in. (mm)

d_g Gusset dimension transverse to member axis, in. (mm)

e_{crit} Location of force F_{Ycrit} with respect to intersection of critical diagonal section and gusset edge, in. (mm)

e_g Eccentricity parallel to member axis of gusset midpoint from workpoint (e.g., beam centerline at column connection), in. (mm)

e_m Transverse eccentricity from member flange to workpoint, typically equal to half the member depth, in. (mm)

e_z Length of moment arm between centroids of z regions, in. (mm)

k Distance from outer face of flange to web toe of fillet, in. (mm)

r_u Required strength per unit length, kips/in. (N/mm)

t_g Gusset thickness, in. (mm)

t_w Member web thickness, in. (mm)

w Weld size, in. (mm)

x Distance from gusset midpoint along member axis, in. (mm)

z Length of concentrated stress region at ends of gusset, in. (mm)

γ Brace angle from member longitudinal axis, deg

ϕ_b Resistance factor for bending (0.9)

ϕ_c Resistance factor for compression (0.9)

ϕ_n Resistance factor for nonductile limit states such as web crippling and weld rupture (0.75)

ϕ_t Resistance factor for tension (0.9)

ϕ_w Resistance factor for web local yielding (1.0)

ϕ_v Resistance factor for shear (1.0)

Subscripts are employed in some equations to distinguish actions and dimensions related to one gusset or one brace from another. Gussets are designated "1" and "2," and dimensions and forces associated with each gusset are given the corresponding subscript. The subscript "*Tot*" refers to total forces, combining those from gusset "1" and gusset "2."

Brace axial forces have two subscripts. The first pertains to which gusset the brace connects to ("1" or "2"). The second pertains to which of the two braces is indicated. Sign conventions match the figures such that positive brace axial forces $F_{1,2}$ and $F_{2,1}$ correspond to compression and positive brace axial force $F_{1,1}$ and $F_{2,2}$ correspond to tension. Forces and angles pertaining to each brace carry the same designation subscript.

The design equations are presented in a general form such that they can be used for both column and beam gussets. To permit this, certain general terms are used, such as "member" in lieu of "beam" or "column." This approach carries through to the symbols.

Brace-force components acting on the gusset–member interface are described as (gusset) "shear" or "normal" forces. Gusset shear forces, F_V, are parallel to the member axis (horizontal for the chevron beam and vertical for the column); normal forces on the connection, F_N, are perpendicular to the member axis (vertical for the chevron beam and horizontal for the column).

The term "workpoint" refers to the intersection of brace centerlines with each other or with the column centerline. This workpoint is typically also at the beam centerline.

Figure 6 shows dimensions noted on beam and gusset-plate diagrams. Braces may occur above the beam, below the beam, or both. The diagram shows a symmetrical condition, but the connection calculations apply for asymmetrical cases. (Beam shear and moment require adjustment for asymmetrical applications.) Figure 7 shows dimensions noted on column and gusset-plate diagrams. Braces may occur in various combinations, and the column may continue up past the connection or may terminate as shown in the upper diagram. The diagram shows a full-height gusset: a gusset plate that comes between the beam and the column.

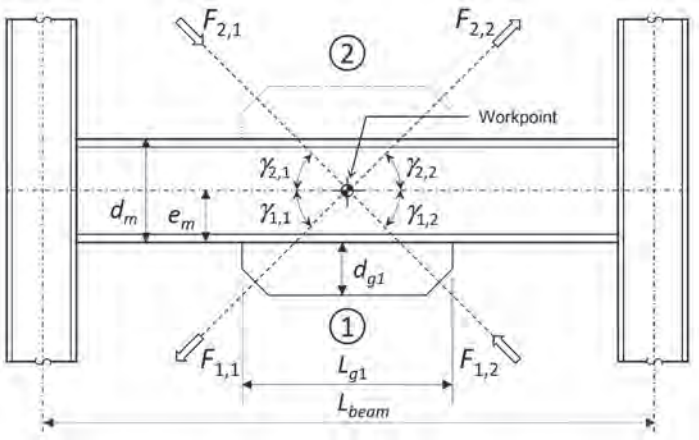

Fig. 6. Chevron gusset geometry.

STATICS

Although the methods developed in this paper are intended to facilitate the design of connections of multiple members (such as is shown in Figure 7), in essence the methods simply provide designers with the means of designing an attachment to a wide-flange member (such as is shown in Figure 8) for a set of known, in-plane forces, converting these to a normal force transverse to the member axis, F_N, a shear force parallel to the member axis, F_V, and a moment in the plane of the web, M_f. The design of this connection includes evaluation of local limit states within the member, including web local yielding, web crippling, and local shear. This local shear (in the gray zone in the center diagram in Figure 8) is essentially panel-zone shear, and determination of the effective depth of the force couple is central to the design methods presented. The right-hand diagram in Figure 8 illustrates that while the member flange and bracket rotate in unison, the panel-zone section of the member web can undergo large shear strains while the bracket remains elastic, and thus the member can yield in shear even if there is a substantial bracket present. The shear strength of the member is not increased by the addition of the bracket shear strength; a thicker or wider bracket would not preclude panel-zone shear yielding. Instead, the shear demand on the member panel zone can be reduced by using a bracket that extends further along the flange, thus increasing the height of the panel zone.

The same reconstitution of forces is applicable to braced-frame and truss connections, assuming the forces in the connecting members are known. The analysis and design of braces and truss diagonals is typically based on their idealization as pin-pin members. In some cases, this idealization could be modified to permit reduction of the moment M_f (which causes the panel-zone shear in the connection); this introduces design moments for both the main member and the diagonals, and thus requires an integration of member design and connection design.

Figure 9 shows free-body diagrams of the gusset plate at the beam midspan; Figure 10 shows the same at the column. Both figures convert a known set of in-plane forces acting on the gusset plate from connecting members into three forces at the midpoint of the gusset-flange interface: normal force transverse to the member axis, F_N, shear force parallel to the member axis, F_V, and moment in the plane of the web at the face of the member, M_f. The brace forces used for the connection design typically do not include moments, although these could be included in determining the gusset forces.

LOCAL MEMBER FORCES (DERIVATION FOR TWO BRACES)

For simplicity, only two braces are considered in the subsequent derivation: those on "side 1" of the connection. A later section shows the procedure for the inclusion of the effects of an additional gusset on the far side (side 2). These braces may be at equal angles (as is typical for the beam case) or at unequal angles (as happens frequently for the column case

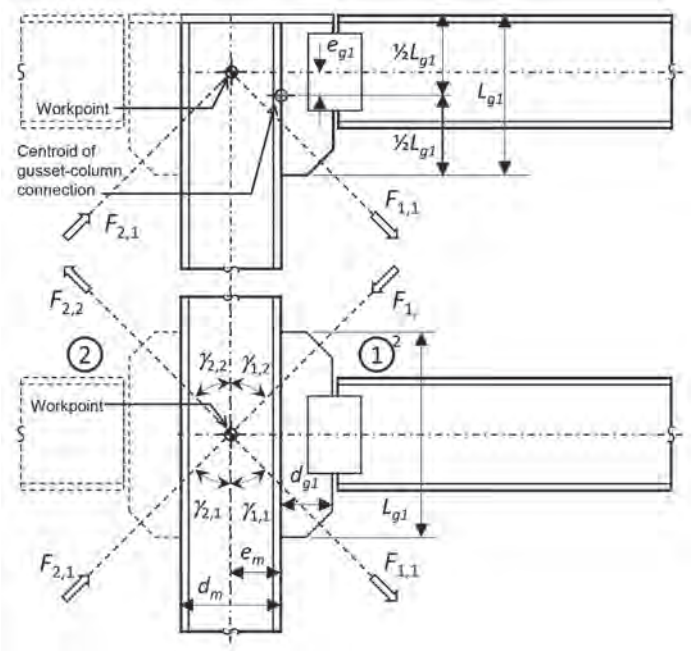

Fig. 7. Column gusset geometry.

and, on occasion, in the beam case). The design equations are presented in general terms applicable to both the beam and the column condition. Minor adjustments to the equations are required for the column case due to the additional forces from the connecting beams; these are noted.

The forces on the gusset-to-flange interface are statically determined. For clarity, brace forces are separated into normal, F_N, and shear, F_V, components. For the column connection, these forces are combined with forces from the beam: V_{Bm}, N_{Bm}, and M_{Bm}, as shown in Figure 10. (For the case of a beam chevron connection, these forces are all zero.) Assuming two braces with forces $F_{1,1}$ and $F_{1,2}$, the shear force is:

$$F_{V1} = F_{1,1}\cos\gamma_{1,1} + F_{1,2}\cos\gamma_{1,2} + V_{Bm1} \tag{1}$$

The normal force is:

$$F_{N1} = F_{1,2}\sin\gamma_{1,2} - F_{1,1}\sin\gamma_{1,1} + N_{Bm1} \tag{2}$$

For the column connection, the collector force N_{Bm1} should be determined from an analysis consistent with brace forces used in the connection design.

In addition to these normal and shear forces, there is a moment (required for static equilibrium). While the moment due to the brace forces is zero at the workpoint, at the flange the moment is:

$$M_{f1} = M_{Ch1} - M_{Bm1} \tag{3}$$

The first term in Equation 3, M_{Ch1}, is the "chevron moment" at the member face. This moment may be conceptualized by considering the forces from the two braces as applied point loads at the locations where their centerlines intersect the member flange. If the brace forces are decomposed into components parallel to and normal to the member axis (Figure 11), the chevron moment can be determined from the normal force components and their eccentricities along the member axis:

$$M_{Ch1} = \left[F_{1,1}\sin(\gamma_{1,1})\right]\left[\frac{e_m}{\tan(\gamma_{1,1})}\right] + \left[F_{1,2}\sin(\gamma_{1,2})\right]\left[\frac{e_m}{\tan(\gamma_{1,2})}\right] \tag{4}$$

which reduces to:

$$M_{Ch1} = F_{V1}e_m \tag{5}$$

The chevron moment is opposed by a moment, M_{FV1}, that corresponds to the parallel components, F_{V1}, multiplied by the eccentricity of the flange from the centerline ($\frac{1}{2}d_m$):

$$M_{FV1} = \left[F_{1,1}\cos(\gamma_{1,1}) + F_{1,2}\cos(\gamma_{1,2})\right]\frac{d_m}{2} = \frac{F_{V1}d_m}{2} \tag{6}$$

which can be simplified to:

$$M_{FV1} = \frac{F_{V1}d_m}{2} \tag{7}$$

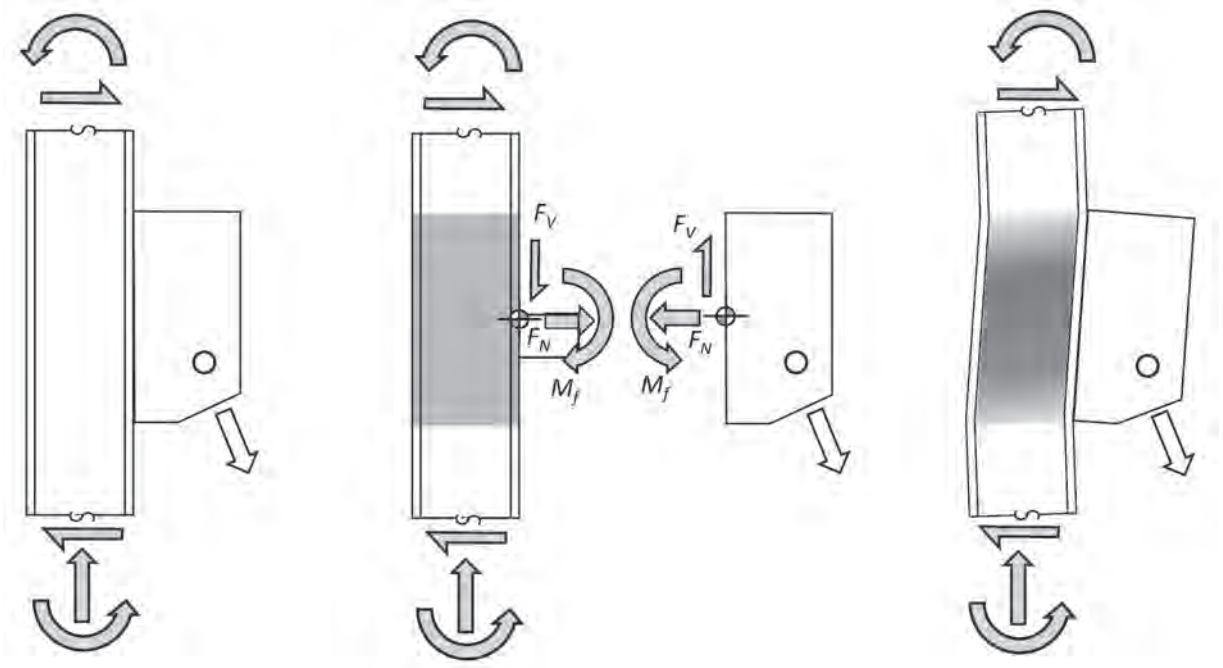

Fig. 8. Free-body diagram of bracket.

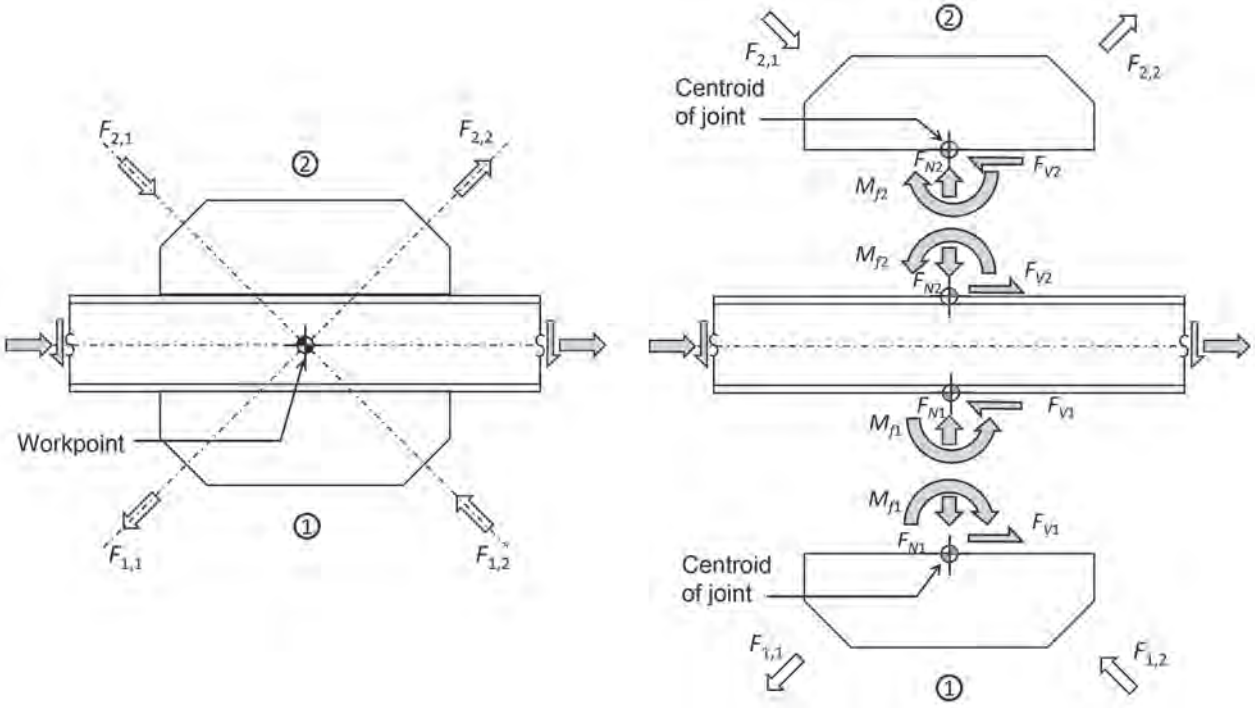

Fig. 9. Force conventions for chevron connection.

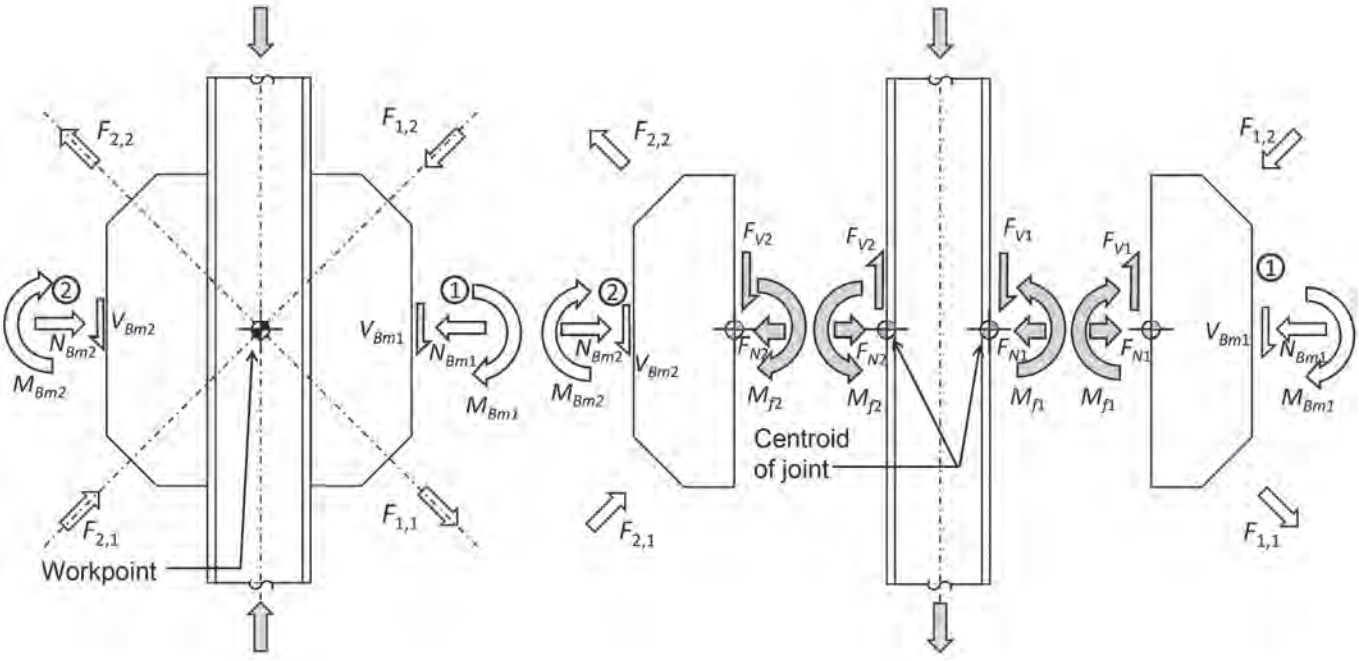

Fig. 10. Force conventions for column connection.

This moment does not affect the gusset or the weld but is necessary for member equilibrium and affects member moment. If the workpoint is at the member centerline (as shown in Figure 9), the distance from the flange to the workpoint, e_m, is:

$$e_m = \frac{d_m}{2} \text{ for the workpoint at the member centerline} \quad (8)$$

If this is the case, the two brace-shear-component-induced moments are equal and opposite ($M_{Ch1} - M_{FV1} = 0$), and there is effectively no moment at the workpoint location on the member centerline due to F_{V1}. If the workpoint is off the member centerline (as shown in Figure 11), the braces induce a moment in the member at the centerline location aligned with the workpoint; this moment causes shear and bending both within and outside of the connection region. Moving the workpoint from the main member centerline toward the gusset reduces the chevron moment while introducing a moment into the main member. In general, such an approach can be economical but requires coordination with member design and building analysis. Similarly, the connection analysis could assign only a portion of this chevron moment to the main member and apply the remainder to the braces. This might reduce the connection demands but would introduce additional design moments into both the main member and the braces, and this member flexure could, in principle, affect the building response to lateral loads. The former approach (modifying the work point) can be integrated with the methods presented in this paper, but the latter approach (assigning counterbalancing moments to the main member and the braces) is separate.

For the column connection, the beam moment, M_{Bm1}, affects the moment at the column flange, M_{f1}. This moment (M_{Bm1}) should be consistent with the brace forces, and the minus sign reflects the direction of forces in Figure 10. Typically, both the beam moment and the brace force are due to the lateral drift. In such cases, the signs are consistent with those shown in Figure 10; when the brace is in compression, the corresponding beam flange is in tension, and vice versa, and thus M_{f1} in Equation 3 is the difference rather than the sum. (The corresponding column shear is additive to the brace forces as discussed later.) Because the effect of the beam moment M_{Bm1} is to reduce the total demand, designers should consider how much of this beneficial effect can be relied on, and a range of this moment could be considered.

For the case of an asymmetric column gusset (such as with only one brace, as shown in the upper diagram of Figure 7), the eccentricity between the gusset midpoint and the beam centerline contributes to the moment:

$$M_{f1} = F_{V1}e_m - M_{Bm1} + F_{N1}e_g \quad (9)$$

A similar adjustment can be made for chevron beams if the gusset midlength and the workpoint are not aligned vertically.

In addition to the "chevron moment," there is a "chevron shear." The chevron shear (V_{Ch1}) is resisted by the gusset and the beam in combination:

$$V_{Ch1} = V_{g1} + V_{mc1} \quad (10)$$

This chevron shear can be determined using static equilibrium on either half segment of the gusset:

$$V_{Ch1} = F_{1,1}\sin\gamma_{1,1} + \frac{1}{2}F_{N1} \quad (11)$$

$$V_{Ch1} = F_{1,2}\sin\gamma_{1,2} - \frac{1}{2}F_{N1} \quad (12)$$

Figure 12 shows a free-body diagrams of beam and gusset segments at the connection, including a transverse section through the beam and gusset showing the sharing of the chevron shear (V_{Ch1}) between the beam shear (V_{mc1}) and the gusset transverse shear (V_{g1}). Note that the location of the centroid of the transverse forces from the gusset segment to the beam flange ($V_{mc1} \pm \frac{1}{2}F_{N1}$) is not specified in the free-body diagrams of the gusset segments; that location may be selected (within certain constraints) in the connection design by the use of a stress distribution model, such as the Elastic Method, the Plastic Method, or the Optimized Plastic Method as described in Section 8 of the AISC *Steel Construction Manual* (2017). Once this location

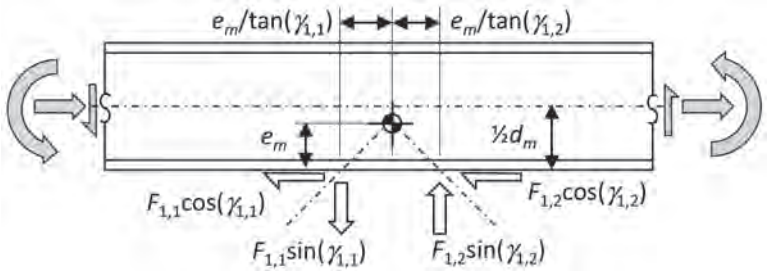

Fig. 11. Brace forces at flange.

is set, the division of V_{Ch1} between V_{mc1} and V_{g1} is statically determined. (Moment at the vertical gusset section is zero, regardless of the stress distribution, for symmetrical conditions with equal brace forces, as shown in the subsequent section, "Gusset Design: Mid-Length Transverse Section.")

The same relationship applies to full-height column gussets. As will be shown in the following sections, the sharing of this chevron shear between the gusset and the beam or column can be controlled by a combination of the gusset dimension selected and the force distribution assumed at the gusset-to-flange interface. In this way, the design methods presented can reduce or eliminate any required web reinforcement.

UNIFORM STRESS METHOD

The Uniform Stress Method is the simplest model for addressing the chevron effect, both for discussion and design purposes. While the treatment of this method here is general, it does not specifically address conditions such as beams with workpoints not at the beam midspan; Fortney and Thornton (2017) provide a more thorough treatment. [The term "Uniform Stress Method" is not employed by Fortney and Thornton. Sabelli and Arber use this term; Hadad and Fortney refer to it as the "Chevron Effects (CE) Method." The term "Uniform Stress Method" has been used in practice and so is used here.]

Fortney and Thornton (2015, 2017) employ the Uniform Stress Method for the transfer of forces over the length of a chevron gusset. In this method, the moment transfer is achieved through two blocks of principal stress in the gusset, each with a length equal to half that of the gusset, as in the "plastic method stress distribution" described in the AISC *Steel Construction Manual*. Figure 13 shows the Uniform Stress Method applied to the column and chevron connections.

Member Shear

Stresses at the member-to-gusset interface are assumed to be distributed uniformly using the full length for the normal and shear forces and a plastic-section-modulus approach for the moment (Fortney and Thornton, 2015). Following this approach, the member shear within the connection region is described by the following equation:

$$V_1(x) = -\frac{2M_{f1}}{L_{g1}} + \frac{4M_{f1}}{L_{g1}^2}|x| + \frac{F_{N1}}{L_{g1}}x + V_M \tag{13}$$

The first two terms are the shear due to the gusset moment, which includes the chevron moment, M_{Ch}, plus any other moment transmitted by the gusset per Equation 3. The third term in the equation is the shear from the unbalanced normal force, and the value at the gusset end ($F_{N1}/2$) is the shear in the member outside of the gusset region for the typical, symmetrical case with $V_M = 0$.

In this equation, x is the distance from the gusset midpoint, as shown in Figure 13. This differs from Fortney and Thornton but is presented in this manner to facilitate combination of forces from gussets of different lengths on opposite flanges of the main member. The member shear is additive for connections with gussets on opposite sides for the typical braced-frame case (with forces as shown in Figures 9 and 10), although the member shear V_M should only be added once. (Hereafter, it is assumed that the member shear V_M is zero in the connection region.)

The maximum shear in the connection region occurs at the gusset midpoint ($x = 0$) and is equal to:

$$V_{mc1} = \frac{2M_{f1}}{L_{g1}} \tag{14}$$

This shear, V_{mc1}, is not equal to the chevron shear, V_{Ch1}, nor to a trigonometric component of either of the brace forces

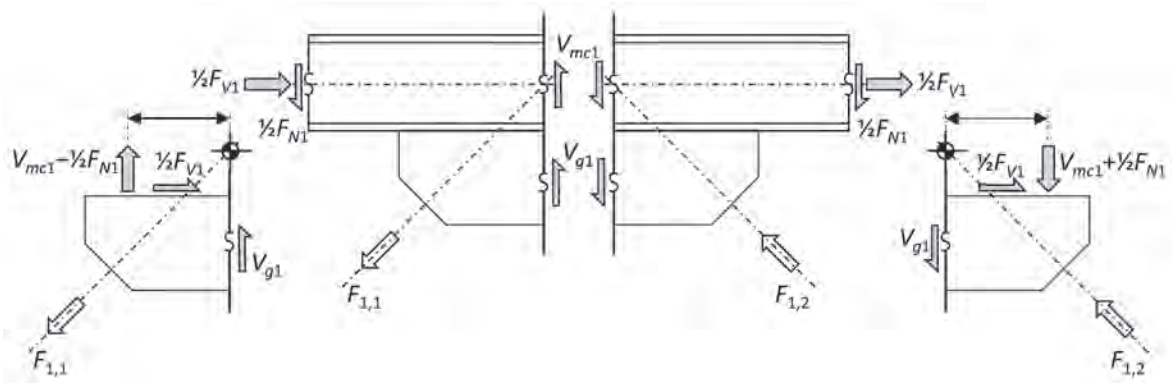

Fig. 12. Transverse section of beam and gusset showing chevron shear.

(e.g., $F_{1,1}\sin\gamma_{1,1}$ or $F_{1,2}\sin\gamma_{1,2}$); it may be greater or smaller than the trigonometric component, depending on the geometry of the connection. The difference between the two is the shear carried by the gusset, V_{g1}, as indicated in Equation 10. The longer the gusset plate, the lower the shear in the main member due to the chevron moment, V_{mc1}, and thus the greater the shear resisted by the gusset, V_{g1}. This is similar to a moment connection in which beam haunches can be used to engage a larger column panel-zone height. In this sense, the gusset plate can be used as external shear reinforcement for the beam, although in this method, it is the length of the gusset that permits it to provide a larger arm for transfer of the chevron moment (and thus reduce the force imposed on the main member) rather than a simple addition of member and gusset shear strength.

Note that this member shear in Equation 14, V_{mc1}, is due only to the force components parallel to the member axis (shear on the connection). The unbalanced normal component does cause shear in the member, but this unbalanced-component shear becomes zero at the workpoint and thus is not considered in conjunction with shear from the balanced component (i.e., the shear from Equation 14). Figure 14 shows a shear diagram for brace-induced shears in a typical pin-end beam consistent with Equation 13.

Note that the maximum member shear occurs at the gusset midpoint (where the member shear neglecting connection effects is zero), and thus the member shear outside of the connection does not affect the maximum shear in the connection region. Concentrated loads within the connection region should be considered by reducing the available shear strength or by engaging the gusset to distribute the load over the gusset length along with the normal force, F_{N1}.

The member shear is the result of both the eccentricity (typically a function of the member depth) and the gusset length. These can be adjusted (within practical bounds) to provide a member that does not require web strengthening. Following this approach, the minimum gusset length to eliminate web strengthening is:

$$L_{g1} \geq \frac{2M_{f1}}{\phi_v V_n} \tag{15}$$

which is equivalent to:

$$L_{g1} \geq \frac{2F_{V1}e_m}{\phi_v V_n} \tag{16}$$

A subsequent section addresses member selection to avoid web reinforcement.

Concentrated Forces

The limit states of web local yielding and web crippling typically can be satisfied without reinforcement at chevron connections, especially those designed using the Uniform Stress Method. These limit states can be evaluated considering two concentrated forces (R_u), each acting on a bearing length of $\frac{1}{2}L_g$:

$$R_{u1} = \frac{F_{N1}}{2} \pm \frac{2M_{f1}}{L_{g1}} \tag{17}$$

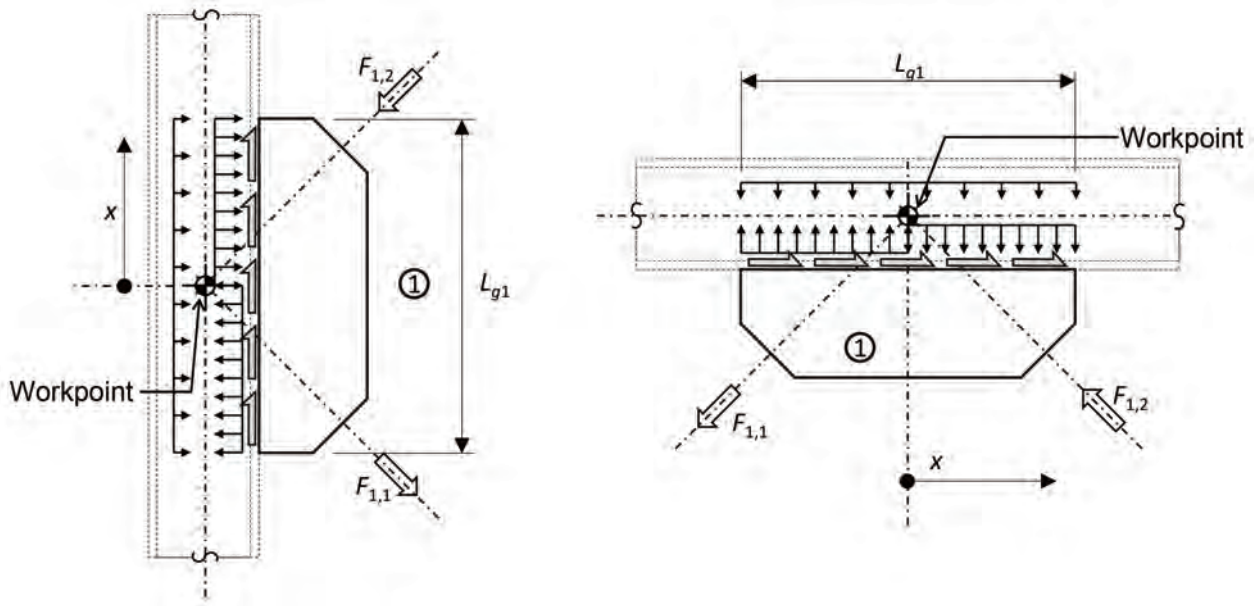

Fig. 13. Uniform Stress Method (after Fortney and Thornton).

Moment

Shear forces in the member have an effect on member moment. While this effect is generally small, Fortney and Thornton (2015) describe conditions in which the beam moment determined using these assumptions (if not considered in design) may necessitate reinforcement using the Uniform Stress Method. Hadad and Fortney (2020) show that in finite element analyses, the beam moments are substantially lower than those calculated using the Uniform Stress Method. While the authors do not propose evaluation of the member moment within the connection region as necessary, examination of the effects that contribute to the moment may aid in understanding of the method.

Beam Moment

In the case of a chevron beam, braces are often considered to be a support point for the beam for wind design. For seismic design of ductile systems, the expected behavior typically entails brace yielding with resulting transverse loading of the beam causing beam shear and bending. [See, for example, AISC *Seismic Provisions* Section F2.3(b).] The beam is evaluated for these forces (adding any gravity loading effects) in combination with the axial force resulting from the components of brace force parallel to the member axis. The combined effect of the moment M_{f1} and the brace force components parallel to the member axis, F_{V1}, produces no shear or flexure outside of the connection region.

For the chevron beam connection, $M_{Bm} = 0$, and thus $M_f = M_{Ch}$. Beam moments within the connection region are described by the following equation:

$$M_1(x) = -\frac{2M_{Ch1}}{L_{g1}}x + \frac{2M_{Ch1}}{{L_{g1}}^2}|x|x - \frac{M_{FV1}}{L_{g1}}x - F_{N1}\left(\frac{L_{beam}}{4} - \frac{L_{g1}}{8} - \frac{x^2}{2L_{g1}}\right) \quad (18)$$

Note that Equation 18 includes more than the integral of the member shear formula (Equation 13). It also includes a distributed moment due to the applied force parallel to the member axis, F_{V1}, at the gusset–flange interface (which, for simplicity, is assumed to be uniformly distributed along the length of the gusset):

$$\frac{M_{FV1}}{L_{g1}} = \frac{F_{V1}e_m}{L_{g1}} \quad (19)$$

Thus:

$$\frac{M_{FV1}}{L_{g1}} = \frac{M_{Ch1}}{L_{g1}} \quad (20)$$

The applied force parallel to the member axis, F_{V1}, thus has two equal and opposing effects: the transverse stress resulting from M_{Ch}, which causes member shear and moment, and the distributed moment corresponding to M_{FV}. These counteracting effects produce zero moment at the ends of the connection region and at the gusset midlength; at other locations, some moment may result based on the differing rates of accumulation over length within the connection region, corresponding to the assumed transverse stress distribution and the assumed distribution of F_{V1} over the gusset length.

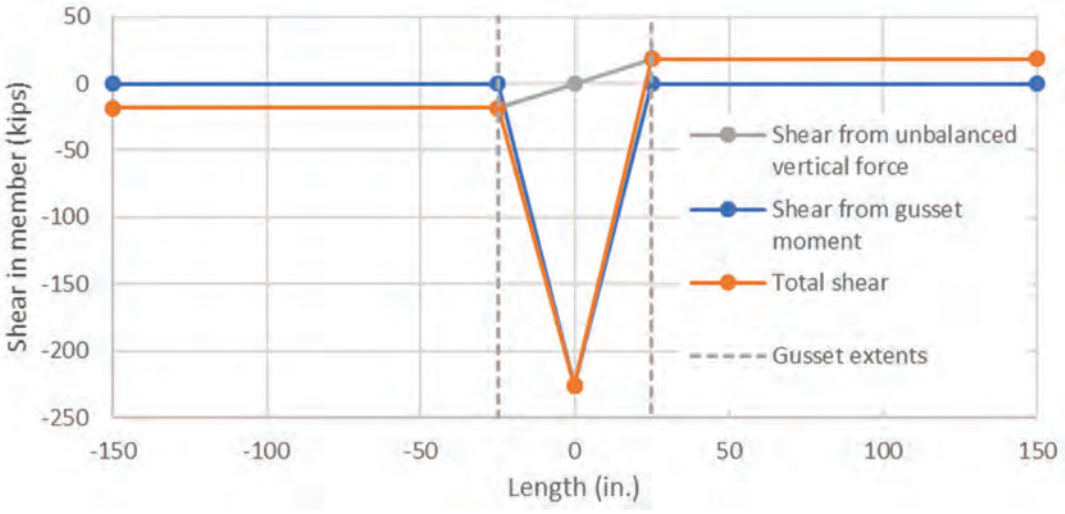

Fig. 14. Brace-induced shears in pin-end beam (Uniform Stress Method).

Equation 18 simplifies to:

$$M_1(x) = -\frac{F_{V1}e_m}{L_{g1}}\left(x - \frac{2}{L_{g1}}x|x|\right) - F_{N1}\left(\frac{L_{beam}}{4} - \frac{L_{g1}}{8} - \frac{x^2}{2L_{g1}}\right) \tag{21}$$

Nonuniform distributions of transfer of the shear force F_V from the gusset to the beam are also admissible, including distributions that minimize or eliminate the local moment effect $M_{Ch}(x) - M_{FV}(x)$. However, the authors have found such approaches unnecessary for demonstrating beam adequacy and, at times, uneconomical for the gusset weld.

A simplified equation can be used to provide a liberal estimate of the maximum brace-induced moment in the beam:

$$M_{max1} \le \left|\frac{F_{V1}e_m}{8}\right| + \left|F_{N1}\left(\frac{L_{beam}}{4} - \frac{L_{g1}}{8}\right) + M_M\right| \tag{22}$$

where M_M is the member moment neglecting brace forces (typically due to gravity). This equation simplifies the determination of moment, providing a liberal upper bound by combining two maxima: the beam moment corresponding to the local shear, $M_{f1}/8$, which occurs at the gusset quarter point, and the midspan moment due to the unbalanced normal force (the second term) and any other beam loading, M_M. (The idealization of the unbalanced normal force as a point load rather than distributed over the gusset length also slightly overestimates the moment.) For the typical braced-frame case (with forces as shown in Figures 9 and 10), the moments from the two gussets are additive, with M_M being added only once.

The first term in Equation 22, $M_{f1}/8$, is a local effect of the connection geometry and is typically small, corresponding to a small eccentricity for the axial force in the beam (which is typically $F_{V1}/4$ at the gusset quarter point).

Column Moment

The column is not required to span to resist the unbalanced brace forces. The column moment in the connection region for the Uniform Stress Method is similar to that from Equation 22:

$$M_{max1} \le \left|\frac{F_{V1}e_m}{8}\right| + |M_M| \tag{23}$$

The effect of any moment M_{Bm} on the member moment is captured in the term M_M, conservatively taken at its full value at the quarter point (where the effect of F_V is at its maximum).

The column moment is typically permitted to be neglected in capacity-design calculations for seismic loads per AISC *Seismic Provisions* D1.4a (AISC, 2016a). For other braced-frame cases this moment is typically very small. The design shear forces outside the connection region are not generally large, especially for frames with pin-ended beams.

CONCENTRATED STRESS METHOD

In the preceding discussion, the Uniform Stress Method stress distribution was assumed to determine the member forces in the connection region. The calculated member shear may be reduced by selecting a more favorable distribution. The Concentrated Stress Method maximizes the moment arm within a given gusset length and thus minimizes the corresponding force caused by the moment. This method is based on the Optimized Plastic Method (AISC, 2017), modified to optimize only for moment resistance (rather than both moment and normal force) and to allow for incorporation of design limits based on both gusset yield and member limit states.

In the Concentrated Stress Method, the moment M_{f1} is assumed to be transferred at the ends of the gusset over lengths z_1. The remaining segment in the middle of the gusset does not participate in transmitting the flexure; it is assumed to resist the unbalanced force F_{N1}. Figure 15 shows this stress distribution.

Member Shear and Minimum Gusset Length

The Concentrated Stress Method converts the moment M_{f1} into a normal force couple R_{z1} with a moment arm of e_{z1}. This normal force R_{z1} is distributed over a length z_1. The values of R_{z1} and e_{z1} are determined such that R_{z1} does not exceed the force that would cause shear yielding of the member.

Figure 16 shows a shear diagram corresponding to this stress distribution for a chevron connection. Note that the maximum beam shear in the Concentrated Stress Method does not occur at the beam midpoint (as it does for the Uniform Stress Method), and thus the beam shear outside of the connection affects the maximum shear within the connection region.

The moment arm e_{z1} is:

$$e_{z1} = L_{g1} - z_1 \tag{24}$$

The normal force from the moment transfer is thus:

$$R_{z1} = \frac{M_{f1}}{e_{z1}} \tag{25}$$

$$R_{z1} = \frac{M_{f1}}{L_{g1} - z_1} \tag{26}$$

This normal force causes shear in the member. For beams, the maximum shear is a combination of the shear due to the unbalanced force and the shear due to delivery of

the chevron moment. The maximum shear is given by the following equation:

$$V_{mc1} = V_{ma1} + R_{z1} \tag{27}$$

The shear outside of the connection region, V_{ma1}, is due to net normal force, F_{N1}, and the member shear from gravity or other sources, V_M:

$$V_{ma1} = \frac{1}{2} F_{N1} + V_M \tag{28}$$

The shear V_M is typically zero adjacent to (and within) the connection region for beams.

If the gusset is long enough, the total connection shear V_{mc} may be set less than or equal to the design shear strength of the member in order to preclude the need for shear reinforcement. For a given gusset length, the maximum moment transfer can be achieved by the highest concentration of stress at the ends. For a minimum gusset length, stiffeners at the gusset edges may be used to create a moment arm

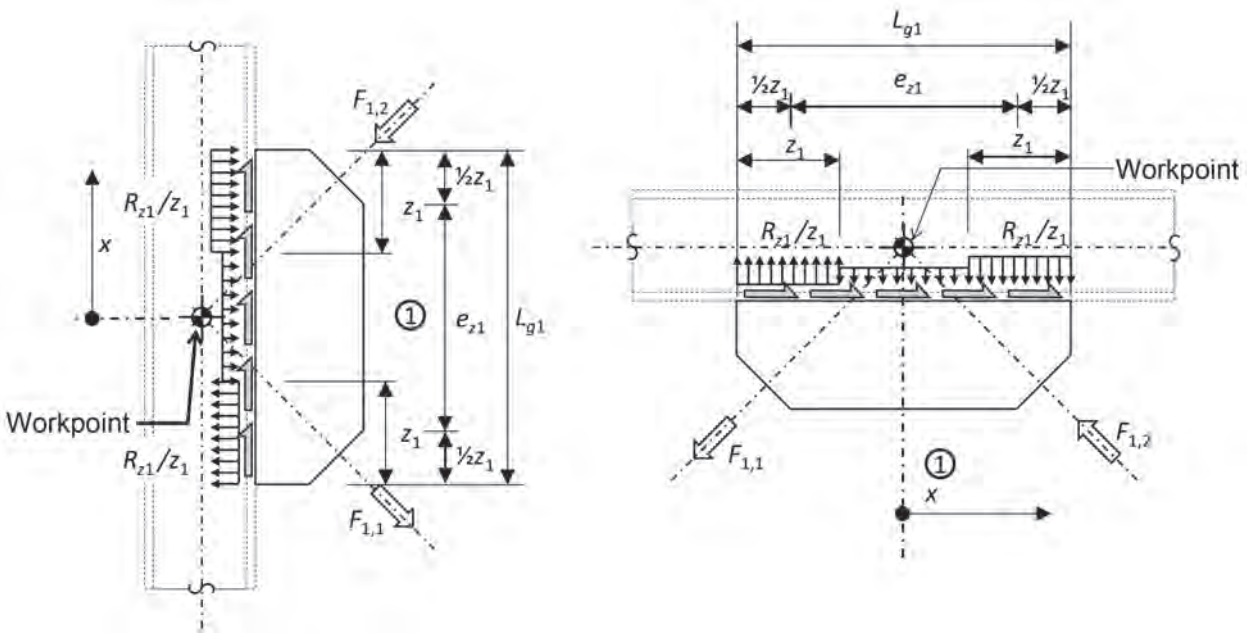

Fig. 15. Stress distribution for the Concentrated Stress Method.

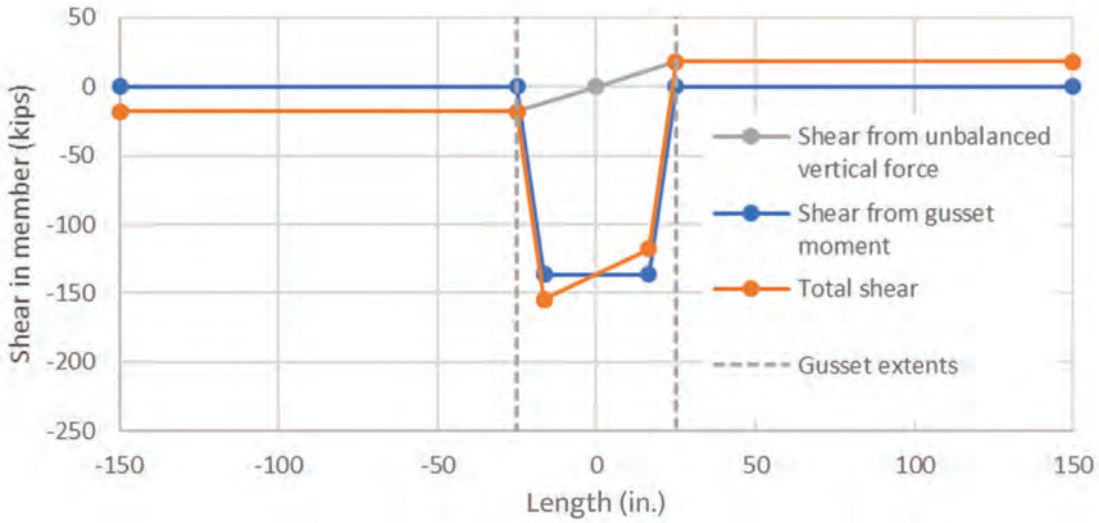

Fig. 16. Brace-induced shear in pin-end beam with Concentrated Stress Method.

equal to the gusset length L_{g1}, similar to a moment connection in which beam flanges deliver moment to the face of a column. For the more typical chevron-moment transfer via the gusset plate, the concentrated stress may be limited by web local yielding, web crippling, or the gusset yielding.

If the gusset length is minimized (without stiffeners), the concentrated stress will be maximized such that the full member shear strength is utilized. Unlike the Uniform Stress Method, in the Concentrated Stress Method the maximum member shear is maintained over a significant portion of the connection length, and thus (for beams) occurs at locations that also have shear induced by the unbalanced normal force from braces. Considering that some of the shear strength is utilized in resisting this unbalanced force, the remaining member shear strength that can be utilized for the moment transfer is:

$$V_{ef1} = \phi_v V_n - V_{ma1} \tag{29}$$

For designs with a gusset on the opposite flange, both the design shear strength (ϕV_n) and the net shear outside the connection ($V_{ma1} - V_{ma2}$) can be apportioned between the two gusset designs. This is addressed in a later section.

The Concentrated Stress Method is derived such that the maximum shear from Equation 26 does not exceed the effective shear strength from Equation 29:

$$R_{z1} \le V_{ef1} \tag{30}$$

The minimum gusset length possible corresponds to the use of stiffeners (flanges) to transfer the moment M_{f1}. Thus as z_1 approaches zero, Equation 26 (combined with Equation 30) gives the minimum gusset length dimension:

$$L_{g1} = \frac{M_{f1}}{V_{ef1}} \ for\ z_1 = 0 \tag{31}$$

Without such stiffeners, there is a finite length of gusset z_1 over which the force R_{z1} is transferred to the beam. The minimum length z_1 may be governed by the limit states of web local yielding, web crippling, or yielding of the gusset. For web local yielding, AISC *Specification* Equation J10-2 (AISC, 2016b) can be rearranged to solve for the minimum bearing length z_1:

$$z_1 \ge \frac{R_{z1}}{\phi_w w F_y t_w} - 5k \tag{32}$$

The corresponding minimum gusset length based on the web local yielding limit state is:

$$L_{g1} \ge e_{z1} + z_1 \tag{33}$$

Combining Equations 24, 32, and 33:

$$L_{g1} \ge \frac{M_{f1}}{R_{z1}} + \frac{R_{z1}}{\phi_w F_y t_w} - 5k \tag{34}$$

This length is minimized by taking the maximum normal force R_{z1} that the member can resist based on its effective shear strength per Equation 30.

Considering combined shear and tension in the gusset, the minimum gusset thickness corresponding to the minimum length selected using Equation 34 and the maximum normal force R_{z1} (equal to V_{ef1}) is determined using the von Mises yield criterion, with shear stress over the full gusset length and the moment delivered by a force couple.

A gusset that satisfies this criterion is required:

$$t_{g1} \ge \sqrt{\left(\frac{F_{V1}}{\phi_v 0.6 F_y L_{g1}}\right)^2 + \left(\frac{R_{z1}}{\phi_t F_y (L_{g1} - e_{z1})}\right)^2} \tag{35}$$

which is equivalent to:

$$t_{g1} \ge \sqrt{\left(\frac{F_{V1}}{\phi_v 0.6 F_y L_{g1}}\right)^2 + \left[\frac{R_{z1}}{\phi_t F_y \left(L_{g1} - \frac{M_{f1}}{R_{z1}}\right)}\right]^2} \tag{36}$$

The center zone may be similarly examined, although generally this zone is much less stressed:

$$t_{g1} \ge \sqrt{\left(\frac{F_{V1}}{\phi_v 0.6 F_y L_{g1}}\right)^2 + \left(\frac{F_{N1}}{\phi_t F_y (L_{g1} - 2z_1)}\right)^2} \tag{37}$$

which is equivalent to:

$$t_{g1} \ge \sqrt{\left(\frac{F_{V1}}{\phi_v 0.6 F_y L_{g1}}\right)^2 + \left[\frac{F_{N1}}{\phi_t F_y \left(\frac{2M_{f1}}{R_{z1}} - L_{g1}\right)}\right]^2} \tag{38}$$

If the required gusset thickness is excessive, a longer gusset may be employed. The gusset length required for a given gusset thickness is the root of a fourth-power polynomial, for which various solution methods are available, including trial-and-error and computer solvers. A closed-form solution may also be derived using Ferrari's formula (Euler, 1765). A simple approximate formula can be obtained, however, if the shear, F_{V1}, is neglected and R_{z1} is set equal to V_{ef1}:

$$L_{g1} > \frac{M_{f1}}{V_{ef1}} + \frac{V_{ef1}}{t_{g1} \phi_t F_y} \tag{39}$$

As in the design example, a length slightly greater than that indicated by Equation 39 is generally satisfactory.

Because of the complexity of the equations for web crippling, that limit state is not integrated into the equations for minimum gusset length but may be evaluated after the gusset length is determined, as shown in the subsequent section.

Gussets Longer than the Minimum Length

In many cases, the gusset length will exceed the minimum from Equation 34, due to design considerations such as the required gusset thickness or the brace-to-gusset attachment. For gussets longer than the minimum, the designer has some flexibility in selecting a stress distribution that transfers the moment. Maximizing the length z decreases the moment arm and thus increases the force to be resisted; it also leaves less weld length for the forces that are resisted in the center zone. The authors have found that the total weld volume tends to be minimized by minimizing the length z_1 for optimized weld lengths and sizes. However, in many cases, the weld size in the center zone is controlled by a minimum weld size, or a proportioning requirement to ensure deformation compatibility is used to size the center-zone weld or the minimum length for z_1; in such cases, maximizing the length z_1 may be more economical.

The minimum length z_1 is determined considering web local yielding, web crippling, and gusset yielding, considering the normal force R_{z1} acting over the length z_1 (and combined with a shearing force for the gusset evaluation). The force R_{z1} corresponding to the length z_1 is determined by Equation 26 and is bounded by Equation 30.

Considering web local yielding, the minimum length z_1 is:

$$z_1 \geq \frac{L_{g1}}{2} - \sqrt{\frac{{L_{g1}}^2}{4} - \frac{M_{f1}}{\phi_w F_y t_w}} - 5k \tag{40}$$

The von Mises yield criterion is used to determine the minimum length z_1 that, for the design loads and a given gusset thickness and length, will result in effective stresses at the yield limit in the gusset. The shear stress is due to F_{V1} and the normal stress is due to the moment M_{f1}. The thickness should satisfy Equation 36. The length z_1 corresponding to the gusset length and thickness selected is obtained by combining Equations 24, 26, and 36:

$$z_1 \geq \frac{L_{g1}}{2} - \sqrt{\frac{{L_{g1}}^2}{4} - \frac{M_{f1}/\phi_t}{\sqrt{\left(F_y t_g\right)^2 - \left(\frac{F_{V1}}{\phi_v 0.6 L_{g1}}\right)^2}}} \tag{41}$$

Considering web crippling, the minimum length z_1 can be determined by rearranging AISC *Specification* Equation J10-4:

$$z_1 \geq \left[\frac{R_{z1}}{\phi_n 0.80 t_w^2}\sqrt{\frac{t_w}{E F_y t_f}} - 1\right]\left(\frac{d_m}{3}\right)\left(\frac{t_f}{t_w}\right)^{1.5} \tag{42}$$

Due to the number of terms of Equation 42, it is convenient to use the maximum value of $R_{z1} = V_{ef1}$ per Equation 30 rather than solving for z_1 using Equations 26 and 42. Alternatively, web crippling can be evaluated using R_{z1} corresponding to the larger of the values from Equations 40 and 41.

The minimum value of z_1 is the largest of the values from Equations 40, 41, and 42. Larger values of z_1 may be used up to a maximum value of z_1 limited by the minimum moment arm corresponding to the maximum transverse force:

$$z_1 \leq L_{g1} - \frac{M_{f1}}{V_{ef}} \tag{43}$$

Above this value of z_1, the length of the moment arm e_z is insufficient and the transverse force required to transmit the moment will exceed V_{ef}. If this maximum value is negative the gusset is too short to transmit the moment regardless of how concentrated the force delivery can be.

In principle, the maximum value of z_1 may also be limited by stresses in the center region. Use of the additional bearing length of $5k$ (as opposed to $2.5k$) in Equation 40 distributes some of the force R_{z1} into the center region. For cases with high unbalanced load (or very small dimension e_z), $2.5k$ may be used in Equation 40, or the following evaluation can be made based on the total transverse force $R_{z1} + F_{N1}$ acting on a length $L_{g1} - z_1$:

$$z_1 \leq L_{g1} - \frac{R_{z1} + F_{N1}}{\phi_w F_y t_w} + 5k \tag{44}$$

Similarly, if the normal force F_{N1} is large (or the center zone is very short), the gusset stress in the center region should also be considered. Using the von Misses yield criterion gives this maximum:

$$z_1 \leq \frac{1}{2}\left[L_{g1} - \frac{F_{N1}/\phi_t F_y t_{g1}}{\sqrt{1 - \left(\frac{F_{V1}}{\phi_v 0.6 F_y t_{g1} L_{g1}}\right)^2}}\right] \tag{45}$$

Concentrated Stress Method Validation

Richards et al. (2018) analyzed a number of braced-frame beams using finite element models and compared internal forces with those obtained from the Uniform Stress Method and the Concentrated Stress Method (as presented by Sabelli and Arber, 2017). Figure 17 shows the results of one such analysis (from Figure 3.32 from Richards et al.). The finite element analysis results (FE) are shown along with the shears determined using the Uniform Stress Method (USM) and the Concentrated Stress Method (CSM, using the modified method as presented in this paper); the beam shear strength, ϕV_n, is also indicated. The values of maximum shear are reasonably consistent between the finite element analysis and the Concentrated Stress Method for this example, and while the total shear in the finite element model is less than the beam shear capacity, the finite element analysis indicated local yielding in the web.

Nevertheless, the point of maximum shear is not identical between the finite element analysis and the Concentrated Stress Method, indicating that the Concentrated Stress Method, while useful for design, is not a perfect representation of the internal stresses.

It should be noted that both Richards et al. (2018) and Hadad and Fortney (2020) found that the Uniform Stress Method is generally representative of the beam shear at levels of loading that do not result in web shear yielding. At higher levels of loading, the work of Richards et al. (2018) indicates adequate performance of gussets meeting the minimum required length for the Concentrated Stress Method and exceeding the length required for the Uniform Stress Method. Additional comparisons of finite-element analyses from Richards et al. with the two design models are presented in Sabelli et al. (2020).

Moment

Shear, such as shown in the three analyses represented in Figure 17, implies moment. The authors do not propose evaluation of the member moment within the connection region as necessary but present the equations for moment to facilitate understanding of the Concentrated Stress Method. Hadad and Fortney (2020) show that in finite element analyses, the beam moments are substantially lower than those calculated using the Uniform Stress Method.

Beam Moment

The beam moment is the combination of the integral of the beam shear and the distributed moment M_{FV} (Equation 19).

The beam shear in the center region is:

$$V_1(x) = -R_{z1} + \frac{F_{N1}}{L_{g1}}x \qquad \text{for } |x| \le L_{g1}/2 - z_1 \tag{46}$$

In the z_1 region, the beam shear is:

$$V_1(x) = -R_{z1}\left(\frac{L_{g1}}{2z_1} - \frac{|x|}{z_1}\right) + \frac{F_{N1}}{2}\frac{|x|}{x} \tag{47}$$
$$\text{for } |x| \ge L_{g1}/2 - z_1$$

Similar to the Uniform Stress Method, the distributed moment M_{FV} may be assumed to be transferred over the length L_{g1} using Equation 19. The brace-induced moment in the beam is:

$$M_1(x) = -R_{z1}x + \frac{M_{FV1}}{L_{g1}}x - F_{N1}\left(\frac{L_{beam}}{4} - \frac{L_{g1}}{8} - \frac{x^2}{2L_{g1}}\right) \tag{48}$$
$$\text{for } |x| \le L_{g1}/2 - z_1$$

Similar to the Uniform Stress Method, the two equal and opposing effects of the applied force parallel to the member axis, F_{V1}, are included in Equation 48: the transverse stress resulting from M_{Ch}, which causes member shear in addition to moment, and the distributed moment corresponding to M_{FV}, which does not affect the shear. The shape of the shear diagram in the Concentrated Stress Method results in a somewhat smaller moment within the connection region than that corresponding to the Uniform Stress Method.

A liberal estimate may be made by computing the connection-induced moment and combining with the mid-span moment due to overall beam flexure:

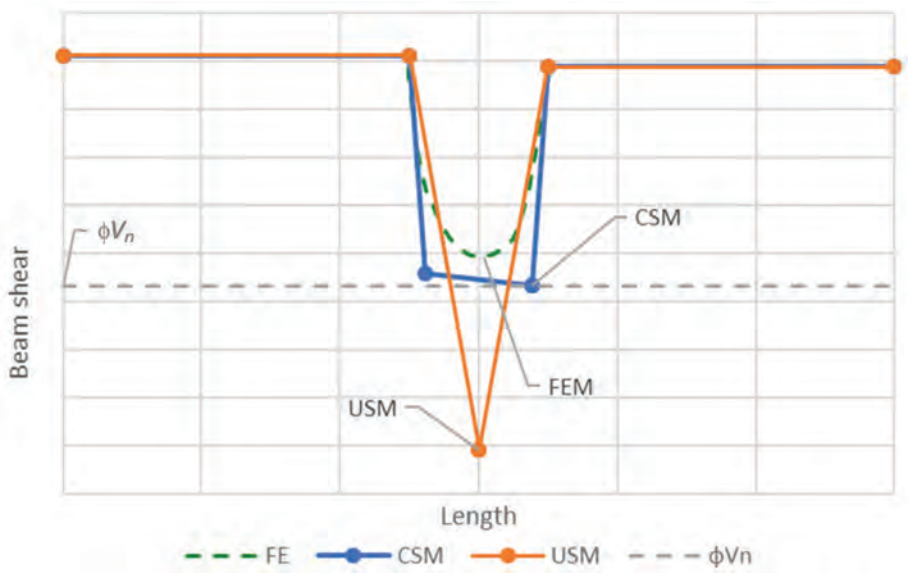

Fig. 17. Concentrated Stress Method (CSM) and Uniform Stress Method (USM) analysis of beam from Richards et al. (2018).

$$M_{max1} \le \frac{|M_{Ch1}|}{2}\left[\frac{z_1}{L_{g1}} - \left(\frac{z_1}{L_{g1}}\right)^2\right] + F_{N1}\left(\frac{L_{beam}}{4} - \frac{L_{g1}}{8}\right) + M_M \tag{49}$$

The connection-induced moment due to M_{Ch} never exceeds $M_{Ch}/8$ (the value for $z_1 = L_{g1}/2$, which corresponds to the Uniform Stress Method distribution). The moment is additive with the moment from gusset 2 for the typical braced-frame case.

Column Moment

Similar methods can be applied to calculate moment in the column within the connection region. Column moments due to frame behavior, which reverse over the connection depth, are typically additive to the effect of M_{Ch}.

$$M_{max1} \le \frac{M_{Ch1}}{2}\left[\frac{z_1}{L_{g1}} - \left(\frac{z_1}{L_{g1}}\right)^2\right] + M_M \tag{50}$$

The effect of any moment M_{Bm} on the member moment is captured in the term M_M, conservatively taken at its full value. Similar to the beam moment, the column moment due to the chevron effect tends to be small.

COMBINATION OF FORCES FOR TWO GUSSET PLATES

The member forces derived are for braces on one side with opposite forces (one brace in tension and the other in compression). These forces may be combined with gravity-induced forces and with shear due to flexural restraint for frames with moment connections. While the diagrams show the left brace in tension and the right brace in compression, forces corresponding to the opposite case are easily determined by using negative values for the brace forces.

For a configuration with braces on both sides of the member (such as a two-story X-configuration in a beam), brace-induced shears and moments will be additive for the typical case in which the story shears are in the same direction. The effective web shear resistance may be apportioned between the two gussets, considering the relative magnitudes of their moments, M_f, to permit independent design of the two gussets:

$$V_{ef1} = \frac{M_{f1}}{M_{Tot}} V_{efTot} \tag{51}$$

and

$$V_{ef2} = \frac{M_{f2}}{M_{Tot}} V_{efTot} \tag{52}$$

where

$$M_{Tot} = M_{f1} + M_{f2} \tag{53}$$

Other methods of apportionment are admissible, but this method allows for design of the gusset connections based on member forces established prior to gusset design and without additional interdependence.

Uniform Stress Method

In the Uniform Stress Method, the full member shear strength generally may be utilized:

$$V_{efTot} = \phi_v V_n \tag{54}$$

Gusset plates may be of different lengths, but for simplicity, they may be set to be equal. If equal-length gussets are used ($L_{g1} = L_{g2}$), Equation 15 for the minimum gusset-plate length to preclude the need for reinforcement can be modified thus:

$$L_g \ge \frac{2M_{Tot}}{V_{efTot}} \tag{55}$$

Concentrated Stress Method

In the Concentrated Stress Method, the effective beam shear strength is reduced:

$$V_{efTot} = \phi_v V_n - \left|\frac{F_{N1}}{2} - \frac{F_{N2}}{2}\right| - |V_M| \tag{56}$$

If equal-length gussets are used, Equation 34 for the minimum gusset-plate length to preclude the need for reinforcement can be modified thus:

$$L_g \ge \frac{M_{Tot}}{V_{efTot}} + \frac{V_{efTot}}{\phi_w F_y t_w} - 5k \tag{57}$$

Similarly, Equation 39 based on gusset yielding can be modified thus:

$$L_{g1} > \frac{M_{Tot}}{V_{efTot}} + \frac{V_{efTot}}{t_{g1}\phi_t F_y} \tag{58}$$

MEMBER SELECTION

The procedures described earlier allow for the design of a connection based on design forces and the strength of a member already selected. Economy in steel construction can often be achieved by consideration of connection requirements in member selection. Equations for required beam strength, rather than required gusset length, can be derived from the methods presented. Fortney and Thornton (2015) suggest a preliminary assumption of a gusset length of one-sixth of the beam span for chevron connections; this value can be used to facilitate member selection.

The chevron shear at the connection is due mainly to the chevron moment, M_{ch}, which is proportional to the eccentricity, e_m, typically half the member depth. Selection of a shallower member reduces the eccentricity and thus reduces the chevron shear. Because the shear capacity is also proportional to the depth, the member depth appears in both the demand and capacity terms, and the required web thickness is not a function of member depth.

Uniform Stress Method

Using the Uniform Stress Method equation for minimum gusset length for a given member strength (Equation 15), the minimum shear strength is

$$\phi_v V_n = \phi_v 0.6 F_y d_m t_w \tag{59}$$

$$\phi_v V_n \geq \frac{2M_{f1}}{L_{g1}} + \frac{2M_{f2}}{L_{g2}} \tag{60}$$

$$\phi_v V_n \geq \frac{F_{V1} d_m}{L_{g1}} + \frac{F_{V2} d_m}{L_{g2}} \tag{61}$$

Note that the member depth appears both in the demand, M_{f1}, and in the resistance, ϕV_n, and thus cancels out in Equation 62 for the minimum member web thickness:

$$t_w \geq \frac{F_{V1}/L_{g1} + F_{V2}/L_{g2}}{\phi_v 0.6 F_y} \tag{62}$$

For beams or columns with small moments due to unbalanced normal forces, a shallow member meeting this requirement may be economical. Note that the optimal gusset length may be a function of member depth.

Concentrated Stress Method

Use of a member with web thickness less than that required by Equation 62 necessitates either reinforcement of the web or use of a greater moment arm to deliver the moment M_{f1} than is assumed in the Uniform Stress Method (such as e_{z1} in the Concentrated Stress Method). There is not a corresponding simple equation for minimum web thickness using the Concentrated Stress Method. However, the minimum gusset length based on beam shear strength with $z_1 = 0$ (Equation 31) represents a limiting value. This minimum gusset length corresponds to a moment arm e_{z1} equal to L_{g1} (rather than $\frac{1}{2}L_{g1}$, as corresponds to the Uniform Stress Method and Equation 62), and thus, if there are no other member shear demands to consider, the required web thickness for this limiting case is half of that from Equation 62. A web thickness of 60% to 75% of that given by Equation 62 (based on an assumed gusset length) generally permits use of the Concentrated Stress Method without the need for web reinforcement, albeit with possible moderate adjustment in gusset length. (Use of 75% of the value from Equation 62 requires $e_{z1} \sim \frac{2}{3} L_{g1}$; use of 60% requires $e_{z1} \sim \frac{5}{6} L_{g1}$.)

GUSSET AND WELD DESIGN

The stress distributions assumed in the Uniform Stress Method and the Concentrated Stress Method impose different demands on gusset plates and welds. The design of those elements should be compatible with each other (and with the checks on member local limit states, such as web local yielding, web crippling, and panel-zone shear), or the connection may not be able to resist the applied forces. For example, if the design for local limit states is based on the Uniform Stress Method, but the gusset thickness is sized using the optimized plastic stress method (which is implicit in the interaction Equation 9-1 in the AISC *Steel Construction Manual*), the member may be subject to a combination of web local yielding and gusset plate yielding prior to developing the required strength. It is recommended that the method used for member local limit states be carried through the design of the gusset and the weld.

Gusset Design: Section Parallel to Member Axis

Uniform Stress Method

For the Uniform Stress Method, the gusset section at the interface with the flange can be evaluated using an interaction method such as the von Mises yield criterion and solving for the required thickness:

$$t_g \geq \sqrt{\left(\frac{|4M_{f1}|}{\phi_t F_y L_{g1}^2} + \frac{|F_{N1}|}{\phi_t F_y L_{g1}}\right)^2 + \left(\frac{F_{V1}}{\phi_v 0.6 F_y L_{g1}}\right)^2} \tag{63}$$

Concentrated Stress Method

For the Concentrated Stress Method, the gusset section at the interface with the flange is implicitly designed by use of a length z conforming to Equations 36 and 38.

Gusset Design: Mid-Length Transverse Section

Statics require that certain forces be transferred across the midpoint of the gusset. Figure 18 shows free-body diagrams of half of a gusset for both the Uniform Stress Method (a) and the Concentrated Stress Method (b).

The normal force on the gusset transverse section (i.e., the force parallel to the member axis) for both models is:

$$N_{g1} = \frac{1}{2} F_{V1} - F_{1,1} \cos \gamma_{1,1} \tag{64}$$

which is equivalent to:

$$N_{g1} = \frac{1}{2}(F_{1,2}\cos\gamma_{1,1} - F_{1,1}\cos\gamma_{1,2}) \tag{65}$$

Uniform Stress Method

The shear on this gusset section transverse to member axis (for the Uniform Stress Method) is:

$$V_{g1} = F_{1,1}\sin\gamma_{1,1} - \frac{2M_{f1}}{L_{g1}} + \frac{F_{N1}}{2} \tag{66}$$

The gusset moment (for the Uniform Stress Method) is:

$$M_{g1} = \left(\frac{2M_{f1}}{L_{g1}} - \frac{F_{N1}}{2}\right)\frac{L_{g1}}{4} + N_{g1}\left(e_m + \frac{d_{g1}}{2}\right) - \frac{F_{V1}}{2}e_m \tag{67}$$

which simplifies to:

$$M_{g1} = N_{g1}\left(e_m + \frac{d_{g1}}{2}\right) - \frac{F_{N1}L_{g1}}{8} \tag{68}$$

Concentrated Stress Method

The gusset shear transverse to member (for the Concentrated Stress Method) is:

$$V_{g1} = F_{1,1}\sin\gamma_{1,1} - R_{z1} + \frac{F_{N1}}{2} \tag{69}$$

The gusset moment (for the Concentrated Stress Method) is:

$$M_{g1} = R_{z1}\left(\frac{L_{g1}}{2} - \frac{z_1}{2}\right) - \frac{F_{N1}}{2}\left(\frac{L_{g1}}{4} - \frac{z_1}{2}\right) + N_{g1}\left(e_m + \frac{d_{g1}}{2}\right) - \frac{F_{V1}}{2}e_m \tag{70}$$

which simplifies to:

$$M_{g1} = N_{g1}\left(e_m + \frac{d_{g1}}{2}\right) - \frac{F_{N1}L_{g1}}{8} + \frac{F_{N1}z_1}{4} \tag{71}$$

Note that the terms related to M_{f1} and F_{V1} cancel out in both Equations 68 and 71. Thus, the gusset moment is only due to the unequal brace force components transverse to the member axis (resulting in an unbalanced transverse force F_{N1}) and to unequal brace force components parallel to the member axis (resulting in a force transfer N_{g1} from one half of the gusset to the other), with those two effects offsetting each other.

The gusset should be evaluated for the interaction of these shear, normal, and moment forces. This may be done using von Mises yield criteria or other methods as discussed in the AISC *Steel Construction Manual* (AISC, 2017).

Gusset Design: Diagonal Section (Concentrated Stress Method)

Brace-to-gusset connections are typically evaluated for the limit state of block shear without consideration of the subsequent load path through the gusset. This may not

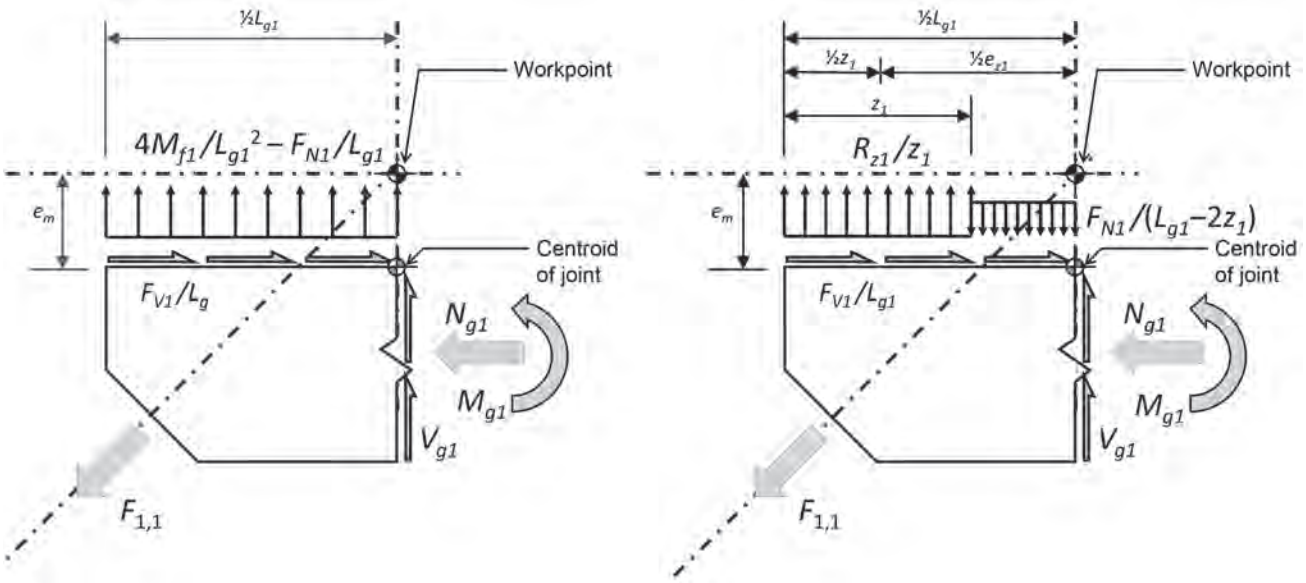

(a) Uniform Stress Method *(b) Concentrated Stress Method*

Fig. 18. Free-body diagrams of half gusset.

present any significant inconsistency for the Uniform Stress Method, which assumes a uniform stress over each half of the gusset, but may for the Concentrated Stress Method, in which high stresses are assumed at the gusset zones z_1. In order to ensure that the gusset has sufficient strength to transfer the force R_{z1} to the region z_1 in the gusset-to-beam connection, the gusset should be evaluated along a diagonal section, as shown in Figure 19. That section is aligned with the outside shear area used in the block-shear calculation and projected to the beam–gusset interface.

The intersection of the diagonal section with the gusset edge occurs at a point defined by the dimension X_{crit}:

$$X_{crit} = \frac{L_g}{2} - \frac{e_m}{\tan\gamma} - \frac{W}{2\sin\gamma} \tag{72}$$

thus,

$$X_{crit} = \frac{L_g}{2} - \frac{d_m\cos\gamma + W}{2\sin\gamma} \tag{73}$$

The length of the section is determined using the dimensions indicated in Figure 19:

$$\frac{D_{clip}}{\sin\gamma} = X_{crit}\tan\gamma - (d_g - Y_{clip}) \tag{74}$$

$$D_{crit} = \frac{X_{crit}}{\cos\gamma} - D_{clip} \tag{75}$$

$$D_{crit} = X_{crit}\cos\gamma + (d_g - Y_{clip})\sin\gamma \tag{76}$$

Note that this length is somewhat greater than the length of one of the shear areas used for the block-shear rupture check in the gusset plate. In some cases, a simplified check with that portion of the block-shear area suffices.

The forces acting to the left of that section are:

$$F_{X\,crit} = \frac{X_{crit}}{L_g} F_V \tag{77}$$

If X_{crit} is less than or equal to z:

$$F_{Ycrit} = \frac{X_{crit}}{z} R_z \tag{78}$$

$$e_{crit} = \frac{X_{crit}}{2} \tag{79}$$

$$M_{crit} = F_{Ycrit}\left(e_{crit} - \frac{D_{crit}\cos\gamma}{2}\right) + F_{Xcrit}\frac{D_{crit}\sin\gamma}{2} \tag{80}$$

If X_{crit} is greater than z_1:

$$F_{Ycrit} = R_z + F_N\frac{X_{crit} - z}{L_g - 2z} \tag{81}$$

Note that on one side of the gusset, the two terms of Equation 81 will be additive; that is the more critical condition.

$$e_{crit} = \frac{R_z\left(X_{crit} - z/2\right) + F_N\dfrac{(X_{crit} - z)^2}{2(L_g - 2z)}}{F_{Ycrit}} \tag{82}$$

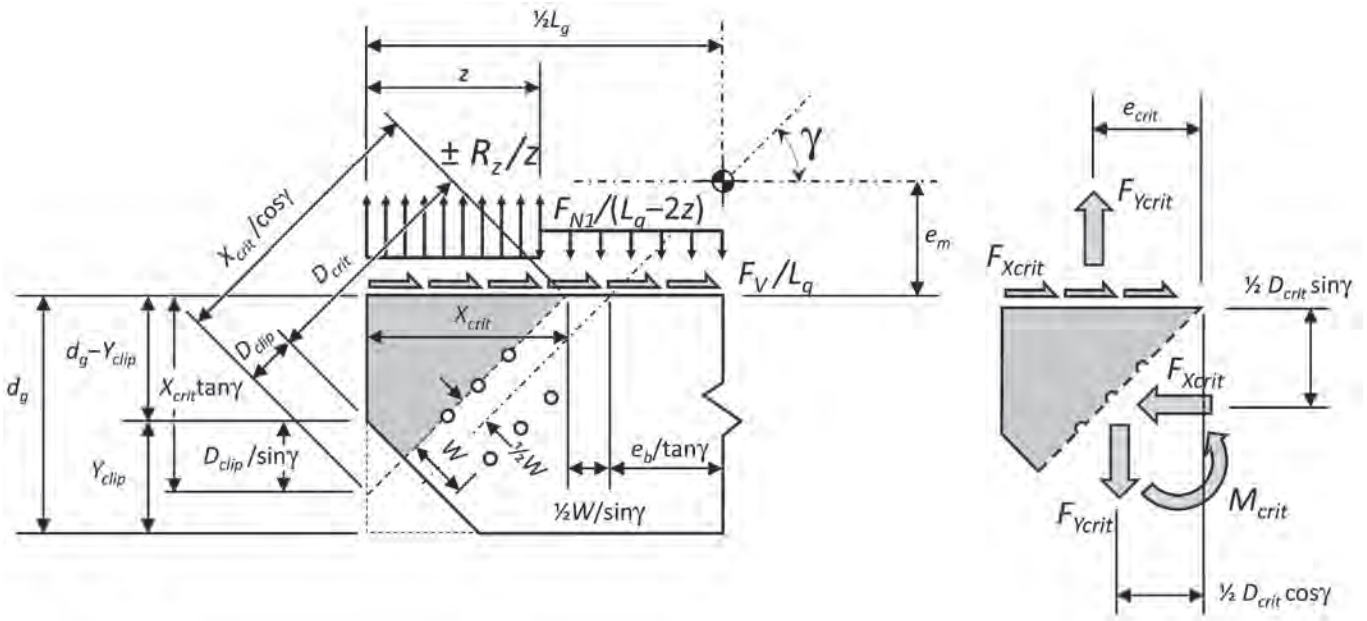

Fig. 19. Critical gusset section.

$$M_{crit} = F_{Ycrit}\left(e_{crit} - \frac{D_{crit}\cos\gamma}{2}\right) + F_{Xcrit}\frac{D_{crit}\sin\gamma}{2} \quad (83)$$

The forces are transformed to act on the diagonal section:

$$V_{crit} = F_{Xcrit}\cos\gamma + F_{Ycrit}\sin\gamma \quad (84)$$

$$N_{crit} = F_{Xcrit}\sin\gamma - F_{Ycrit}\cos\gamma \quad (85)$$

The gusset should be evaluated for these forces using an interaction method such as the von Mises yield criterion or interaction Equation 9-1 in the AISC *Steel Construction Manual*.

Weld Design

The design of welds should provide adequate strength to transfer forces across the gusset-to-beam interface (F_V, F_N, and M_f) and adequate ductility to achieve the assumed stress distribution. The weld size for a double fillet need not exceed ⅝ of the gusset thickness (for an adequately sized gusset), as discussed for single-plate connections in the AISC *Steel Construction Manual* (2017); this weld size permits yielding of the gusset before weld rupture. (This proportioning rule implicitly accepts use of a resistance factor greater than 0.75.) Weld sizes greater than ⅝ of the gusset thickness are not effective in developing their full force because they are limited by the gusset capacity (and thus also indicate an inadequate gusset thickness); however, increasing a weld that requires less than ⅝ of the gusset thickness up to this value allows for yielding of the gusset before weld rupture and thus permits stress redistribution.

Uniform Stress Method

Under the Uniform Stress Method, the weld adequacy should be evaluated using methods from the AISC *Steel Construction Manual*, such as the instantaneous center of rotation, which represents both weld strength and the limits on weld ductility. As a minimum, the weld should be large enough to resist the local stress consistent with the Uniform Stress Method. The required strength per unit length is:

$$r_u = \sqrt{\left(\frac{|4M_{f1}|}{L_{g1}^2} + \frac{|F_{N1}|}{L_{g1}}\right)^2 + \left(\frac{F_{V1}}{L_{g1}}\right)^2} \quad (86)$$

The AISC *Seismic Design Manual* (2018) utilizes the 25% increase related to gussets at beam-column-brace connections to promote ductility per the AISC *Steel Construction Manual* and Hewitt and Thornton (2004). Hadad and Fortney (2020) determined a ratio of maximum to average stress of approximately 3 (including a standard deviation) for weld stresses in their finite element analyses of chevron connections. They suggest that the factor of 3 be applied in the design of the weld (which need not exceed the size corresponding to the gusset-plate strength).

Concentrated Stress Method

The Concentrated Stress Method inherently addresses nonuniform stress in the gusset and may indicate stresses in the z region much higher than indicated by the Uniform Stress Method. As such, the increase to address nonuniform stress is not proposed for this method.

For designs employing the Concentrated Stress Method, stresses may redistribute along the weld due to beam inelasticity. As such, the stress distribution corresponding to the instantaneous center of rotation method may be impossible to achieve with the beam web strength provided. The weld in the z_1 zones should be evaluated for the force normal to the member axis, R_{z1}. For welds in the center region ($L_{g1} - 2z_1$), the normal force is F_{N1}. The shear force (parallel to the member axis) in both regions may be taken as F_{V1}/L_{g1}. Often the weld size required in the z regions will be substantially greater than that required in the center region.

To address strain compatibility of the linear weld group consisting of a larger weld size in the z regions and a smaller size in the center, two measures are proposed. First, the weld size in the z region may be sized to develop the strength of the gusset plate (e.g., a double fillet weld of at least ⅝ of the gusset thickness); this ensures that the deformation required of that zone of the joint may be provided by the gusset, and thus the full strength of both that region and the center region can be achieved.

Second, the two welds may be proportioned so that their strains are consistent with the design strength utilized. This may be done by analyzing the deformation of the different weld elements, as in the instantaneous center of rotation method. The authors have found satisfactory designs by proportioning the weld group with the weld in the center zone being ⅝ of the size of the welds in the z region and then extending the larger z-region weld to the ¼ point of the gusset at each end. It is expected that, with more study, those minima could be reduced or eliminated. Alternatively, the weld size selected for the z region may be used for the entire gusset length.

PROPOSED DESIGN PROCEDURE

The design of chevron and full-height gussets may be governed by design considerations other than the local forces addressed in this paper. In such cases, the material efficiency of the Concentrated Stress Method cannot be realized, and the Uniform Stress Method (which is simpler to implement) may be convenient. The following design procedure may be used to minimize the complexity of the required calculations:

1. Establish parameters.

   1.1 Determine the forces F_V, F_N, and M_f, acting on the gusset-member interface.

   1.2 Determine the optimal gusset-plate length based on the brace-to-gusset connection (and any other considerations). If desired, determine the optimal gusset thickness.

   1.3 For connections with gussets on opposite flanges, determine shear-strength apportionment for the two gussets per Equations 51 and 52.

2. Try the Uniform Stress Method.

   2.1. Check if the optimal gusset-plate length exceeds the minimum length required for the Uniform Stress Method using Equation 15 or 55. If so:

   2.2. Check member.

      2.2.1. Determine V_{mc} (Equation 14); check shear.

      2.2.2. Evaluate web local yielding and web crippling Equation 17.

   2.3. Design gusset.

      2.3.1. Design the gusset section parallel to the member axis using the Uniform Stress Method Equation 63.

      2.3.2. Check the transverse gusset section for the forces from Equations 65, 66, and 68. (Any procedure in the AISC *Manual* may be used.)

   2.4. Design the gusset–member interface weld. (Design for peak stress using the Uniform Stress Method distribution; apply appropriate ductility factor or size to develop the gusset plate strength.)

3. If the Uniform Stress Method design is unsatisfactory, try the Concentrated Stress Method.

   3.1 Select gusset length.

      3.1.1. Check minimum length required for the Concentrated Stress Method (Equation 34). Use the maximum of the optimal gusset-plate length and this minimum length. If this length is excessive, consider reinforcing the member web (or using a different member).

      3.1.2. Determine the required gusset thickness per Equations 36 and 38. Revise gusset length if necessary.

   3.2. Analyze connection and check member

      3.2.1. Determine the length of the zone z (Equations 40, 41, and 42). Use the maximum length from these three equations.

      3.2.2. Determine the concentrated force R_z (Equation 26).

      3.2.3. Determine V_{mc} (Equation 27); check member shear.

   3.3. Design gusset.

      3.3.1. Check the gusset section at the interface with the flange in the center zone. (Gusset horizontal section at the interface with the flange in the z zone is implicitly checked by the required thickness calculation.)

      3.3.2. Check the transverse gusset section for the forces from Equations 65, 69, and 71. (Any procedure in the AISC *Manual* may be used.)

      3.3.3. Check the diagonal gusset section for the forces from Equations 80 (or 83), 84, and 85. (Any procedure in the AISC *Manual* may be used.)

   3.4 Design weld.

      3.4.1. Design zone z weld.

      3.4.2. Design center-zone weld.

Note that this recommended design procedure implicitly checks member shear in the connection region for both the Uniform Stress Method and the Concentrated Stress Method. It does not include a check of the member for combined axial and bending forces within the connection region based on the authors' experience and judgment.

Table 1. Brace Forces			
	Brace Axial Force *F* (kips)	**Shear Component *F* cos(γ) (kips)**	**Normal Component *F* sin(γ) (kips)**
$F_{1,1}$	568	364	436
$F_{1,2}$	653	418	502
$F_{2,2}$	511	327	393
$F_{2,1}$	588	376	451

DESIGN EXAMPLE

The connection shown in Figure 20 will be designed following the recommended procedure, proceeding from the Uniform Stress Method to the Concentrated Stress Method developed in this study to eliminate reinforcement.

Given:

The brace design forces are presented in Table 1. All brace angles are 50.2° from horizontal. To facilitate subsequent calculations, the shear and normal components of the brace forces are determined and presented in the table.

Both beam and gusset are Grade 50 material. The beam is a W24×94 (ϕV_n = 375 kips; A=27.7 in.^{2}; Z=254 in.^{4}), 25 feet long. The workpoint is at the beam centerline:

$$e_m = \frac{d_m}{2} = 12.15 \text{ in.} \tag{8}$$

The beam moment due to loading other than from braces, M_M, is 80 kip-ft.

Based on the brace-to-gusset connection (not shown), the minimum gusset length is 48 in. For the brace-to-gusset connection design, a ¾-in.-thick gusset is optimal, and the depth required is 21 in.

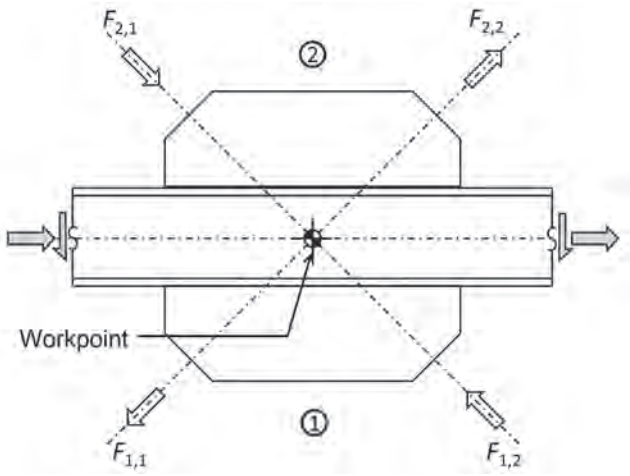

Fig. 20. Design example.

Table 2. Connection Forces				
	Equation	Gusset 1	Gusset 2	Combination (total or difference)
$F_{V\,(i)}$ (kips)	1	782	703	78.5
$F_{N\,(i)}$ (kips)	2	65.5	58.9	6.6
$M_{f\,(i)}$ (kip-in.)	3	9500	8550	18000
$V_{ef\,(i)}/V_{efTOT}$	51; 52	0.526	0.474	1.0

Solution:

Design of Gusset 1

1. Establish Parameters

Optimal gusset dimensions have been given. The forces acting on the flange from each of the gussets is shown in Table 2, which also shows the apportionment factors for beam effective shear strength.

2. Try the Uniform Stress Method

The minimum gusset length is determined from:

$$\begin{aligned} L_g &\geq \frac{2M_{Tot}}{V_{efTot}} \\ &= \frac{18{,}000 \text{ kip-in.}}{375 \text{ kips}} \\ &= 96.1 \text{ in.} \end{aligned} \tag{55}$$

For 48-in. gussets both above and below the beam, the Uniform Stress Method requires a web thickness of:

$$\begin{aligned} t_w &\geq \frac{F_{V1}/L_{g1} + F_{V2}/L_{g2}}{\phi_v 0.6F_y} \\ &= \frac{F_{V1} + F_{V2}}{\phi_v 0.6F_y L_g} \\ &= \frac{782 \text{ kips} + 703 \text{ kips}}{(1.0)0.6(50 \text{ ksi})(48 \text{ in.})} \\ &= 1.03 \text{ in.} \end{aligned} \tag{62}$$

This would require a W24×250. (Using the same gusset length, a W21×248 or a W18×211 would also be suitable.) Alternatively, an increase in effective shear strength of 96.1/48 = 2.0 could be achieved by a web doubler of ¾ × 18 in.:

$$\begin{aligned} L_g &\geq \frac{2M_{Tot}}{V_{efTot}} \\ &= \frac{2M_{Tot}}{(\phi_v V_{n_{beam}} + \phi_v V_{n_{doubler}})} \\ &= \frac{2(18{,}000 \text{ kip-in.})}{[375 \text{ kips} + 1.0(0.6)(0.75 \text{ in.})(18 \text{ in.})(50 \text{ ksi})]} \\ &= 46.2 \text{ in.} \end{aligned} \tag{55}$$

The minimum extents of the doubler can be determined using Equation 13.

The Uniform Stress Method would require a 96-in. gusset without reinforcement, a much heavier beam, or significant reinforcement to permit a gusset on the order of the optimal 48-in. length. As none of these is desirable, the design will proceed with the Concentrated Stress Method.

3. Try the Concentrated Stress Method

For the Concentrated Stress Method, the effective shear strength, V_{efTOT}, must be reduced considering the net unbalanced force:

$$V_{efTot} = \phi_v V_n - \left| \frac{F_{N1}}{2} - \frac{F_{N2}}{2} \right| \tag{56}$$
$$= 375 \text{ kips} - \left| \frac{6.6 \text{ kips}}{2} \right|$$
$$= 372 \text{ kips}$$

The lower gusset will be designed to utilize no more than 52.6% of the available member shear strength per Equation 51.

$$V_{ef1} = \frac{M_{f1}}{M_{Tot}} V_{efTot} \tag{51}$$
$$= \frac{9{,}500 \text{ kip-in.}}{18{,}000 \text{ kip-in.}} (372 \text{ kips})$$
$$= 196 \text{ kips}$$

Minimum Gusset Length and Corresponding Thickness

Assuming (for preliminary design) that the transverse force R_{z1} is equal to this effective shear strength, the minimum gusset length is:

$$L_{g1} > \frac{M_{f1}}{V_{ef1}} + \frac{V_{ef1}}{\phi_w F_y t_w} - 5k \tag{34}$$
$$= \frac{9{,}500 \text{ kip-in.}}{196 \text{ kips}} + \frac{196 \text{ kips}}{(1.0)(50 \text{ ksi})(0.515 \text{ in.})} - 5(1.38 \text{ in.})$$
$$= 49.2 \text{ in.}$$

The approximate length that corresponds to a ¾-in. gusset is:

$$L_{g1} > \frac{M_{f1}}{V_{ef1}} + \frac{V_{ef1}}{\phi_t F_y t_{g1}} \tag{39}$$
$$= \frac{9{,}500 \text{ kip-in.}}{196 \text{ kips}} + \frac{196 \text{ kips}}{(0.9)(50 \text{ ksi})(0.75 \text{ in.})}$$
$$= 54.3 \text{ in.}$$

As this length does not include the effect of the shear, a slightly larger value will be used, and the effect of shear addressed in the determination of the minimum length z_1. A 56-in. effective gusset length will be investigated. (The length also results in an economical weld design, which is presented later in the example.) The detailed length is 58 in., recognizing that the weld will not extend to the very end of the gusset.

The minimum bearing length z_1 based on the limit states of web local yielding and web crippling is:

$$z_1 \geq \frac{L_{g1}}{2} - \sqrt{\frac{L_{g1}^2}{4} - \frac{M_{f1}}{\phi_w F_y t_w}} - 5k \tag{40}$$

$$= \frac{56.0 \text{ in.}}{2} - \sqrt{\frac{(56.0 \text{ in.})^2}{4} - \frac{9{,}500 \text{ kip-in.}}{(1.0)(50 \text{ ksi})(0.515 \text{ in.})}} - 5(1.38 \text{ in.})$$

$$= 0.73 \text{ in.}$$

$$z_1 \geq \left[\frac{V_{ef1}}{\phi_n 0.80 t_w^2}\sqrt{\frac{t_w}{EF_y t_f}} - 1\right]\left(\frac{d_m}{3}\right)\left(\frac{t_f}{t_w}\right)^{1.5} \tag{42}$$

$$= \left[\frac{196 \text{ kips}}{(0.75)(0.80)(0.515 \text{ in.})^2}\sqrt{\frac{0.515 \text{ in.}}{(29{,}000 \text{ ksi})(50 \text{ ksi})(0.875 \text{ in.})}} - 1\right]\left(\frac{24.3 \text{ in.}}{3}\right)\left(\frac{0.875 \text{ in.}}{0.515 \text{ in.}}\right)^{1.5}$$

$$= -3.87 \text{ in.}$$

The low value from Equation 40 and the negative value from Equation 42 indicate that the force being developed, R_z, does not require a significant bearing length to satisfy the limit states of web local yielding and web crippling.

The minimum length z_1 corresponding von Mises yield criterion for stresses in the gusset is obtained from Equation 41:

$$z_1 = \frac{L_{g1}}{2} - \sqrt{\frac{{L_{g1}}^2}{4} - \frac{M_{f1}/\phi_t}{\sqrt{(F_y t_{g1})^2 - \left(\frac{F_{V1}}{\phi_v 0.6 L_{g1}}\right)^2}}} \tag{41}$$

$$= \frac{56.0 \text{ in.}}{2} - \sqrt{\frac{(56.0 \text{ in.})^2}{4} - \frac{9{,}500 \text{ kip-in.}/0.9}{\sqrt{[(50 \text{ ksi})(0.75 \text{ in.})]^2 - \left(\frac{782 \text{ kips}}{(1.0)(0.6)(56 \text{ in.})}\right)^2}}}$$

$$= 7.38 \text{ in.}$$

The maximum length z_1 is:

$$z_1 \leq L_{g1} - \frac{M_{f1}}{V_{ef_1}} \tag{43}$$

$$= 56.0 \text{ in.} - \frac{9{,}500 \text{ kip-in.}}{196 \text{ kips}}$$

$$= 7.51 \text{ in.}$$

The value from Equation 41 will be used. The corresponding transverse force is:

$$R_{z1} = \frac{M_{f1}}{L_{g1} - z_1} \tag{26}$$

$$= \frac{9{,}500 \text{ kip-in.}}{56.0 \text{ in.} - 7.38 \text{ in.}}$$

$$= 195 \text{ kips}$$

The limit states of web local yielding, web crippling, and gusset combined tension and shear yielding are implicitly checked by the gusset-length selection and this length z_1 determined above (Equations 40, 42, and 41). This value may also be used to check gusset stress using Equation 36; however, gusset stress is implicitly checked by the selection of a dimension z_1 that complies with Equation 41.

The beam shear is evaluated considering 52.6% of the shear due to the total unbalanced force:

$$V_{mc1} = V_{ma1} + R_{z1} \tag{27}$$

$$= \left(\frac{M_{f1}}{M_{Tot}}\right)\frac{F_{N1} - F_{N2}}{2} + R_{z1}$$

$$= 0.526\left(\frac{6.6 \text{ kips}}{2}\right) + (195 \text{ kips})$$

$$= 197 \text{ kips}$$

$$\frac{V_{mc1}}{\phi_v V_n} = \frac{197 \text{ kips}}{375 \text{ kips}}$$

$$= 0.525 \le 0.526 \quad \textbf{o.k.}$$

This is consistent with the apportionment of available beam shear strength between the two gussets established in Table 2.

Beam Moment and Axial Force in Gusset Region

For completeness, the combined effects of the internal beam moment and axial force are evaluated. (The proposed design procedure does not include this evaluation.)

Although Equation 49 permits a more precise calculation of beam moment, the moment is typically small, and the upper-bound value is used here for convenience for gusset 2, as that design has not been performed. Adapting Equation 49 to include the effect of two gussets gives:

$$M_{max} = \frac{M_{Ch1}}{2}\left[\frac{z_1}{L_{g1}} - \left(\frac{z_1}{L_{g1}}\right)^2\right] + \frac{M_{Ch2}}{2}\left[\frac{z_2}{L_{g2}} - \left(\frac{z_2}{L_{g2}}\right)^2\right] + \frac{(F_{N1} - F_{N2})L_{beam}}{4} + M_M$$

For gusset 1:

$$\frac{1}{2}\left[\frac{z_1}{L_{g1}} - \left(\frac{z_1}{L_{g1}}\right)^2\right] = \frac{1}{2}\left[\frac{7.38 \text{ in.}}{56.0 \text{ in.}} - \left(\frac{7.38 \text{ in.}}{56.0 \text{ in.}}\right)^2\right]$$

$$= 0.0572$$

For gusset 2, the dimension z_2 has not been determined. In this example (with $M_{f2} < M_{f1}$), z_2 could reasonably be assumed to be less than or equal to z_1 if $L_{g2} = L_{g1}$. The general limit is:

$$\frac{1}{2}\left[\frac{z_2}{L_{g2}} - \left(\frac{z_2}{L_{g2}}\right)^2\right] \le \frac{1}{8}$$

$$M_{max} \le 0.0572\left(\frac{9{,}500 \text{ kip-in.}}{12 \text{ in./ft}}\right) + 0.125\left(\frac{8{,}550 \text{ kip-in.}}{12 \text{ in./ft}}\right) + \frac{(65.5 \text{ kips} - 58.9 \text{ kips})(25 \text{ ft})}{4} + 80 \text{ kip-ft}$$

$$\le 255 \text{ kip-ft}$$

The axial force is conservatively taken as the maximum at the end of the connection region, assuming a symmetric distribution of collector forces:

$$P_u = \left|\frac{F_{V1}}{2} - \frac{F_{V2}}{2}\right|$$

$$= \left|\frac{782 \text{ kips}}{2} - \frac{703 \text{ kips}}{2}\right|$$

$$= 39.5 \text{ kips}$$

Assuming the section is fully braced at this location, the full section strength is used:

$$\phi_c P_n = \phi_c A_s F_y$$
$$= (0.9)(27.7 \text{ in.}^2)(50 \text{ ksi})$$
$$= 1{,}250 \text{ kips}$$

$$\phi_b M_n = \phi_b Z F_y$$
$$= (0.9)(254 \text{ in.}^3)(50 \text{ ksi})$$
$$= 11{,}400 \text{ kip-in.}$$
$$= 953 \text{ kip-ft.}$$

$$\frac{P_u}{\phi_c P_n} = 0.03$$

$$\frac{M_u}{\phi_b M_n} = 0.27$$

The interaction check from AISC *Specification* Equation H1-1b is used:

$$\frac{1}{2}\frac{P_u}{\phi_c P_n} + \frac{M_u}{\phi_b M_n} = \frac{1}{2}(0.06) + 0.27 \qquad \text{(from } \textit{Spec.} \text{ Eq. H1-1b)}$$
$$= 0.30 \quad \textbf{o.k.}$$

Gusset Selection

A ¾-in.-thick, 21-in.-deep, and 58-in.-long (56-in. effective length) gusset will be investigated.

$t_{g1} = 0.75$ in.
$d_{g1} = 21.0$ in.
$L_{g1} = 56.0$ in.

Gusset Check at Section Parallel to the Member Axis at Beam Flange

The Concentrated Stress Method implicitly checks the gusset over the lengths z_1 for combined stresses in determining the minimum length z_1 (Equation 41). For the center zone between the lengths z_1, Equation 38 gives the interaction ratio:

$$\sqrt{\left(\frac{F_{V1}}{\phi_v 0.6 F_y t_{g1} L_{g1}}\right)^2 + \left(\frac{F_{N1}}{\phi_t F_y t_{g1}(L_{g1} - 2z_1)}\right)^2} \qquad (38)$$
$$= \sqrt{\left[\frac{782 \text{ kips}}{0.6(50 \text{ ksi})(0.75 \text{ in.})(56.0 \text{ in.})}\right]^2 + \left\{\frac{65.5 \text{ kips}}{(0.9)(50 \text{ ksi})(0.75 \text{ in.})[56.0 \text{ in.} - 2(7.38 \text{ in.})]}\right\}^2}$$
$$= 0.622$$

Gusset Check at Mid-Length Transverse Section

The adequacy of the gusset depth is verified examining a section of the gusset transverse to the member axis. (See Figure 18.) The gusset force in direction of member is:

$$N_{g1} = \frac{1}{2}(F_{1,2}\cos\gamma_{1,2} - F_{1,1}\cos\gamma_{1,1}) \qquad (65)$$
$$= \frac{1}{2}(418 \text{ kips} - 364 \text{ kips})$$
$$= 27 \text{ kips}$$

The axial resistance of the gusset is:

$$\begin{aligned}\phi_t P_n &= 0.9 F_y d_{g1} t_{g1} \\ &= (0.9)(50 \text{ ksi})(21.0 \text{ in.})(0.75 \text{ in.}) \\ &= 709 \text{ kips}\end{aligned}$$

The gusset moment is:

$$\begin{aligned}M_{g1} &= N_{g1}\left(e_m + \frac{d_{g1}}{2}\right) - \frac{F_{N1}}{2}\left(\frac{L_{g1}}{4} - \frac{z_1}{2}\right) \\ &= (27 \text{ kips})\left(12.15 \text{ in.} + \frac{21.0 \text{ in.}}{2}\right) - \frac{65.5 \text{ kips}}{2}\left(\frac{56 \text{ in.}}{4} - \frac{7.38 \text{ in.}}{2}\right) \\ &= 280 \text{ kip-in.}\end{aligned} \tag{71}$$

The flexural resistance of the gusset is:

$$\begin{aligned}\phi_b M_n &= 0.9 F_y \frac{d_{g1}^2 t_{g1}}{4} \\ &= 0.9(50 \text{ ksi})\frac{(21.0 \text{ in.})^2 (0.75 \text{ in.})}{4} \\ &= 3{,}720 \text{ kip-in.}\end{aligned}$$

Gusset shear transverse to member:

$$\begin{aligned}V_{g1} &= F_{1,1} \sin\gamma_{1,1} - R_{z1} + \frac{F_{N1}}{2} \\ &= 436 \text{ kips} - 195 \text{ kips} + \frac{65.5 \text{ kips}}{2} \\ &= 274 \text{ kips}\end{aligned} \tag{69}$$

The shear resistance is:

$$\begin{aligned}\phi_v V_n &= 1.00(0.60 F_y) d_{g1} t_{g1} \\ &= 1.00(0.60)(50 \text{ ksi})(21.0 \text{ in.})(0.75 \text{ in.}) \\ &= 473 \text{ kips}\end{aligned}$$

Using the von Mises interaction equation:

$$\begin{aligned}\sqrt{\left(\frac{M_{g1}}{\phi_t M_n} + \frac{N_{g1}}{\phi_t P_n}\right)^2 + \left(\frac{V_{g1}}{\phi_v V_n}\right)^2} &= \sqrt{\left(\frac{280 \text{ kip-in.}}{3{,}720 \text{ kip-in.}} + \frac{27 \text{ kips}}{709 \text{ kips}}\right)^2 + \left(\frac{274 \text{ kips}}{473 \text{ kips}}\right)^2} \\ &= 0.590\end{aligned}$$

Gusset Check along Diagonal Section

The gusset will be checked along the critical diagonal section (Figure 19). The bolt gage, W, is 8 in. and the transverse dimension Y_{clip} is 8.0 in.

$$\begin{aligned}X_{crit} &= \frac{L_{g1}}{2} - \frac{d_m \cos\gamma + W}{2\sin\gamma} \\ &= \frac{56.0 \text{ in.}}{2} - \frac{(24.3 \text{ in.})\cos(50.2°) + 8 \text{ in.}}{2\sin(50.2°)} \\ &= 12.7 \text{ in.}\end{aligned} \tag{72}$$

This value is greater than z_1.

The diagonal section length is:

$$D_{crit} = X_{crit}\cos\gamma + (d_{g1} - Y_{clip})\sin\gamma \tag{75}$$
$$= (12.7 \text{ in.})\cos(50.2°) + (21.0 \text{ in.} - 8 \text{ in.})\sin(50.2°)$$
$$= 18.1 \text{ in.}$$

The forces acting on the section are:

$$F_{Xcrit} = \frac{X_{crit}}{L_{g1}} F_{V1} \tag{77}$$
$$= \frac{12.7 \text{ in.}}{56.0 \text{ in.}}(782 \text{ kips})$$
$$= 177 \text{ kips}$$

$$F_{Ycrit} = R_{z1} + F_{N1}\frac{X_{crit} - z_1}{L_{g1} - 2z_1} \tag{81}$$
$$= 195 \text{ kips} + (65.5 \text{ kips})\frac{12.7 \text{ in.} - 7.38 \text{ in.}}{56.0 \text{ in.} - 2(7.38 \text{ in.})}$$
$$= 204 \text{ kips}$$

$$e_{crit} = \frac{R_{z1}\left(X_{crit} - \frac{z_1}{2}\right) + F_{N1}\frac{(X_{crit} - z_1)^2}{2(L_g - 2z_1)}}{F_{Ycrit}} \tag{82}$$
$$= \frac{(195 \text{ kips})\left(195 \text{ kips} - \frac{7.38 \text{ in.}}{2}\right) + (65.5 \text{ kips})\frac{(12.7 \text{ in.} - 7.38 \text{ in.})^2}{2[56.0 \text{ in.} - 2(7.38 \text{ in.})]}}{204 \text{ kips}}$$
$$= 8.72 \text{ in.}$$

$$M_{crit} = F_{Ycrit}\left(e_{crit} - \frac{D_{crit}\cos\gamma}{2}\right) + F_{Xcrit}\frac{D_{crit}\sin\gamma}{2} \tag{83}$$
$$= (204 \text{ kips})\left[8.72 \text{ in.} - \frac{(18.1 \text{ in.})\cos(50.2°)}{2}\right] + (177 \text{ kips})\frac{(18.1 \text{ in.})\sin(50.2°)}{2}$$
$$= 1{,}825 \text{ kip-in.}$$

$$V_{crit} = F_{Xcrit}\cos\gamma + F_{Ycrit}\sin\gamma \tag{84}$$
$$= 270 \text{ kips}$$

$$N_{crit} = F_{Xcrit}\sin\gamma - F_{Ycrit}\cos\gamma \tag{85}$$
$$= (177 \text{ kips})\sin(50.2°) - (204 \text{ kips})\cos(50.2°)$$
$$= 5 \text{ kips}$$

The gusset is evaluated for these forces using the von Mises yield criterion:

$$\sqrt{\left(\frac{4|M_{crit}|}{\phi_t F_y t_{g1} {D_{crit}}^2} + \frac{N_{crit}}{\phi_t F_y t_{g1} D_{crit}}\right)^2 + \left(\frac{V_{crit}}{\phi_v 0.6 F_y t_{g1} D_{crit}}\right)^2}$$
$$= \sqrt{\left[\frac{4(1{,}825 \text{ kip-in.})}{(0.9)(50 \text{ ksi})(0.75 \text{ in.})(18.1 \text{ in.})^2} + \frac{5 \text{ kips}}{(0.9)(50 \text{ ksi})(0.75 \text{ in.})(18.1 \text{ in.})}\right]^2 + \left[\frac{270 \text{ kips}}{1.00(0.60)(50 \text{ ksi})(0.75 \text{ in.})(18.1 \text{ in.})}\right]^2}$$
$$= 0.94 \le 1.0 \quad \textbf{o.k.}$$

Gusset Weld (z-Region)

The weld along the length z_1 must deliver a normal force equal to R_{z1}; it must also deliver a shear force proportional to its length:

$$N_{weld} = R_{z1}$$
$$= 195 \text{ kips}$$

$$V_{weld} = \frac{z_1}{L_g} F_{v1}$$
$$= \frac{7.38 \text{ in.}}{56.0 \text{ in.}}(782 \text{ kips})$$
$$= 103 \text{ kips}$$

The weld in this zone therefore resists a force at an angle:

$$P_u = \sqrt{N_{weld}{}^2 + V_{weld}{}^2}$$
$$= \sqrt{(195 \text{ kips})^2 + (103 \text{ kips})^2}$$
$$= 221 \text{ kips}$$

The angle θ is $\tan^{-1}(195/103) = 62°$ from the weld axis. Using AISC *Specification* Equation J2-5:

$$P_u \le \phi R_n$$
$$= \phi_n 0.6 F_{EXX} (1.0 + 0.5 \sin^{1.5} \theta) \frac{\sqrt{2}}{2} w L_w$$
$$w \ge \frac{P_u}{\phi_n 0.6 F_{EXX} (1.0 + 0.5 \sin^{1.5} \theta) \frac{\sqrt{2}}{2} (2 z_1)}$$
$$w \ge \frac{221 \text{ kips}}{(0.75) 0.6 (70 \text{ ksi}) \left[1.0 + 0.5 \sin^{1.5} (62.2°)\right] \sqrt{2} (7.38 \text{ in.})}$$
$$= 0.474 \text{ in.}$$

A double-sided ½-in. fillet weld will be used. The weld size need not exceed ⅝ of the gusset plate thickness:

$$w \le \frac{5}{8} t_{g1}$$
$$= \frac{5}{8}(0.75 \text{ in.})$$
$$= 0.469 \text{ in.}$$

This weld must include the z region; a 14-in. length will be used to extend to the gusset ¼ points. Because this weld fully develops the gusset strength, deformation compatibility is inherently addressed.

Gusset Weld (Center Region)

The weld in the center region must be checked. The required strength is based on:

$$L_{g1} - 2z_1 = 56.0 \text{ in.} - 2(7.38 \text{ in.})$$
$$= 41.2 \text{ in.}$$

$$N_{weld} = F_{N1}$$
$$= 65.5 \text{ kips}$$

$$V_{weld} = F_{V1}\frac{L_{g1} - 2z_1}{L_{g1}}$$
$$= (782 \text{ kips})\frac{56.0 \text{ in.} - 2(7.38 \text{ in.})}{56.0 \text{ in.}}$$
$$= 576 \text{ kips}$$
$$P_u = \sqrt{N_{weld}{}^2 + V_{weld}{}^2}$$
$$= \sqrt{(65.5 \text{ kips})^2 + (576 \text{ kips})^2}$$
$$= 579 \text{ kips}$$

The angle θ is $\tan^{-1}(65.5/576) = 6.5°$. Using AISC *Specification* Equation J2-5:

$$w \geq \frac{P_u}{\phi_n 0.6F_{EXX}(1.0 + 0.5\sin^{1.5}\theta)\frac{\sqrt{2}}{2}2(L_{g1} - 2z_1)}$$
$$= \frac{579 \text{ kips}}{(0.75)0.6(70 \text{ ksi})\left[1.0 + 0.5\sin^{1.5}(6.5°)\right]\sqrt{2}(41.2 \text{ in.})}$$
$$= 0.310 \text{ in.}$$

A pair of the 5⁄16-in. fillet welds will be used.

The weld group consisting of the *z*-region and center welds conforms to both of the deformation compatibility recommendations: the *z*-region welds develop the gusset strength and extend to the gusset ¼ points, and the center region welds are 5⁄8 of the size of the welds in the *z*-regions.

Design Summary

Figure 21 shows the design based on the calculations above. The ½-in. fillet welds in the *z*-regions are presented as 3⁄16-in. fillet welds over the 5⁄16-in. full-length fillet welds.

A similar design is required for gusset 2. If the same method is followed, the beam shear resulting from the two gussets (each designed for a portion of V_{ef}) combined with the net unbalanced load will not exceed the beam shear capacity.

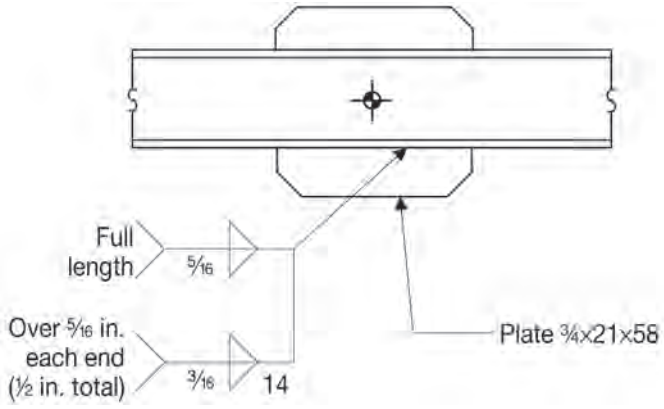

Fig. 21. Gusset design.

CONCLUSIONS

This study provides equations that can be used in the design of bracing connections to eliminate the need for web reinforcement. Recommendations are made for the selection of braced-frame beams and columns to facilitate connection design. The design method allows engineers to use the gusset plate to limit the shear demand on the member web. These equations can be used to assess the effects of member depth and gusset length on the required member shear strength in order to optimize member selection and gusset design. The Concentrated Stress Method presented allows for significantly smaller gusset plates than the Uniform Stress Method for an unreinforced section. For cases in which the Uniform Stress Method requires an undesirably large gusset or the use of a web doubler, the Concentrated Stress Method may permit a more economical design.

ACKNOWLEDGMENTS

The authors would like to recognize their debt to the pioneering work of William Thornton and the late Pat Fortney. Leigh Arber provided invaluable assistance in the review of this paper.

REFERENCES

AISC (2012), *Seismic Design Manual*, 2nd Ed., American Institute of Steel Construction, Chicago, Ill.

AISC (2016a), *Seismic Provisions for Structural Steel Buildings,* ANSI/AISC 341-16, American Institute of Steel Construction, Chicago, Ill.

AISC (2016b), *Specification for Structural Steel Buildings,* ANSI/AISC 360-16, American Institute of Steel Construction, Chicago, Ill.

AISC (2017), *Steel Construction Manual*, 15th Ed., American Institute of Steel Construction, Chicago, Ill.

AISC (2018), *Seismic Design Manual*, 3rd Ed., American Institute of Steel Construction, Chicago, Ill.

Euler, L. (translated by Hewlett, J.) [published 1765; 1822 translation], "Of a New Method of Resolving Equations of the Fourth Degree," *Elements of Algebra*, Longman, Hurst, Rees, Orme, and Company, London.

Fortney, P.J. and Thornton, W.A. (2015), "The Chevron Effect—Not an Isolated Problem," *Engineering Journal*, AISC, Vol. 52, No. 2, pp. 125–164.

Fortney, P.J. and Thornton, W.A. (2017), "The Chevron Effect and Analysis of Chevron Beams—A Paradigm Shift," *Engineering Journal*, AISC, Vol. 54, No. 4, pp. 263–296.

Hadad, A.A. and Fortney, P.J. (2020), "Investigation on the Performance of a Mathematical Model to Analyze Concentrically Braced Frame Beams with V-Type Bracing Configurations," *Engineering Journal*, AISC, Vol. 57, No. 2, pp. 91–108.

Hewitt, C.M. and Thornton, W.A. (2004), "Rationale Behind and Proper Application of the Ductility Factor for Bracing Connections Subjected to Shear and Transverse Loading," *Engineering Journal*, AISC, Vol. 41, No. 1, pp. 3–6.

Richards, P., Miller, B., and Linford, J. (2018), *Finite Element Evaluation of the Chevron Effect in Braced Frames,* Brigham Young University Report No. SSRP-2018/02.

Sabelli, R. and Arber, L. (2017), "Design of Chevron Gusset Plates," 2017 SEAOC Convention Proceedings.

Sabelli, R., Saxey, B., and Richards, P. (2020), "The Chevron Effect in Web Shear at Midspan Gussets," *Proceedings of the 17th World Conference on Earthquake Engineering*, Sendai, Japan.

Thornton, W.A. (1984), "Bracing Connections for Heavy Construction," *Engineering Journal*, AISC, Vol. 21, No. 3, pp. 139–148.

Guide for Authors

Scope

Engineering Journal is dedicated to the improvement and advancement of steel construction. Its pages are open to all who wish to report on new developments or techniques in steel design, research, the design and/or construction of new projects, steel fabrication methods, or new products of significance to the uses of steel in construction. Only original papers should be submitted.

General

Papers intended for publication should be submitted by email Margaret Matthew, editor, at **matthew@aisc.org**.

The articles published in the *Engineering Journal* undergo peer review before publication for (1) originality of contribution; (2) technical value to the steel construction community; (3) proper credit to others working in the same area; (4) prior publication of the material; and (5) justification of the conclusion based on the report.

All papers within the scope outlined above will be reviewed by engineers selected from among AISC, industry, design firms, and universities. The standard review process includes outside review by an average of three reviewers, who are experts in their respective technical area, and volunteers in the program. Papers not accepted will not be returned to the author. Published papers become the property of the American Institute of Steel Construction and are protected by appropriate copyrights. No proofs will be sent to authors. Each author receives three copies of the issue in which his contribution appears.

Manuscripts

Manuscripts must be provided in Microsoft Word format. Include a PDF with your submittal so we may verify fonts, equations and figures. View our complete author guidelines at **aisc.org/ej**.

Smarter. Stronger. Steel.

American Institute of Steel Construction
130 E Randolph St, Ste 2000, Chicago, IL 60601
312.670.2400 | aisc.org/ej